CHARACTERIZATION OF A NOVEL IRE1 SUBSTRATE PACT AND INTERACTING miRNAS

A DISSERTATION SUBMITTED TO

THE GRADUATE SCHOOL OF ENGINEERING AND SCIENCE

OF BILKENT UNIVERSITY

IN PARTIAL FULFILLMENT OF THE REQUIREMENTS FOR

THE DEGREE OF

DOCTOR OF PHILOSOPHY

IN

MOLECULAR BIOLOGY AND GENETICS

By

Aslı Ekin Doğan

June 2022

CHARACTERIZATION OF A NOVEL IRE1 SUBSTRATE PACT AND INTERACTING miRNAs

By ASLI EKİN DOĞAN

JUNE 2022

We certify that we have read this dissertation and that in our opinion it is fully adequate, in scope and in quality, as a thesis for the degree of Doctor of Philosophy.

Dr. Ebru Erbay

(Advisor)

Dr. Michelle Marie Adams

Dr. Hasan Tayfun Özçelik

Dr. Çağdaş Devrim Son

Dr. Erkan Yılmaz

Approved for the Graduate School of Engineering and Science

Dr. Ezhan Karaşan

Director of the Graduate School of Engineering and Science

ABSTRACT

Characterization of a Novel IRE1 Substrate PACT and Interacting miRNAs

Aslı Ekin Doğan

Molecular Biology and Genetics, PhD

Advisor: Ebru Erbay

June 2022

The double-stranded RNA-dependent protein kinase activator A (PACT) anchors the RNA-induced silencing complex (RISC) to the endoplasmic reticulum (ER)'s membranous platform where RISC nucleation occurs and thus, PACT plays a key role in microRNA (miR)-mediated translational repression. Previous studies have shown that ER stress leads to PACT phosphorylation while simultaneously inducing changes in the expression of many miRs. Here, we demonstrate that PACT is phosphorylated by the ER-resident Inositol-requiring enzyme-1 (IRE1), a bifunctional kinase/endoribonuclease (RNase), both under ER stress and no stress conditions. While the role of IRE1 as a stress-induced RNase driving the unfolded protein response (UPR) is well understood, the function or the target(s) of its kinase activity have remained unexplored. Findings of this thesis show that IRE1-mediated phosphorylation of PACT regulates mature miR-181c levels, which suppresses the expression of key regulators of mitochondrial biogenesis (mitobiogenesis). Phosphorylation by IRE1 causes PACT-mediated suppression of mitobiogenesis and respiration. Partial PACT-deficiency in mice leads to enhanced mitobiogenesis during brown fat activation in cells and mice. Furthermore, cardiopulmonary bypass-induced ischemia/reperfusion injury downregulates PACT protein expression in human hearts while simultaneously inducing mitobiogenesis. Collectively, these findings demonstrate PACT-miR-181c signaling axis is a key regulator of mitochondrial biogenesis and energetics.

Keywords: ER stress, inter-organelle communication, protein phosphorylation, mitobiogenesis, miRNAs, brown adipose tissue

ÖZET

IRE1 Kinaz Substratı PACT'ın ve Bağlandığı miRNA'ların Karakterizasyonu

Aslı Ekin Doğan

Moleküler Biyoloji ve Genetik, Doktora

Tez Danışmanı: Ebru Erbay

Haziran 2022

RNA bağlayıcı protein, çift sarmallı RNA'ya bağlı protein kinaz aktivatörü A (PACT), RNA kaynaklı susturma kompleksinin (RISC), çekirdeklenmesi için membranöz bir platform sağlayarak merkezi bir rol oynayan Endoplazmik Retikuluma (ER) tutturur ve mikroRNA (miR) aracılı translasyonel baskıda rol alır. Önceki çalışmalar, ER stresin PACT fosforilasyonuna yol açarken aynı anda birçok miR'in ifadesinde değişikliklere neden olduğunu göstermiştir. Bu tez bulguları, PACT'ın hem ER stress altında hem de bazal koşullarda ER bağlantılı Inositol gerektiren enzim-1 (IRE1), (çift endoribonükleaz (RNaz) ve kinaz) tarafından fosforile edildiğini gösterir. ER stresin aktive ettiği IRE1 RNaz fonksiyonu, katlanmamış protein tepkisini (UPR) tetiklerken, fizyolojik koşullarda bazal IRE1 kinaz aktivitesinin işlevi veya hedefleri bilinmemektedir. Bu tezin bulguları fosforile edilmiş PACT'ın, mitokondriyal biyogenezin (mitobiyogenez) kilit düzenleyicilerinin ekspresyonunu baskılayan olgun miR-181c seviyelerini düzenlediğini göstermektedir. IRE1 ile fosforilasyon, PACT aracılı mitobiyogenez ve mitokondriyel oksijen kullanımının baskılanması için gereklidir. Farelerde kısmi PACT eksikliği, hücre kültüründe olduğu kadar in vivo olarak da kahverengi adipoz doku aktivasyonu sırasında daha güçlü mitobiyogeneze yol açar. Ayrıca, kardiyopulmoner baypas kaynaklı iskemi/perfüzyon hasarı, insan kalp dokusunda PACT protein ekspresyonunu azaltırken aynı zamanda mitokondriyal biyogenezi indükler. Toplu olarak, bu bulgular PACT-miR181c sinyal ekseninin mitokondriyal biyogenez ve enerjinin önemli bir düzenleyicisi olduğunu göstermektedir.

Anahtah Sözcükler: ER stresi, organeller arası komunikasyon, protein fosforilasyonu, mitobiyogenez, mikro-RNA, kahverengi yağ dokusu

Dedicated to my mom and dad…

ACKNOWLEDGEMENTS

First, I would like to thank my advisor Dr. Ebru Erbay for her mentorship and guidance throughout my PhD and providing the best scientific environments for my work. I also want to thank our lab members, Asli Dilber Yildirim, Zehra Yildirim, Hamid Syed and Kikkie Poels for their friendship, support, and help. I am also thankful to my thesis committee members Prof. Michelle Adams and Prof. Tayfun Özçelik for their feedback and guidance.

Notably, I would like to thank Prof. Roberta Gottlieb for her valuable scientific input and support during the most difficult years of my PhD. I also want to express my gratitude to Gottlieb lab members, Jon Sin, Juliana Germano, Savannah Sawaged, Honit Piplani, Reetu Thakur and Kristina Song for their precious friendship and sharing their scientific expertise about mitochondria.

I am thankful to Dr. Celine Riera and her lab members for sharing their knowledge and resources with me to complete the in vivo part of my thesis work.

I also would like to thank Prof. Ganes Sen for providing the most essential tools for my thesis project, including the cell lines, plasmids and transgenic mice.

I am grateful for Prof. Moshe Arditi's moral support and guidance when I needed the most, during very stressful times.

I gratefully acknowledge European Research Council (Starting Grant 336643), National Institutes of Health (Grant R01HL149972) and Cedars-Sinai Medical Center Institutional Support for enabling me to complete my thesis work.

I would like to thank my dearest friends Fotis Nikolos, Kazukuni Hayashi, Zehra Yildirim and Mark Alonzo for their endless support, keeping me motivated and treating me as family.

Most importantly, I owe a huge thank you to my family. The only reason for me to persevere during hard times is the support of my precious mom and dad. I am eternally grateful to them for teaching me the importance of science, hard work, diligence, and dedication. No words can express my love and admiration for them.

Lastly, I am thankful to have the most supportive, caring, and loving fiancé. He kept me going and cheered me up when I felt like I should give up. I am incredibly lucky to have him in my life.

CONTENTS

ABSTRACT ..... **III**

ÖZET ..... **IV**

ACKNOWLEDGEMENTS ..... **VII**

CONTENTS ..... **IX**

LIST OF FIGURES ..... **XIII**

LIST OF TABLES ..... **XV**

ABBREVIATIONS ..... **XVI**

1. CHAPTER 1. INTRODUCTION **1**

1.1. The Endoplasmic Reticulum 1

1.2. Function of the Endoplasmic Reticulum 1

1.3. Unfolded Protein Response 3

1.4. Mitochondrial Structure and Dynamics 6

1.5. Mitochondria and ER Connection 7

1.6. Mitochondrial Biogenesis 10

1.7. ROS Formation and Defense Mechanisms 12

1.8. MicroRNAs and RNA-induced Silencing Complex 15

1.9. PACT and Its Functions 17

1.10. miR-181c And Its Implication in Regulation of Mitochondrial Dynamics 20

1.11. Brown Adipose Tissue Activation and Mitobiogenesis 22

1.12. Mitochondrial Dynamics in Cardiac Ischemia/Reperfusion (I/R) Injury 24

1.13. Hypothesis and Study Aims 28

2. CHAPTER 2. MATERIALS AND METHODS **31**

2.1. Materials 31

2.1.1. Reagents 31

2.1.2. Cell Culture Reagents 34

TABLE 2.2. CELL CULTURE REAGENTS **34**

2.1.3. Antibodies 35

TABLE 2.3. ANTIBODIES AND WORKING CONDITIONS **35**

2.1.4. Solutions 36

TABLE 2.4. SOLUTIONS **36**

2.1.5. Primers 39

TABLE 2.5. PRIMERS **39**

2.1.6. Plasmids and Cell Lines 40

2.1.7. Transgenic mice 40

2.2. METHODS 41

2.2.1. Study Design 41

2.2.2. Cell Culture and Transfections 41

2.2.3. Inhibitor Treatments 42

2.2.4. Palmitate (PA)-BSA Complex Preparation and Treatment 42

2.2.5. Animals 43

2.2.6. Toe Numbering and Genotyping for Prkra$^{-/-}$ mice 43

TABLE 2.6. PRIMERS AND PCR DETAILS FOR GENOTYPING **43**

2.2.7. RNA Isolation and qRT-PCR 43

2.2.8. Protein Lysates, SDS/PAGE Electrophoresis, Transfer and Western Blotting 44

2.2.9. Immuno-precipitation 44

2.2.10. IRE1 Kinase Assay 45

2.2.11. Site Directed Mutagenesis 45

TABLE 2.7. SITE DIRECTED MUTAGENESIS REACTION BUFFER **45**

TABLE 2.8. PCR CYCLE CONDITIONS **46**

2.2.12. Phospho-Proteomics Analysis 46

2.2.13. SeaHorse Mito Stress Test 48
2.2.14. SeaHorse Mitochondrial Fuel Flex Test 48
2.2.15. MitoTracker Staining 49
2.2.16. mtROS Measurement 49
2.2.17. Assessment of mtDNA Copy Number 49
2.2.18. Mitochondrial Enrichment 50
2.2.19. CL-316,243 Treatment 50
2.2.20. Metabolic Cages 51
2.2.21. EchoMRI 51
2.2.22. Histological Analysis 51
2.2.23. In vitro DICER or IRE1 cleavage assay 52
2.2.24. miRNA profiling by microarray 52
2.2.25. Statistics 52

3. CHAPTER 3. RESULTS 53

3.1. PACT IS AN IRE1 KINASE SUBSTRATE 53
3.1.1. Inhibiting IRE1 kinase domain but not RNase domain impacts PACT protein levels 53
3.1.2. IRE1 interacts with and phosphorylates PACT 56
3.2. PACT IS A SUPPRESSOR OF MITOBIOGENESIS 59
3.2.1. PACT regulates mitochondrial mass in vitro 59
3.2.2. PACT is involved in human I/R injury related mitobiogenesis 60
3.2.3. PACT blocks mitochondrial biogenesis in mouse and human cells 62
3.2.4. PACT has a role in the regulation of mitochondrial fusion and fission 66
3.3. PACT REGULATES MITOCHONDRIAL ENERGETICS 68
3.3.1. PACT is a regulator of mitochondrial oxygen consumption 68
3.3.2. PACT is a regulator of mitochondrial oxygen consumption in human cells 70
3.3.3. Mitochondrial substrate utilization is altered by PACT 71
3.3.4. Mitochondrial MTCO1 protein levels are dependent on PACT 72
3.3.5. Phospho-mutant PACT does not regulate mitochondrial oxygen consumption 73

3.3.6. Loss of PACT downregulates mitochondrial reactive oxygen species production 74
3.3.7. PACT does not regulate mitochondrial or cytosolic ROS metabolizing enzymes 75
3.3.8. PACT is not involved in mitophagy pathway 76
3.4. PACT SUPPRESSES MITOBIOGENESIS THROUGH MIR-181C 79
3.4.1. PACT regulates maturation of miR-181c 79
3.4.2. miR-181c is also a suppressor of mitobiogenesis 82
3.5. LOSS OF PACT AUGMENTS B_3-AR AGONIST-INDUCED BROWN ADIPOSE MITOBIOGENESIS 85
3.5.1. PACT is crucial for differentiated brown adipose cell mitobiogenesis and oxygen consumption 85
3.5.2. In-vivo brown adipose tissue activation and related mitobiogenesis is more pronounced in Prkra$^{+/-}$ mice 87
3.5.3. Energy expenditure of Prkra$^{+/-}$ mice is higher compared to Prkra$^{+/+}$ mice 89
3.5.4. PACT is not involved in iWAT activation and mitobiogenesis 91
3.6. ABLATION OF IRE1 ALONE IS NOT SUFFICIENT TO UPREGULATE MITOBIOGENESIS 92
3.7. IRE1- DEPENDENT MIR EXPRESSION CHANGES DURING ER-STRESS 93
CHAPTER 4. DISCUSSION 96
CHAPTER 5. FUTURE PERSPECTIVES 100
BIBLIOGRAPHY 102
COPYRIGHT PERMISSIONS 117
PUBLICATIONS 120

LIST OF FIGURES

Figure 1.1 Unfolded protein response. 4
Figure 1.2 Schematics of mitochondrial dynamics and quality control. 7
Figure 1.3 MAMs and related signaling. 10
Figure 1.4 Cellular pathway of mitochondrial biogenesis signal. 12
Figure 1.5 ROS metabolism and antioxidant enzymes. 14
Figure 1.6 Canonical RISC functioning and subunits. 16
Figure 1.7 Domains and functions of PACT. 20
Figure 1.8 miR-181c signaling in the mitochondrial matrix. 21
Figure 1.9 Brown adipocyte activation. 24
Figure 1.10 Overview of mitochondrial quality control during I/R injury. 27
Figure 1.11 Graphical Abstract. 30
Figure 3.1 PACT's phosphorylation is IRE1 kinase activity dependent. 54
Figure 3.2 PACT's phosphorylation is not dependent on IRE1 RNAse activity and mRNA levels are not affected by IRE1. 55
Figure 3.3 PACT's phosphorylation is not dependent on IRE1 in vivo. 56
Figure 3.4 PACT's phosphorylation is not dependent on IRE1 in vivo. 57
Figure 3.5 PACT is phosphorylated on S18 and T20 by IRE1. 58
Figure 3.6 Mitochondrial mass is regulated by PACT in vitro. 60
Figure 3.7 PACT is involved in upregulation of mitobiogenesis in human I/R condition. 61
Figure 3.8 PACT is a suppressor of mitobiogenesis in mouse cells. 63
Figure 3.9 PACT is a suppressor of mitobiogenesis in human cells. 66
Figure 3.10 PACT has an impact on mitochondrial fusion and fission. 67
Figure 3.11 PACT is a regulator of mitochondrial oxygen consumption and ATP production. 69
Figure 3.12 PACT is a regulator of mitochondrial oxygen consumption in human cells. 70
Figure 3.13 PACT knock-out or reconstitution changes mitochondrial substrate utilization. 71
Figure 3.14 PACT regulates ETC protein levels. 73
Figure 3.15 Mut-PACT cannot regulate mitochondrial OCR. 73
Figure 3.16 Knocking-out PACT decreases mtROS production. 74
Figure 3.17 PACT does not affect cytosolic or mitochondrial ROS metabolizing enzymes. 76
Figure 3.18 PACT does not regulate mitophagy. 78
Figure 3.19 WT-PACT but not Mut-PACT regulates maturation of miR-181c. 80
Figure 3.20 PACT impacts DICER cleavage of pre-miR-181c. 81
Figure 3.21 miR-181c blocks mitochondrial biogenesis and oxygen consumption. 82
Figure 3.22 miR-181c blocks mitochondrial biogenesis and oxygen consumption. 84
Figure 3.23 PACT is important for brown adipocyte mitobiogenesis and respiration. 86
Figure 3.24 PACT is involved in brown adipose tissue mitobiogenesis. 88

Figure 3.25 Partial PACT loss increases energy expenditure and oxygen consumption in mice. 90
Figure 3.26 PACT is not involved in iWAT mitobiogenesis. 91
Figure 3.27 Ablation of IRE1 or its kinase activity is not sufficient to induce mitobiogenesis. 93
Figure 3.28 IRE1-dependent changes in miRNA expression in ER-stress. 94
Figure 3.29 miR-2137 is regulated by IRE1 RNase activity. 95

LIST OF TABLES

Table 2.1. Reagents and Chemicals 31
Table 2.2. Cell Culture Reagents 34
Table 2.3. Antibodies and Working Conditions 35
Table 2.4. Solutions 36
Table 2.5. Primers 39
Table 2.6. Primers and PCR Details for Genotyping 43
Table 2.7. Site Directed Mutagenesis Reaction Buffer 45
Table 2.8. PCR cycle conditions 46

ABBREVIATIONS

Abbreviation	Explanation
ATP	Adenosine Triphosphate
ATF	Activating Transcription Factor
BAT	Brown Adipose Tissue
Bip/GRP78	Binding-immunoglobulin protein/Glucose Regulated Protein 78
β_3-AR	β_3-Adrenergic Receptor
DNA	Deoxyribonucleic Acid
DRP1	Dynamin-Related-Protein 1
ECL	Enhanced Chemiluminescence
EDTA	Ethylenediaminetetraacetic Acid
ETC	Electron Transport Chain
ER	Endoplasmic Reticulum
ERAD	ER Associated Degradation
eIF2α	Eukaryotic Initiation Factor 2
FACS	Fluorescence-Activated Cell Sorting
FBS	Fetal Bovine Serum
HEPES	4-(2-Hydroxyethyl)-1-Piperazineethanesulfonic Acid
IFN	Interferon
IMM	Inner Mitochondrial Membrane
IRE1	IRE1 Inositol-Requiring Enzyme-1
IP3R	Inositol 1,4,5-Triphosphate Receptors
i.p.	Intraperitonel
iWAT	Inguinal White Adipose Tissue
MAM	Mitochondria Associated Membranes
MFN	Mitofusin
MCU	MCU

NLR	Nucleotide Binding and Oligomerization Domain (NOD)- Like Receptors
NRF1	Nuclear Respiratory Factor 1
OMM	Outer Mitochondrial Membrane
OXPHOS	Oxidative Phosphorylation
OPA1	Optic Atrophy 1
PACT	PKR Activating Protein
PRKRA	Double-Stranded RNA-Dependent Protein Kinase Activator
PERK	Protein Kinase RNA-Like ER Kinase
PGC1α	Peroxisome proliferator-activated receptor-gamma coactivator 1 alpha
PKR	Protein Kinase RNA
RISC	RNA-Induced Silencing Complex
RNA	Ribonucleic Acid
RT-PCR	Reverse Transcriptase PCR
ROS	Reactive Oxygen Species
SERCA	Sarcoplasmic Reticulum Ca^{2+} ATPase pump
siRNA	Small Interfering RNA
SIRT1	Sirtuin 1
SOD	Superoxide Dismutase
TBS	Tris-Buffered Saline
TFAM	Transcription Factor A, Mitochondrial
UCP1	Uncoupling protein 1
UPR	Unfolded Protein Response
XBP1	X-Box Binding Protein 1
VDAC	Voltage dependent anion channel

1. CHAPTER 1. INTRODUCTION

1.1. The Endoplasmic Reticulum

Endoplasmic reticulum (ER) is built from intertwined branching tubules and sacs. It covers around the nucleus and extends into the cytosol of the cell. Smooth ER regions do not include ribosomes whereas the rough ER is associated with ribosomes and therefore is involved in protein synthesis. Moreover, some parts of the ER are in close contact with mitochondria through formations called mitochondria associated membranes (MAMs). These structures play important role in exchanging signal molecules in-between ER and mitochondria. ER is also in close contact with Golgi apparatus through vesicles and tubules, which also have roles in intracellular molecule trafficking (1).

1.2. Function of the Endoplasmic Reticulum

ER is the main intracellular site for protein synthesis and folding, lipid synthesis and calcium storage.

Protein Synthesis and Folding

Folding of proteins mainly occur in the ER, either secreted or transmembrane. Translation of these proteins take place in the rough ER, which are attached to ribosomes that may be later released to the cytosol. During translation of proteins on the rough ER, polypeptide chains are relocated into the ER lumen via membrane channels. Here, ER functioning is crucial to achieve successful folding of the nascent proteins. After folding, mature proteins are transferred back to the ER membrane to be sent to its destination inside the cell or on the cell membrane. If the protein is targeted to be secreted outside the cell, it is further

processed by Golgi apparatus. Post-translational modifications are also made in the ER, such as N-glycosylation or oligomerization, to allow for the protein to be shipped into its target compartment and to function properly (2).

Endoplasmic Reticulum Associated Degradation (ERAD)

After folding inside the ER lumen, misfolded proteins are eliminated by ER's quality control mechanism, called the ERAD. In a condition where such proteins are detected, these are sent back to cytosol to be degraded, where they are ubiquitinylated to be degraded by the proteasome (3).

Membrane Biogenesis

ER is also associated lipid synthesis and biogenesis. It is responsible for the synthesis of phospholipids and cholesterol to form cell or organelle membranes. It forms close contacts with mitochondria and Golgi apparatus to synthesize these lipids (4).

Calcium

One of the major sites for calcium storage and maintenance is the ER. Calcium acts as a secondary messenger inside the cells and is involved in inter-organelle communications. For example, calcium concentration differences drive muscle contractions that ultimately change the shape of ER (2). Furthermore, an increase in calcium release from the ER to the mitochondria can directly impact mitochondrial energetics, oxidative phosphorylation, mitochondrial membrane potential or ATP production. These signals are also crucial for the initiation of programmed cell death signaling (5-7).

Since ER stores calcium, it has also specific channels to achieve its transfer. Specifically, Sarcoplasmic Reticulum Ca^{2+} ATPase (SERCA) pump and, inositol 1,4,5-triphosphate receptors (IP3R) are used for the export of calcium from the cell or import of it into the cell to achieve optimal concentration for cellular processes (2). As mitochondria and ER are in close contact through membrane formations, and mitochondria also needs calcium for optimal functioning, it has also specific calcium channels on its outer membrane, called the Voltage dependent anion channel (VDAC) or mitochondrial calcium uniporter (MCU) to allow for the transportation of it through mitochondria (8).

1.3. Unfolded Protein Response

The disruption of ER's functions can activate an elaborate, adaptive stress response that is known as the Unfolded Protein Response (UPR), comprised of transcriptional and translational layers of signaling that aims to restore ER homeostasis. The UPR-induced adaptive changes include expansion of ER's membranes, production of protein-folding chaperons and attenuation of general translation to reduce ER protein folding load (1).

There are various conditions that drive UPR to be activated. Viral infections, high load of protein synthesis with low levels of ATP production or oxidative stress stemming from environmental demands, that might lead to perturbations of ER functioning. Furthermore, an increase in cholesterol or fatty acids in the cells due to obesity might again obstruct proper ER functioning. These disruptions collectively or separately can induce ER stress, that activates an elaborate signaling cascade to fight the excess protein load or stress (9). All these can be referred to as the UPR.

UPR starts in the ER and has three distinct arms to cope with and resolve stress. These arms include Inositol-Requiring Enzyme-1 (IRE1), protein kinase RNA (PKR) like ER kinase (PERK) and the activating transcriptional factor 6 (ATF6) (10) (Figure 1.1). In basal conditions, these three proteins are bound the ER chaperone named Binding-

immunoglobulin protein/Glucose Regulated Protein 78 (Bip/GRP78) inside the ER lumen. When unfolded protein response is triggered, GRP78 releases all three proteins to activate the UPR signaling (1).

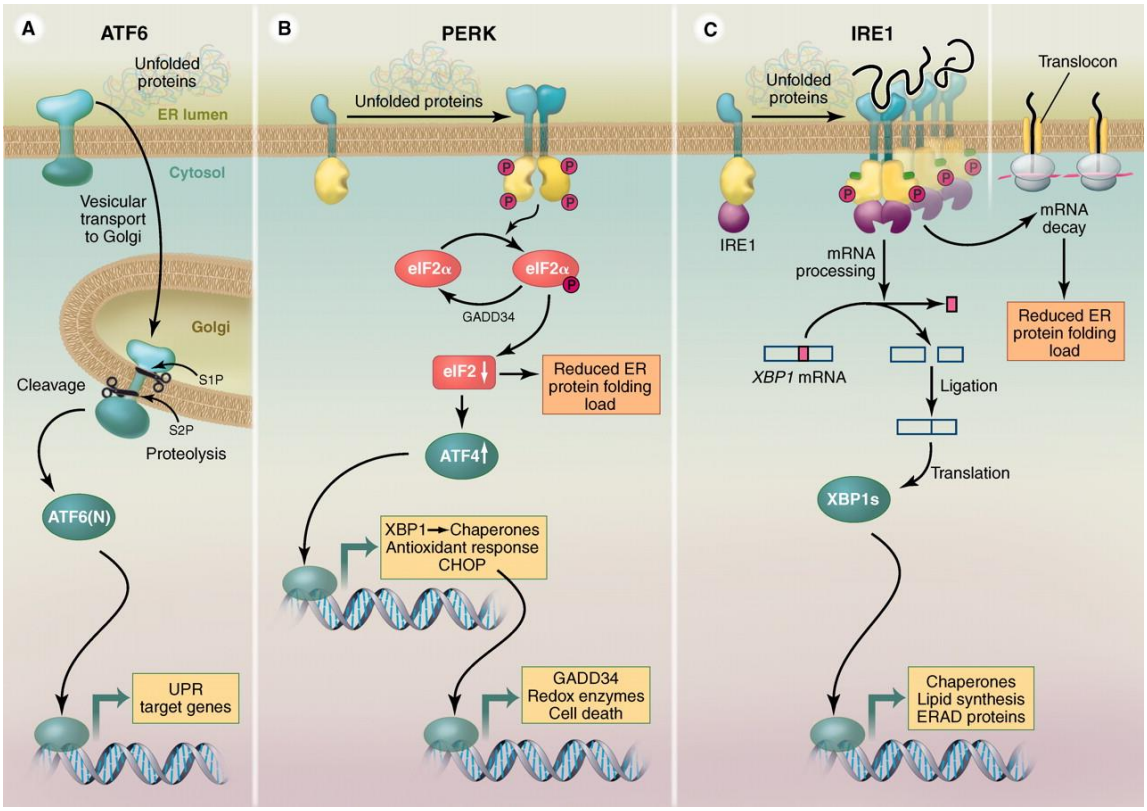

Figure 1.1 Unfolded protein response. IRE1 is the most conserved arm of unfolded protein response from yeast to mammals, targeting XBP1 mRNA. Mature sXBP1 is located into the nucleus to drive expression of mainly ER chaperones to resolve ER stress (1).

IRE1

The ER membrane-anchored, Inositol-Requiring Enzyme-1 (IRE1) regulates the evolutionarily most conserved arm of the three-partite UPR signaling. IRE1 can sense misfolded proteins via its luminal domain and signals to the nucleus through its dual kinase

and endoribonuclease (RNase) domain (1). More recently, it has been shown that IRE1 can be activated by membrane bilayer stress that occurs when increased amounts of saturated fatty acids or cholesterol are incorporated into the ER membranes. The addition of these lipids has been shown to alter ER membrane biophysical properties, prompting IRE1 oligomerization and autophosphorylation (11, 12). The current understanding of IRE1 signaling is largely limited to its RNase activity and its specific substrate, X-box binding protein 1 (XBP1) mRNA. Whether IRE1 kinase also has a specific protein substrate is not known (13-15). In the recent years, IRE1 has also been shown to degrade some ER-associated mRNA and specific micro RNAs (miRs), small non-coding RNAs of 19-23 bases with its RNase activity (16-22).

PERK

PERK is the second kinase that resides on the ER membrane and gets activated during UPR. Upon dissociation from GRP78, PERK oligomerizes and autophosphorylates and ultimately is activated (23). Activated PERK phosphorylates eukaryotic initiation factor 2α (eIF2 α), which attenuates the global protein translation. Interestingly, certain genes are exempt from this inhibition, which have alternative open reading frames. One major target gene that is expressed during PERK activation is activating transcription factor 4 (ATF4). ATF induced the transcription of genes involved in amino-acid import, autophagy, metabolism, and survival (23, 24).

ATF6

The third arm is ATF6, which is a transcription factor. It has a luminal and a cytosolic domain, that includes a bZIP DNA binding motif. A third domain of ATF6 is the transmembrane domain, which has a Golgi translocation signal. When UPR is induced, ATF6 is shipped to the Golgi apparatus via ER vesicles, where it gets cleaved and activated (25). This cleavage is done by membrane bound transcription factor site 1 and 2 (S1P, S2P).

Mature ATF6 is then transported into the nucleus where it targets genes to resolve UPR such as chaperones or proteins that are responsible for protein folding/synthesis (26).

1.4. Mitochondrial Structure and Dynamics

Mitochondria are first discovered and considered as the energy house of a cell, responsible for production of energy to maintain cellular metabolism through oxidative phosphorylation (OXPHOS) (27, 28). Currently, mitochondria are known to participate in apoptosis, immunity, calcium signaling and autophagy (28-30). Mitochondria have a double membrane structure, where the outer mitochondrial membrane (OMM) is in contact with the cytosol, and the inner mitochondrial membrane convolutes inside the mitochondrial matrix. Mitochondria also have their own circular DNA, called the mitochondrial DNA (mtDNA). mtDNA encodes for crucial proteins that are involved in OXPHOS functioning, mostly electron transport chain (ETC) complex subunits (31). Recent findings have revealed that mitochondria are highly dynamic organelles with a tubular network structure that constantly undergo fusion and fission. This balance is maintained to protect optimal functioning and respiration of the mitochondria (Figure 1.2) (32).

Fission of mitochondria refers to the division of the organelle into two and fusion is merge of two separate mitochondria to create one bigger organelle. Balance between these two events is crucial for mitochondrial function and also as a reaction to cellular events such as nutrients or metabolic state (33). A high-rate fission might implicate mitochondrial dysfunction to cope with mitochondrial damage and is usually linked to cellular stress and death (34). Moreover, fission is also important during the G2/M phase of cell division, where it serves as an increase in motility and mtDNA inheritance (35). Fusion, on the other hand, favors an increase in OXPHOS activity and is usually stimulated during nutrient starvation to protect from autophagy (36, 37).

Mitochondrial fission is achieved by Dynamin-related-protein 1 (Drp1) and Dynamin 2 (Dnm2), where Drp1 is responsible for constriction of the membranes and Dnm2 is involved in membrane cleavage (38). Fusion is done via the activity of Mitofusins 1 and 2 (MFN1, 2) and optic atrophy 1 (OPA1). MFN proteins carry out OMM fusion and OPA1 mediate IMM fusion (39).

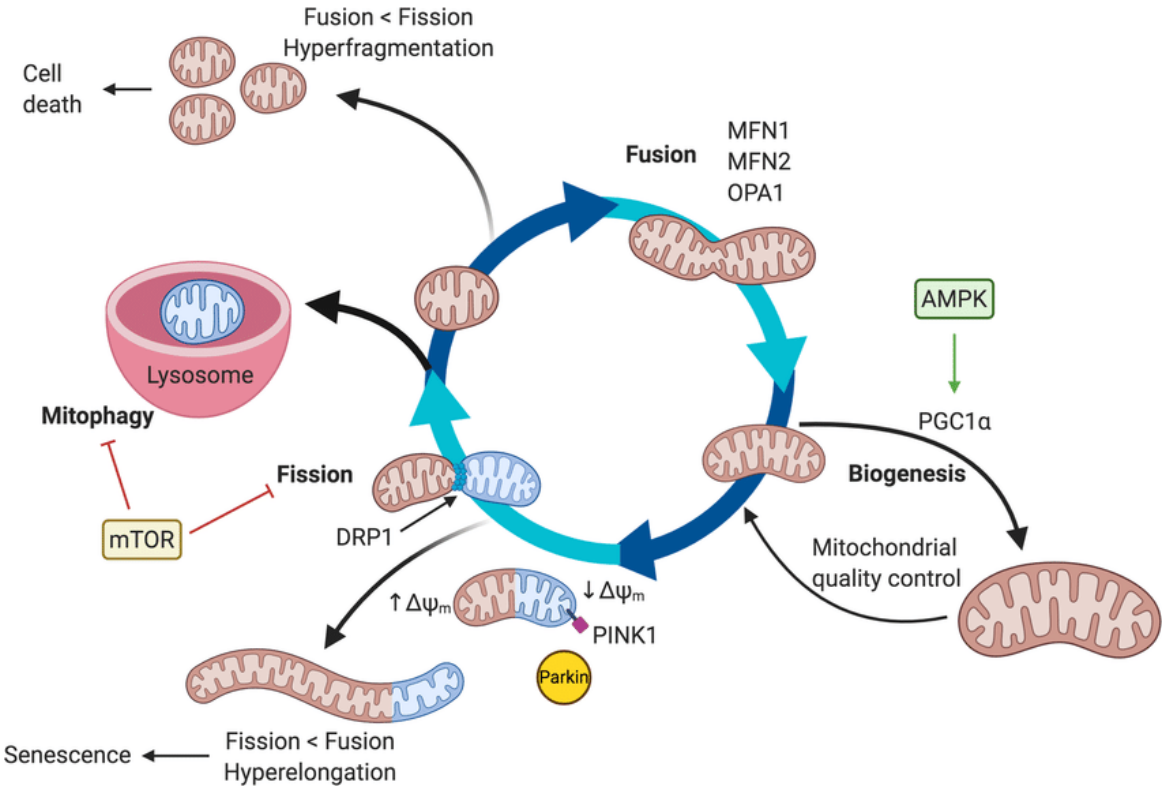

Figure 1.2 Schematics of mitochondrial dynamics and quality control. Mitochondrial dynamics are achieved by a constant quality control via fusion, fission, mitophagy and mitobiogenesis to maintain and replenish functioning mitochondria. Master regulators of these pathways are depicted here; PGC1α for mitobiogenesis, DRP1 for fission, MNFs and OPA1 for fusion, PINK1 and Parkin for mitophagy (40).

1.5. Mitochondria and ER Connection

ER and mitochondria are in close contact and exchange material for optimal functioning of both organelles, and to maintain homeostasis during various environmental stimuli. These two organelles are associated through ER-mitochondria membrane contact sites (MAMs) (Figure 1.3) (41, 42) . MAMs allow for the exchange of calcium or lipids. Various channel

proteins reside on MAMs such as VDAC or IP3Rs, mitochondrial fission and fusion proteins and ubiquitin ligases. The stability of MAMs is achieved by the mitochondrial fusion proteins (43). UPR kinases IRE1 and PERK are also shown to be on these contact sites (44, 45).

A crucial role of MAMs is the calcium transport between the two organelles. Calcium from the ER released into the cytoplasm by the IP3R receptors is taken up by the mitochondrial VDAC or MCU channels (46).

Moreover, a mitochondrial chaperone, GRP75, is also responsible for the maintenance of MAMs via stabilizing IP3Rs. Specifically, IP3Rs are predisposed to degradation by the proteasomes and Grp75 builds a connection between VDACs and IP3Rs to assure regular calcium transfer (47). On the ER, Sigma-1 Receptor (Sig1R) responsible for calcium transfer is stabilized by the ER chaperone GRP78 to allow for extended signaling (48).

When ER stress is not resolved for long periods of time, calcium release is upregulated from the ER. This higher release of calcium interferes with the mitochondrial membrane potential that results in the depolarization of the IMM. Consequently, cytochrome c of the ETC is released into the cytosol from the IMM, that in turn drives B-cell lymphoma 2 associated X (Bax)/B-cell lymphoma 2 homologous agonist killer (Bak) dependent apoptosis (49).

Mitochondrial dynamics are also highly dependent on MAMs. Fusion or fission mechanisms maintain optimal number of mitochondria for the cell's needs for survival (41, 50) . Mitochondrial fission protein DRP1, a cytosolic GTPase, is transported to the mitochondrial fission site when needed. Fission takes place at MAMs, where ER tubules connect and constrict mitochondria and position DRP1 for scission (51). Fusion GTPases MFN1,2 form dimers with one another on the OMM during fusion. Formation of dimers ensures the proper distance between ER and mitochondria, together with maintenance of ER-mitochondria contacts (43, 52). OPA1, another fusion factor of the IMM regulates mitochondrial cristae structure (53, 54).

MAMs are also implicated in the early stages of UPR activation, as it has been shown that silencing PERK in this context ER stress induced apoptosis is downregulated, as a results of less MAM formation and augmented ROS release (45, 55). Moreover, IRE1 on the MAMs govern the activity of IP3Rs to ensure necessary transfer of calcium to mitochondria (56). MAMs also play a role in ROS and inflammasome formation. Nucleotide oligomerization domain-like receptors (NLRs) are involved in detecting cytosolic changes like infection, stress or cell damage. Upon sensing these, NLRs build a multiprotein complex called the inflammasome, to resolve insults to regular cell functioning (24). NLRP3 inflammasome is localized to both ER and cytoplasm, however, it can also be translocated to the MAMs together with its adaptor ASC, in order to detect and resolve mitochondrial damage (56).

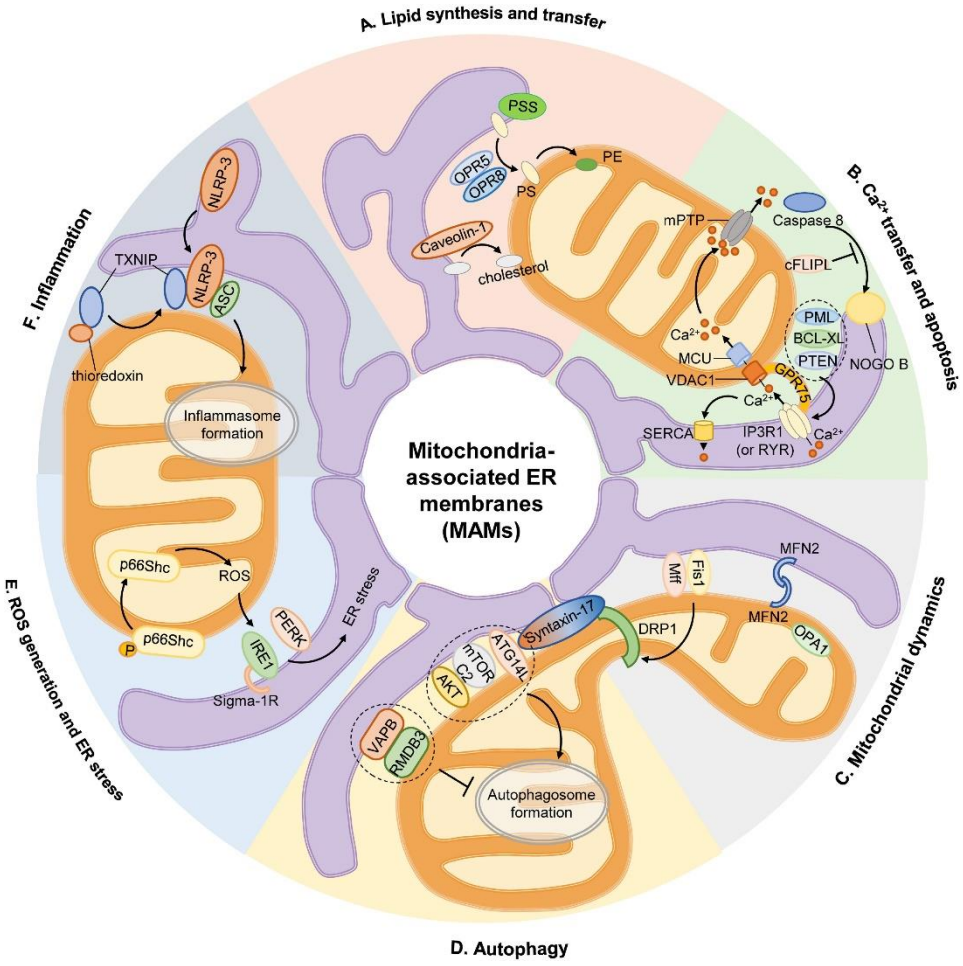

Figure 1.3 MAMs and related signaling. MAMs are hubs for communication between ER and mitochondria during inflammation, lipid synthesis, calcium trafficking, ROS generation, ER stress signaling, autophagy and mitochondrial dynamics (57).

1.6. Mitochondrial Biogenesis

New mitochondria biogenesis (mitobiogenesis) is important for maintaining healthy mitochondrial capacity that is proportional to metabolic demand. Mitobiogenesis is also needed to replenish the damaged mitochondria removed by mitochondria-specific autophagy (mitophagy) (58). Mitobiogenesis can be triggered by numerous external stimuli such as exercise, cold, or caloric restriction (59-61). Several molecular regulators of

mitobiogenesis have been characterized in mammals such as transcription factors and co-activators that are responsible for coordinating mitochondrial and nuclear gene expression. Overall, Peroxisome-proliferator-activated receptor coactivator-1 α (PGC1α) is a master regulator of the mitobiogenesis pathway. Nutritional and metabolic cues is relayed to PGC1α by the NAD+-dependent deacetylase, Sirtuin 1 (SIRT1) that deacetylates and activates PGC1α. PGC1α co-activates the transcription factor, nuclear respiratory factor 1 (NRF1), which induces the mitochondrial Transcription factor A (TFAM). TFAM is required for the transcription of mitochondrial DNA (mtDNA) replication (62-64). PGC1α also increases the transcription of numerous genes encoding mitochondrial proteins by co-activating peroxisome proliferator activated receptor gamma (PPARγ) (64). Mitobiogenesis pathway starts by the activation of PGC1α, which in turn stimulates nuclear transcription factors 1 and 2 (NRF1, 2) and estrogen-related receptor- α (ERR- α). These are followed by an upregulation of expression of TFAM (65). Next step is the translation of genes that are encoded in the mtDNA, via specific nuclear encoded transcription and elongation factors (Figure 1.4). Importantly, most of the mitochondrial proteins are encoded in the nuclear DNA and are imported into the mitochondria after being synthesized. These proteins are directed into the mitochondria via an amino-terminal cleavable targeting signal, through mitochondrial translocase TIM23. Here, imported proteins are assembled inside the mitochondrial matrix and are later sorted to their relevant location, either mitochondrial matrix, or the IMM (66, 67).

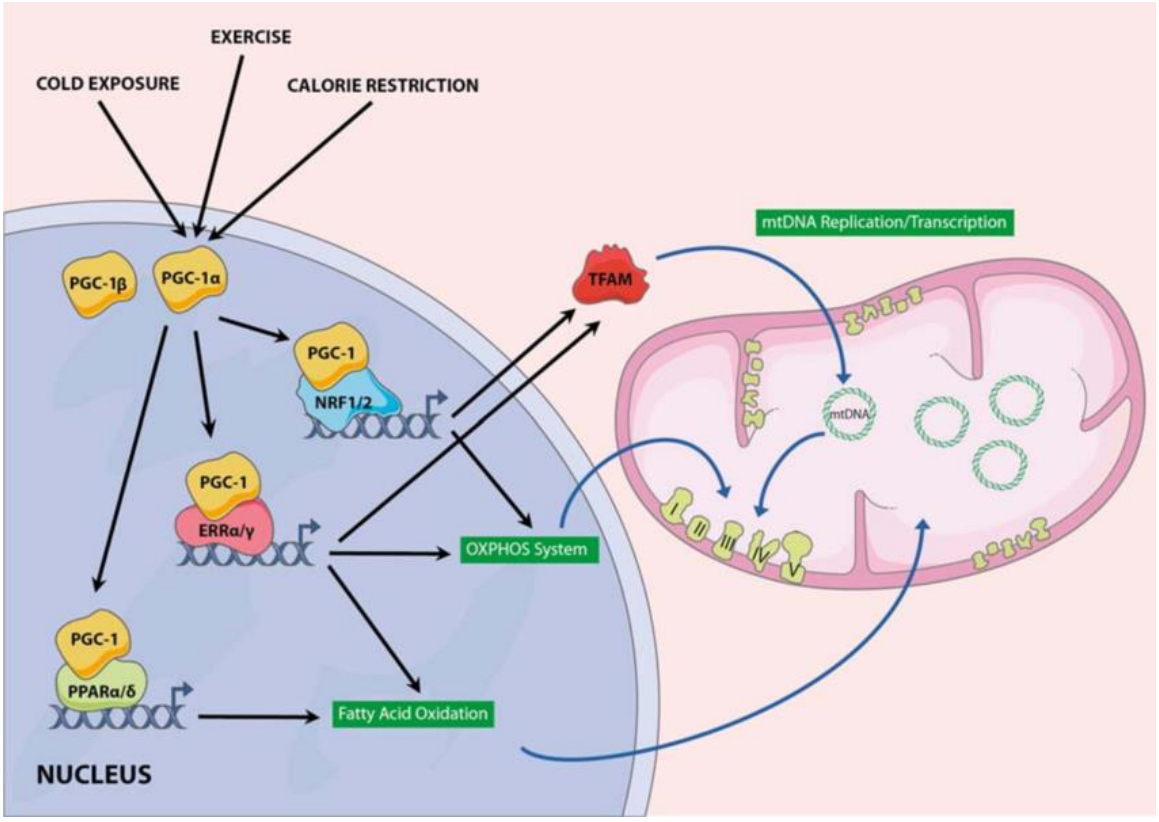

Figure 1.4 Cellular pathway of mitochondrial biogenesis signal. PGC1α is the master regulator of mitobiogenesis and is a co-activator of gene expression in the nucleus. Downstream of PGC1α is NRF1/2 and TFAM that induce mitochondrial DNA replication and protein synthesis to produce new mitochondrion (68).

1.7. ROS Formation and Defense Mechanisms

Oxygen has free outer shell electrons that are able to bond with other molecules since these outer electrons are unpaired. Bonding with one electron at a time allows for the inertness to produce reactive oxygen species (ROS) (69, 70). First electron transfer produces the superoxide anion, second yields hydrogen peroxide, followed by hydroxyl radical and lastly water molecule. Superoxide is unstable as it is quickly scavenged by mitochondrial manganese (Mn)- superoxide dismutases (SODs). However, hydrogen peroxide is less reactive and therefore can diffuse through organelle membranes such as mitochondria, peroxisomes or ER (71). Overall, ROS scavenging systems aim to eliminate various ROS

molecules, most importantly hydrogen peroxide, before these accumulate in different parts of the cell (Figure 1.5).

Mitochondria and ROS

Main sites of ROS formation in the mitochondria are ETC complexes I and III. Complex I is the acceptor of electrons of NADH through its cofactor flavin mononucleotide. These electrons are then passed to coenzyme Q (CoQ). In basal conditions, active respiration and high ATP synthesis is couples with a low proton gradient. In this case, there is less hydrogen peroxide formation and efflux through the membranes (72). In conditions where there is high NADH but low ATP production (stress induced ETC interruption), there is accumulation of superoxide from Complex I. Also, if reduced CoQ is highly abundant with a high proton gradient, electrons flow back to Complex I from reduced CoQ. This gradient enables formation of superoxide anions (73). To eliminate ROS produced mainly by Complex I and III, superoxide is first converted into hydrogen peroxide by the mitochondrial Mn-SOD. Besides, there is another type of SOD, which is referred to as the copper-zinc (Cu-Zn)-SOD that resides in the intermembrane space. These two types of SODs can be found in both mitochondria and peroxisomes (69, 74). As a next step, hydrogen peroxide is further reduced by various enzymes, such as catalase, glutathione peroxidase (GPx) and Peroxidase (Prdx). Catalase mostly resides in the peroxisomes and a little in mitochondria (75). GPx and Prdx also function in the mitochondria (73, 76). GPx is responsible for reduction of hydrogen peroxide and oxidation of glutathione. Glutathione is then reduced further by glutathione reductase. These forms are more soluble in water and more likely to be effluxed out of the cell (77). Moreover, Prdx enzymes also scavenge hydrogen peroxide, with Prdx3 and 5 residing in the mitochondria (78).

Peroxisomes and ROS

Peroxisomes are mainly responsible for the α-oxidation or β-oxidation of fatty acids, purine metabolism or amino acid metabolism (74, 79). Enzymes involved in these processes are called flavoproteins that usually require the transfer of electrons to oxygen. These reactions again yield superoxide anions or hydrogen peroxide, which needs to be turned into less

damaging forms such as water and oxygen, via the activity of catalase. In contrast to mitochondria, where the transfer of electrons are coupled to ATP production by Complex V, in peroxisomes, energy that is yielded during electron transfer produces heat (80). Moreover, if the produced hydrogen peroxide is not eliminated by catalase, it will diffuse into the cytosol and various other parts of the cell to be eliminated by cytosolic SODs (81).

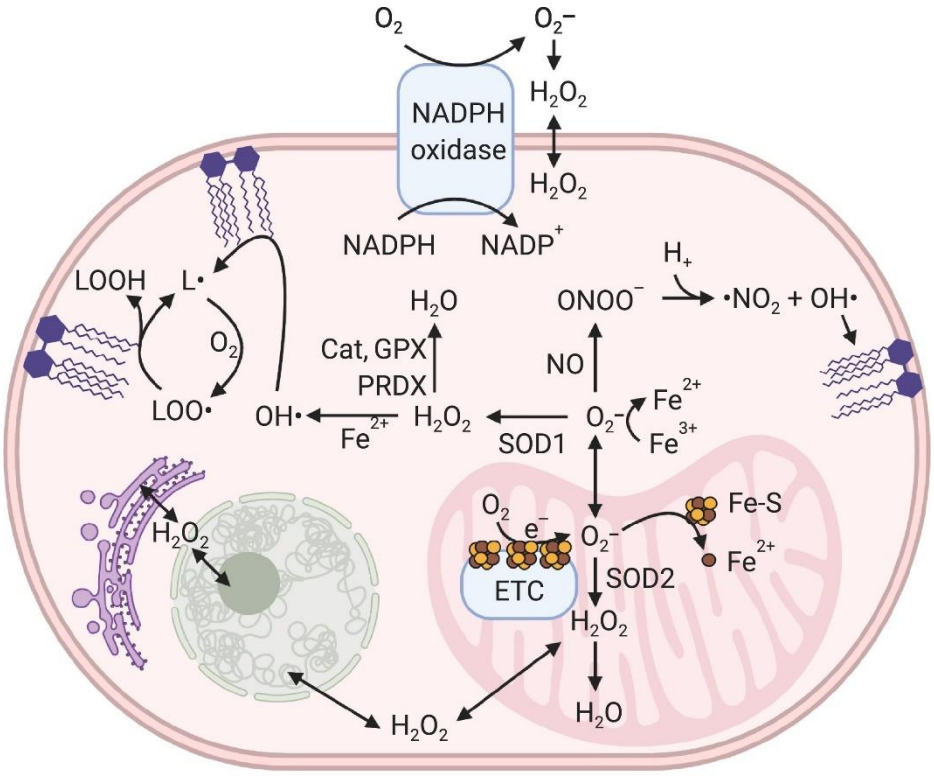

Figure 1.5 ROS metabolism and antioxidant enzymes. Cellular scavenging pathways to eliminate mitochondrial and peroxisomal ROS (82).

1.8. MicroRNAs and RNA-induced Silencing Complex

miRNAs are regulators of gene expression and are first discovered as long non-coding RNAs of 20-22 nucleotides in C. elegans (83). miRNAs are transcribed by RNA Polymerase II and this initial product is referred to as primary miRNAs (pri-miRNAs). Pri-miRNAs are further cleaved inside the nucleus to precursor miRNAs (pre-miRNAs) by Drosha and DGCR8 to have a hairpin structure. Pre-miRNAs are then transported into the cytoplasm through a Ran-GTP dependent channel, Exportin 5. In the cytoplasm, hairpin structured pre-miRNAs are further cleaved by Dicer, yielding a double-stranded miRNA duplex. This duplex is processed to a single-stranded form and is loaded into the RNA-induced silencing complex (RISC), that includes Argonuate proteins. From a single pre-miRNA, two different mature forms can be made; -5p or -3p, named after the 5' or 3' arms of the precursor. RISC detects and blocks target gene expressions via coupling the miRNA to the target mRNA's 3' untranslated region (UTR). Seed sequence of the mature miRNA, a sequence of 7 or 8 nucleotides, complementary to that of the target mRNA is enough to obtain target suppression. This suppression can be done by inhibition of translation or degradation of target mRNA (84-87).

RISC is a ribonucleoprotein complex that functions in gene silencing and nucleates on ER membranes (88). RISC uses single-stranded miRs as a template to recognize complementary mRNA sequences that will be targeted for silencing via transcriptional or translational mechanisms (89, 90). While ER stress can induce significant changes in miR profiles, how ER stress or IRE1 impact RISC function or RISC-mediated changes in gene expression is not well-understood (91).

The RISC consists of several RNA-binding proteins (RNAbp) including Ribonuclease III (Dicer), Argonaute RISC Catalytic Component 2 (Ago2), transactivation response element RNA-binding protein (TRBP) and double-stranded RNA-dependent protein kinase (PKR) activator (PRKRA) or PKR activating protein (PACT) (Figure 1.6) (89, 90). Notably, what happens to PACT-regulated miRNAs during cellular stress conditions that is unclear (92).

PACT has been suggested to alter the maturation of miRs and miR loading to the RISC (93-99). Both TRBP and PACT have been proposed to determine the proper length of a subset of miRNAs (such as miR181c) and which strand in a miRNA duplex (such as pre-miR-674) is loaded onto the RISC (100).

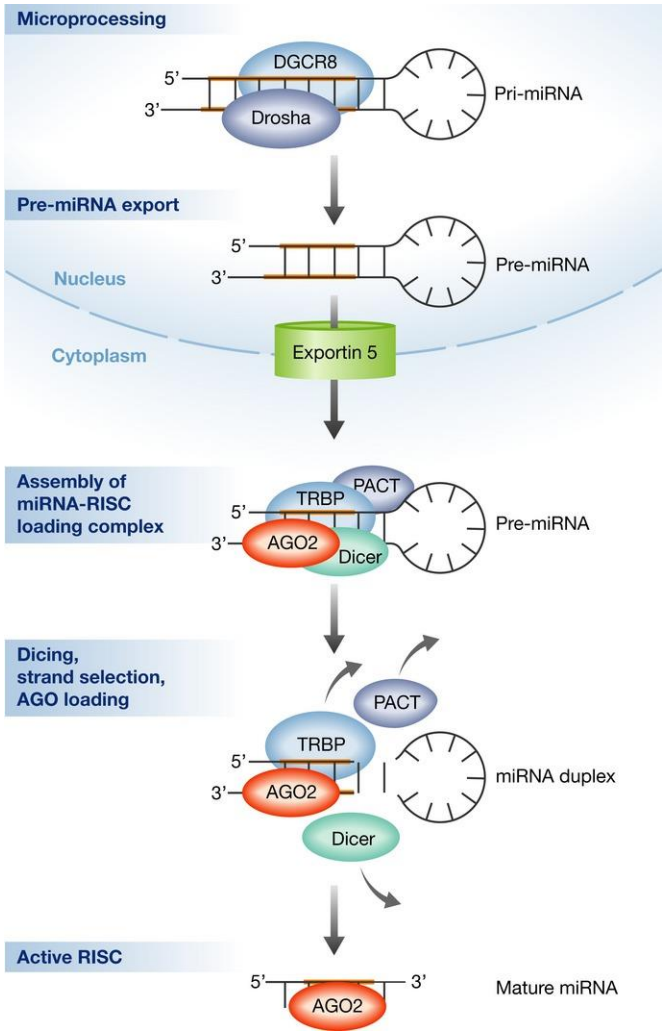

Figure 1.6 Canonical RISC functioning and subunits. Schematic depicting the processing of pri-miRNA exported out of nucleus to be further processed by Dicer and Ago2 complexes to reveal its mature form. Mature miRNA later blocks its target mRNA attached to Ago2 complex in the cytoplasm (101).

1.9. PACT and Its Functions

Double-stranded RNAs (dsRNAs) are very crucial in fine-tuning cellular functions. Importantly, dsRNAs are the central players of miRNA, endogenous short-interfering RNA (siRNA) and piwi-interacting RNA (piRNA) biogenesis (102). Besides, dsRNAs also intermediates for the replication of RNA viruses. Therefore, it is vital for cells to determine self and non-self dsRNAs. Such differentiations are made via proteins that are specialized to identify modifications on foreign dsRNAs such as 5' triphosphate groups. Such proteins that are responsible for detection of foreign dsRNAs are Toll-like receptors (TLRs) 3,4, and 8, as well as Retinoic acid-inducible gene I (RIG-I), Melanoma differentiation associated protein 5 (MDA5) and PKR (103). Notably, PACT is discovered to be an activator of PKR during viral infection and ER stress, and later on shown to interact and activate RIG-I and MDA5 as well (104, 105). It has been shown that PACT is constitutively phosphorylated on Serine 246 and ER stress leads to PACT phosphorylation on Serines 18 and 287 by an unknown kinase (106-108). The phosphorylated PACT associates with Protein kinase R (PKR), resulting in PKR activation and PKR-mediated phosphorylation of eukaryotic initiation factor-2α (eIF2α). This, in turn, results in general translational attenuation (107, 109, 110). However, to date, the identity of the kinase that phosphorylates PACT during ER stress remains unknown (Figure 1.7).

Domains of PACT

PACT has three double-stranded RNA binding domains (dsRBDs). These domains are connected via linker regions (111, 112). Having more than one dsRBDs is evolutionarily advantageous since it increases binding affinity and specificity (113). Between these three domains, the first two bind to dsRNAs and are named A type dsRBDs, since dsRNA has an A form helix with a deeper but narrower major groove compared to dsDNA (114). The third domain is a type B dsRBD, and it does not interact with dsRNAs. This domain is required for protein-protein interactions. PACT interacts with Dicer and PKR through its

third domain (97, 112, 115-117) . It is also known that PACT forms heterodimers with TRBP or homodimers with itself through the functioning of its third domain (109, 118).

Small RNA Biogenesis and PACT

PACT is directly and heavily involved in the RNA interference (RNAi) pathway as mentioned above (Figure 1.5). RNAi serves to silencing of mRNAs transcriptionally or translationally, through the use of short RNAs. Previous studies have shown that PACT interacts with Dicer and Ago2 (93, 99, 115, 116, 119). It mainly partakes in pre-miRNA processing and loading of targets to the RISC (93, 115). PACT is specifically involved in optimizing RISC functioning, along with its interaction partner TRBP. PACT is thought to be involved four aspects of RNAi activity; (i) loading of pre-miRNAs to RISC for Dicer cleavage by its dsRNA affinity, (ii) aiding optimal cleavage of the substrate dsRNA by Dicer by providing the proper orientation, (iii) unloading of the cleaved product from the Dicer complex into Argonuate proteins and (iv) at the last step, determining the type of dsRNA loaded into the Argonuate proteins. Therefore, depleting PACT from either Dicer or Ago2 complexes is shown to decrease the maturation of certain miRNAs, as substrate loading/unloading and affinity is disrupted (92, 96, 97).

PACT and Innate Immunity

As mentioned above, PACT can physically interact with several proteins that are involved in innate immunity. It has been shown that PACT interacts and activates RIG-I during certain viral infections (104, 120, 121). RIG-I and Dicer has been shown to have similar helicase domains that are from the same subfamily, however PACT's interaction to these two might be different, as there are no sequence homologies in the helicase insert domains (122). The most well studied example of PACT mediated RIG-I activation is in the context of Sendai virus infection, where PACT activity induces interferon regulatory factor 3 (IRF3) and interferon-β expression. Similarly, during Ebola infection, it has been shown that PACT overexpression downregulates viral replication (120).

Similarly, PACT also interacts and activated PKR. PKR is a kinase that inhibits general translation through phosphorylating eIF2α when active. This can occur during viral infections or ER stress conditions. During these conditions, PACT interacts and changes the conformation of PKR, to allow its autophosphorylation. Phosphorylated PKR is active and can further phosphorylate its substrates to initiate downstream signaling cascades that lead to apoptosis when prolonged (107).

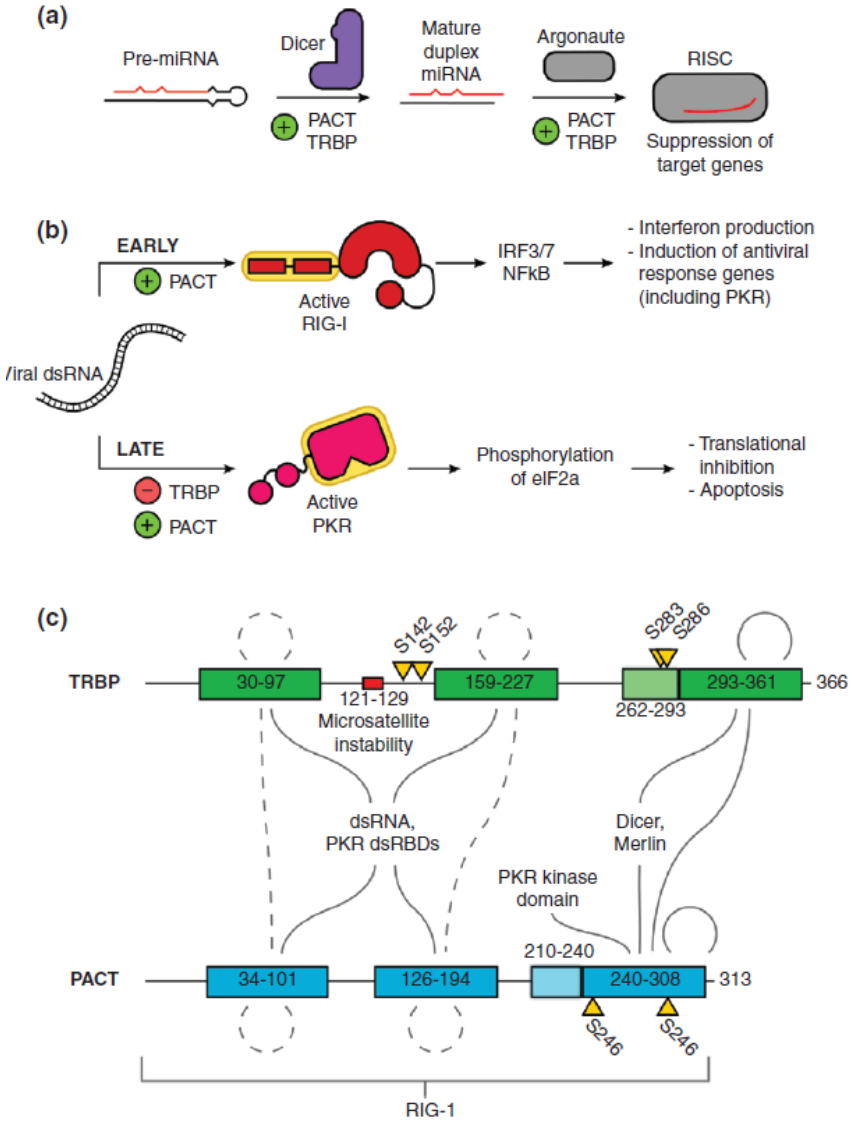

Figure 1.7 Domains and functions of PACT. PACT has two major roles in the cell, (a) optimizing maturation of miRNAs by regulating Dicer and Ago2 functioning, and (b) interacting and activating innate immune proteins like RIG-I and PKR. (c) PACT has three dsRBDs to interact with dsRNA and its protein partners like TRBP (92).

1.10. miR-181c And Its Implication in Regulation of Mitochondrial Dynamics

miR-181c has been studied extensively in cardiomyocytes and previously shown to be imported into the mitochondria even though its encoded in the nucleus and directly targets 3'-UTR of mitochondrial Complex IV Subunit I (MTCO1) as well as mitochondrial ROS production (123). In the same paper, it has been shown that miR-181c suppression of MTCO1 expression results in an increase in the other two subunits of Complex IV, mt-COX2 and 3. Therefore, miR-181c impacts mitochondrial ROS production via Complex IV remodeling stemming from an imbalance between the subunits of this ETC complex (124). Since Complex IV is heavily responsible for electron transport during oxidative phosphorylation to produce ATP in the mitochondria (125), miR-181c targeting of MTCO1 directly impacts ROS production. Later on, a more mechanistic approach to decipher miR-181c's function in the mitochondria, another study showed that overexpression of miR-181c causes an insult on Complex IV functioning and ROS production through increasing the levels of calcium in the mitochondrial matrix. This increase in turn activates ETC Complex III and leads to an increase in mitochondrial membrane polarization. Higher membrane polarization and inhibition of MTCO1 together induces ROS production (Figure 1.8) (124). Overexpression of the miR also causes heart failure and myocardial injury stemming from ischemia-reperfusion as it is involved in regulation of oxidative stress (124). This is mainly because heart tissue requires energy from oxidative phosphorylation through electron transport (126). MTCO1 is the major electron acceptor in Complex IV that resides in the IMM. Decrease of MTCO1 and Complex IV remodeling therefore will obstruct optimal functioning of OXPHOS and will yield less energy than needed for the heart tissue.

Furthermore, other miR181 family members are implicated in mitochondrial disease models. miR181a/b cluster has shown to target mitochondrial biogenesis through regulating SIRT1, PGC1α, NRF1 and multiple Complex IV subunits. It has been also shown that miR181a/b increases both mitobiogenesis and mitophagy when downregulated. Same study shows that in various disease models involving retina and optic neurons, inhibition of miR181a/b protects from cell death and alleviates disease progression (127).

In another study focusing on the effects of insecticides on Parkinson's disease (PD) progression, miR181 is implicated to be involved in disease progression through regulating similar pathways. In a PD cell line, this study shows that cell viability decreases together with an increase ROS levels, apoptosis and inflammation. This phenotype was coupled to an increase in miR181 levels. Supporting these, overexpression of miR181 promoted disease progression, through inhibition of SIRT1/ PGC1α/NRF2 pathway (128). Therefore, elevation of miR181 is also related to downregulation of mitobiogenesis in a wide spectrum of contexts where mitochondrial functioning is crucial to produce energy.

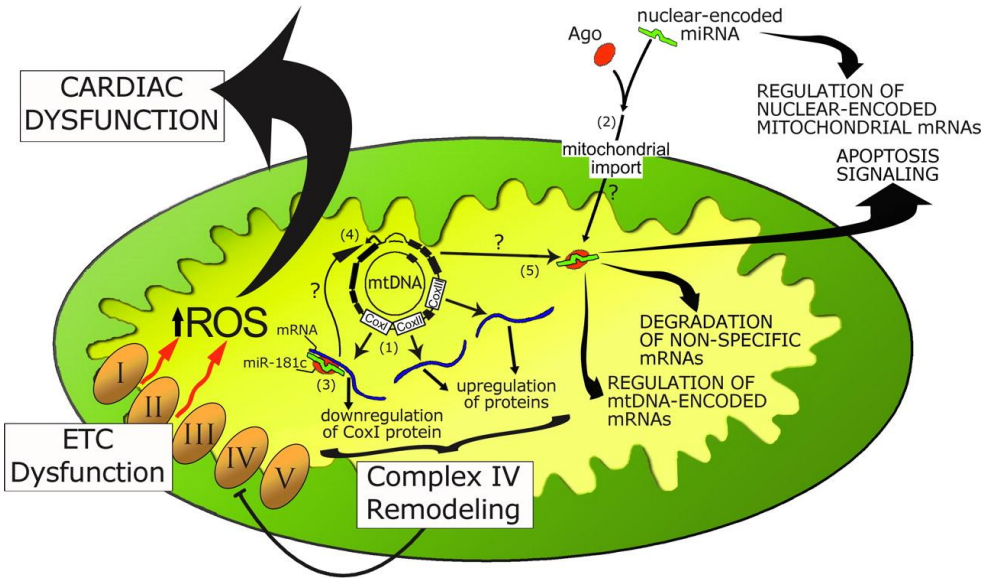

Figure 1.8 miR-181c signaling in the mitochondrial matrix. Nuclear encoded miR-181c is imported into the mitochondria, where it targets and inhibits MTCO1 to result in Complex IV remodeling to result in ETC dysfunction and ROS production (129).

1.11. Brown Adipose Tissue Activation and Mitobiogenesis

In mammals, white adipose tissue (WAT) stores fat and brown adipose tissue (BAT) is mainly responsible for production of heat to the body during cold stimuli. In this context, white adipocytes are able to store triglycerides as one large single lipid droplet whereas brown adipocytes accommodate smaller and numerous lipid droplets around them (130). Brown adipocytes have a significant number of mitochondria with uncoupling protein 1 (UCP1) expression. UCP1 uncouples OXPHOS from ATP production as it can shuttle protons at the IMM (130). The generated energy is released as heat during cold exposure as UCP1 expression is upregulated. Another type of adipose tissue, called inguinal white adipose tissue (iWAT) consists of beige adipocytes, that are capable of expressing UCP1 and upregulate mitobiogenesis during cold exposure. Brown and beige adipocytes function quite similar to one another, and they are responsible for thermogenesis during cold (131). BAT is activated via the sympathetic nervous system and can achieve non-shivering thermogenesis. During external stimuli, norepinephrine binds to the β_3 adrenergic receptor (β_3-AR) on brown adipocytes to induce cyclic adenosine monophosphate (cAMP) and downstream signaling. Upon activation of this pathway, non-esterified fatty acids are released from lipid droplets and directly activate UCP1 activity. This results in an increase in mitochondrial fatty acid oxidation and production of heat (Figure 1.9) (130). This signaling cascade is also crucial in WAT, β_3-AR activation results in free fatty acids to be used as fuels during fasting. Free fatty acids from WAT can actually activate sympathetic nervous system and thus BAT activity, where a feed-forward loop is formed between WAT and BAT (132).

As mentioned above, cold exposure or pharmacological stimulation of β_3-AR in BAT induces the cyclic adenosine monophosphate (cAMP) pathway, which in turn activates PGC1α and downstream UCP1 production. This activation leads to a pronounced upregulation of mitobiogenesis that is coupled to thermogenesis in BAT and iWAT (133).

Strikingly, PACT protein expression is nearly two-fold reduced in mouse brown adipose tissue (BAT), upon cold-induced activation of mitochondrial biogenesis (mitobiogenesis) (134-137). While other RNA binding proteins (RNAbps) have been reported to impact adipocyte metabolism, activation and differentiation, PACT's role in BAT has not been investigated before (138-141). Both white and brown adipose tissue is a major source of exosomal miRNAs in mice and humans (142). Partial Dicer-deficiency in BAT has been shown to disrupt cold-induced thermogenesis (143). Several miRs have been identified to play a role in either activation or inhibition of BAT and subsequent thermogenesis (144-149). These studies collectively demonstrate the importance of miRNAs in BAT's physiological function and suggest that the observed reduction in PACT expression during BAT activation could be relevant to miR-regulated gene expression changes that are needed for BAT activation (134-137).

PACT and several other RNAbps were recently shown to be present in the IRE1 interactome (150). In this study, we show that IRE1 kinase can phosphorylate PACT. IRE1-mediated phosphorylation of PACT results in the inhibition of mitobiogenesis, in part, by controlling miR-181c levels. miR-181c targets key regulators of the mitobiogenesis program such as NRF1, SIRT1 and TFAM. These findings demonstrate that even partial loss-of-function of PACT in mice can significantly enhance β_3-AR agonist-induced BAT activation and subsequent mitobiogenesis induction. These findings further show that PACT-deficiency in mice results in increased energy expenditure in mice. Strikingly, PACT expression is also reduced in human hearts, where mitobiogenesis induction is coupled to cardiac ischemia-reperfusion injury. Collectively, the data demonstrates that PACT and PACT-regulated miR-181c are profound inhibitors of mitochondrial biogenesis in mice and humans.

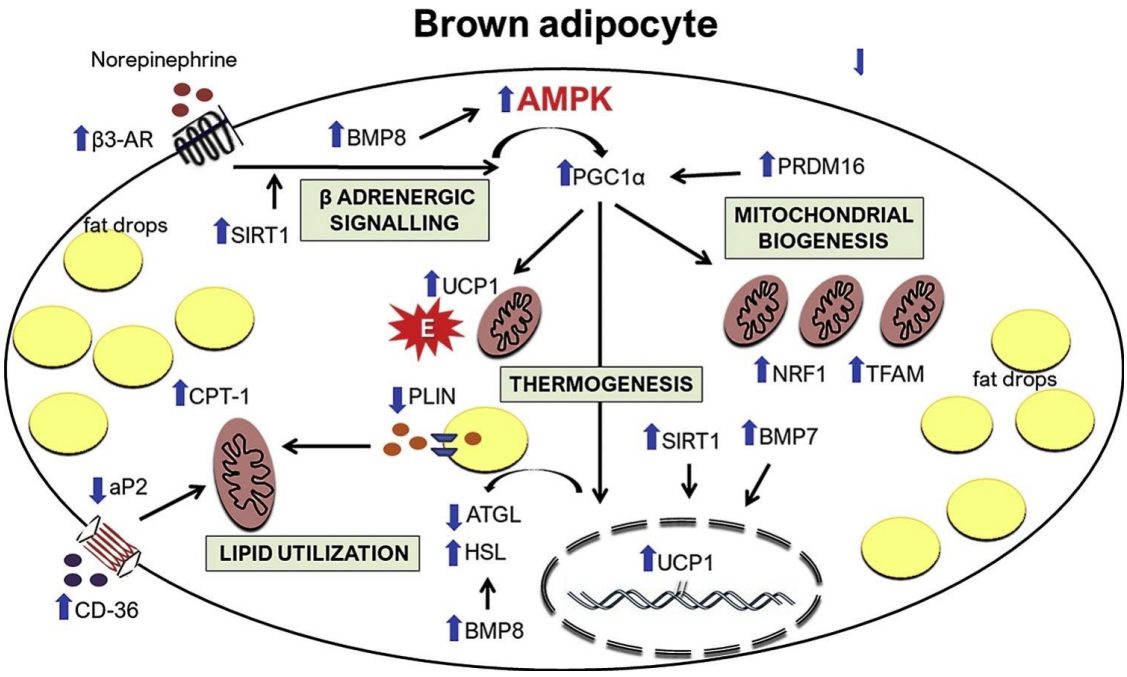

Figure 1.9 Brown adipocyte activation. External stimulus such as cold exposure results in the release and binding of norepinephrine to β_3-AR that results in activation of AMPK and downstream PGC1α. Activated PGC1α in turn upregulates the expression of mitobiogenesis markers and most importantly UCP1 to induce heat production for thermogenesis (151).

1.12. Mitochondrial Dynamics in Cardiac Ischemia/Reperfusion (I/R) Injury

Heart is the supply of oxygen for the tissues through the continuous perfusion of fresh blood. During cases of arterial diseases, blood flow is restricted to the heart, leading to cardiomyocyte death and ultimately blocking pumping of blood to organs (152-154). To overcome this restriction of blood flow, the most common solution is bypass surgeries to replenish perfusion (155). However, *in vivo* experiments now show that during the first few minutes of reperfusion after surgery, cardiomyocytes show augmented cell death, as well as dynamic changes in their mitochondria (156, 157). Molecular mechanisms underlying this phenotype are shown to be an increase in ROS production and release, calcium imbalance, lack of ATP production and most importantly mitochondrial dysfunction (158, 159). It is very important to decipher the mitochondrial mechanisms underlying I/R, since

heart tissue highly relies on mitochondria for energy supply (160). During I/R injury, mitochondria activate a quality control mechanism to cope with the stress to the heart tissue. This adaptive response ensures maintenance of mitochondrial turnover, fusion, fission and mitophagy (Figure 1.10) (157, 161). Specifically, damaged mitochondria are cleared by mitophagy, and new mitochondria are made via mitobiogenesis to endure the required energy demands (162, 163).

During I/R injury, fission is upregulated as mitochondrial damage is induced. Phosphorylation of DRP1 at serine 637 is downregulated, which drives localization of DRP1 to mitochondria to promote fission (164). Induced fission after I/R drives cytosolic calcium overload and further aids cardiomyocyte apoptosis. Levels of mitochondrial fission factor (MFF) are also enhanced after injury, and it has been shown that deletion of MFF in this context block mtDNA damage and augments mitochondrial respiration (165, 166).

In the context of fusion, previous studies have shown that when induced, it can counteract augmented fission to block fission-initiated apoptosis (167). Besides, since fusion favors the long and tubular mitochondrial network formation, membrane potential is shared to allow for a more efficient respiration as well as the recognition of damages parts easier (168). An *in vitro* model of I/R injury has shown that deletion of MFN2 augments apoptosis through a mechanism dependent on caspase-9 and Bcl-2 (169). Furthermore, double deletion of mitochondrial fusion factor MFN1 and 2 resulted in an increase in UPR and damaged mitochondria accumulation (170, 171). Supporting these findings, the other fusion factor OPA1 levels decrease upon I/R injury and its overexpression blocks fission and cardiomyocyte apoptosis (167).

Importantly, clearance of damaged mitochondria is achieved by mitophagy, that is the particular mechanism of mitochondrial autophagy. This mechanism drives the elimination of anomalous mitochondria to prevent cellular dysfunction or death (172). BCL2/adenovirus E1B 19 kDa protein-interacting protein 3 (BNIP3), FUN14 domain

containing 1 (FUNDC1) and NIX are localized to the OMM. These receptors are responsible for the initiation of mitophagy. Furthermore, PARKIN is another master mediator of mitophagy signaling, where it is normally localized to the cytoplasm and is translocated to the mitochondria when the membrane potential is not maintained. Mitochondria that are destined to be cleared by mitophagy are engulfed by the autophagosome through microtubule-associated protein 1A/1B-light chain 3 (LC3) activation and eventually degraded by autophagosomal proteins (173, 174). During I/R, PARKIN dependent mitophagy has shown to augment mitochondrial permeability transition pore (mPTP) and this prompts the diffusion of membrane potential. Consequently, reperfused hearts show increased necroptosis (175). Increased mitophagy also results in a shortage of ATP production and this drives apoptosis (176).

As a fourth mechanism, during I/R injury has been shown to increase mitochondrial biogenesis (157) that drives the decrease in myocardial infarct size (177-179). Here, increased mitobiogenesis is coupled with a higher respiration capacity and ATP production (178). Notably, nitric oxide synthase (NOS) activity is upregulated in this context and its inhibition prevented the cardioprotective impact of mitobiogenesis (177, 178). This mechanism is in fact related to a short-term attempt to cell survival and is called the preconditioning after hypoxia or I/R. It has been shown that, via mimicking pre-conditioning by diazoxide treatment, cAMP response element binding protein (CREB) is upregulated, which is a key player in PGC1α driven mitobiogenesis (180). In line with these findings, I/R injury has also been linked to a decrease in superoxide dismutase activity that copes with ROS in the mitochondria, causing unusual levels of ROS (181, 182). Inducing anti-oxidant enzymes of mitochondria like superoxide dismutase 2 (SOD2) or glutathione peroxidase-1 significantly prevents I/R mediated ROS production and cellular dysfunction (183, 184). Therefore, mitobiogenesis not only aids in making new and functional mitochondria after I/R injury, but also increases cell's resilience to damage via detoxification of ROS.

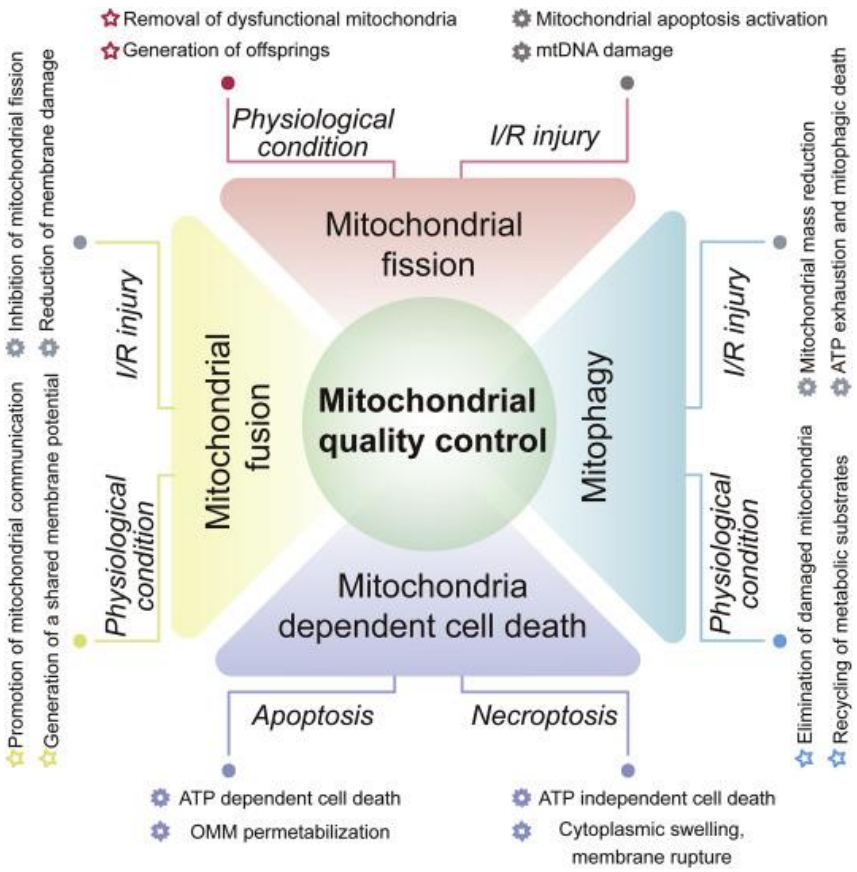

Figure 1.10 Overview of mitochondrial quality control during I/R injury. Fission, fusion, mitophagy and mitochondria-controlled cell death are upregulated to maintain homeostasis in the heart tissue (185).

1.13. Hypothesis and Study Aims

ER resident dual functioning kinase and endoribonuclease IRE1's RNase function and downstream signaling has been extensively studied in the literature (186, 187). However, it's kinase activity and substrates are not well known. From an IRE1 interactome data previously published (188), I screened possible IRE1 kinase targets for their interaction with IRE1 *in vitro*. From this, I have found one possible target, PACT, that is known to be phosphorylated during early stages of ER stress (106), and the kinase responsible for its phosphorylation was not known. Therefore, I first hypothesized that PACT is a kinase substrate of IRE1 and through immunoprecipitation of endogenous PACT and IRE1, I showed that IRE1 interacts with PACT. Furthermore, genetic deletion or small molecule inhibition of kinase activity of IRE significantly downregulated ER stress induced protein levels of PACT, showing that IRE1 is a regulator of PACT. In the next step, *in vitro* kinase assays revealed that PACT is a kinase substrate of IRE1.

In order to decipher the biological consequence of PACT phosphorylation by IRE1, I next turned my attention to inter-organelle signaling. Since ER and mitochondria are in close physical contact (42), I first sought to determine PACT's impact on mitochondrial energetics and biogenesis. By using plasmid overexpression or silencer (si)-RNA mediated knock-down, I was able to show that PACT is a suppressor of mitobiogenesis and oxidative phosphorylation. To understand the exact mechanism by which PACT exerts its effects on mitochondria, I next looked at mitochondrial miRs, since PACT is known to regulate miR biogenesis and maturation (92). I found that PACT regulates the mature levels of miR-181c, which is known to localize to mitochondria target and inhibit MTCO1, as well as augment ROS production (123, 124). Silencing or overexpression of PACT regulated pre- and mature miR-181c levels. Notably, phosphorylation mutant of PACT was not able to regulate mitobiogenesis or miR-181c maturation, suggesting that IRE1 phosphorylation on PACT is crucial for its impact on mitochondrial dynamics. It was also crucial to investigate IRE1's miR targets, since it's known to regulate miR maturation through its RNase domain (19, 189). The rationale for this was to confirm whether miR-181c is also an IRE1 target or

not. miR-181c was not a target for IRE1, however I found multiple important miRs that are significantly regulated by IRE1. One such miR was miR-2137, that significantly increased during ER-stress and reduced upon IRE1 deletion or inhibition of its RNase domain *in vivo* and *in vitro*, suggesting that IRE1 controls the maturation of numerous miRs directly through its RNase activity or through the activity of its kinase targets such as PACT.

To base the hypothesis of IRE1-PACT-miR-181c signaling on an *in vivo* model, I next switched to brown adipose mitobiogenesis, since brown adipose tissue is known to have a high density of mitochondria and can further upregulate mitochondrial mass when activated upon external stimuli (130). To test whether PACT in important for brown adipose tissue mitobiogenesis, I exploited primary adipocyte culture *in vitro* and brown adipose activation under pharmacological stimulation *in vivo* and looked and mitobiogenesis markers. Once again I observed that partial knock-out of PACT in a mouse model augments mitobiogenesis of brown adipose tissue and UCP1 production, which is a hallmark of brown adipose activation (60). Furthermore, metabolic parameters of mice that are PACT haplo-insufficient are significantly higher than the wild-type controls, as seen from energy expenditure, CO_2 production and oxygen consumption. Overall, this study shows that PACT is a mediator of inter-organelle communication and is a suppressor of mitobiogenesis. Activated IRE1 upon lipid or ER stress interacts and phosphorylates PACT, which in turn increases miR181c maturation and subsequently suppresses mitobiogenesis through PGC1α-TFAM-NRF1 pathway (Figure 1.11).

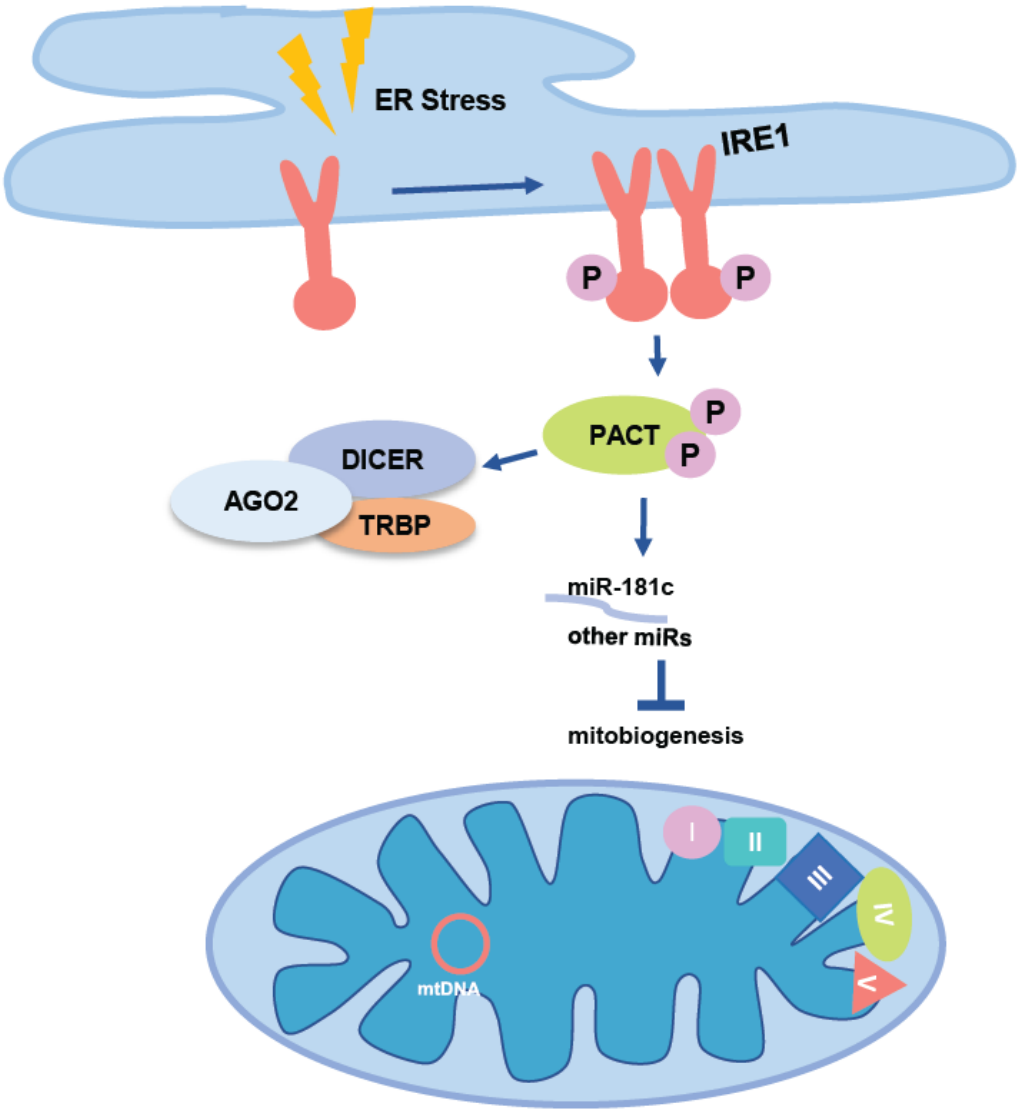

Figure 1.11 Graphical Abstract. Schematics of IRE1-PACT-miR181c signaling.

2. CHAPTER 2. MATERIALS AND METHODS

2.1. Materials

2.1.1. Reagents

General laboratory use chemicals and reagents are summarized in Table 2.1.

Table 2.1. Reagents and Chemicals

Reagent	Company and Catalog Number
Amersham Prime ECL Western Blotting Detection Reagent	GE Healthcare, RPN2236
β-mercaptoethanol	Sigma, M3148-100ML
Acrylamide %40 solution	Biorad, 1610146
Glycine	Santa Cruz, sc-29096C
Bovine Serum Albumin	Goldbio, A-420-1
Fluoroshield Mounting Medium with DAPI	Abcam, Ab104139
DC Protein Assay Reagent	Biorad, 5000116
Page Ruler Prestained Protein Ladder	Thermo Fisher Scientific, 26620
Protease Inhibitor Cocktail EDTA Free	Sigma, P8340-5ML
Phosphatase Inhibitor Cocktail 3	Sigma, P0044
PVDF Transfer Membrane	Pierce-Thermo Scientific, 88518
Nitrocellulose Transfer Membrane	VWR, 27376-991
Chloroform	Sigma, 24216

Reagent	Company and Catalog Number
Absolute Ethanol	Sigma, 32221
Methanol	Sigma, 32213
Triton-X	Sigma, 9036-19-5
Trisure	Bioline Bio, 38033
Tris Base	Sigma, T1503
EDTA	Sigma, E9884
Ammonium Persulfate (APS)	Sigma, A3678
OCT Compound-Tissue Tek	Electron Microscopy Sciences, 62550
Dimethyl Sulfoxide (DMSO)	Sigma, D8418
CL-316,243	Sigma, C5976
4μ8c	Calbiochem, 412512
AMG-18	R&D Systems, 6166/5
KIRA-6	Cayman Chemical, 19151
Palmitic Acid (PA)	Sigma, P0500-25G
Hematoxylin and Eosin Stain Kit	Vector Laboratories, H-3502
Fatty Acid-Free Bovine Serum Albumin	Sigma, A7030-100G
Lambda phosphatase	Santu Cruz, sc-200312
Tunicamycin	Santa Cruz, sc-3506
Thapsigargin	Santa Cruz, sc-24017A
Polyethylinimine (PEI)	Polysciences, 23966

Reagent	Company and Catalog Number
MitoSOX™ Red Mitochondrial Superoxide Indicator	Invitrogen, M36008
MitoTracker® Green FM – Special Packaging	Invitrogen, M7514
PowerUP Sybr Green	Applied Biosystems, A25742
Revert Aid First Strand Cdna Synthesis Kit	Thermo Scientific, K1691
Cremophor EL	EMD Millipore, 238470
ATP-γ-S	Abcam, ab138910
p-Nitrobenzyl mesylate, PNBM	Abcam, ab138910
ERN1 human recombinant protein	SignalChem, E31-11G
Recombinant PACT protein	Novus Biologicals, NBP2-51787
Thioglycolate Solution	Sigma, 70157
Sucrose	Sigma, S0389
Kapa Mastermix	Fisher Scientific, NC0597884

2.1.2. Cell Culture Reagents

Reagents and media used for cell culture experiments are summarized in Table 2.2.

Table 2.2. Cell Culture Reagents

Reagent	Company and Catalog Number
L-Glutamine	Thermo Scientific, 25030081
Dulbecco's modified Eagle's Medium (DMEM)	Thermo Scientific, 11995073
Phosphate Buffer Saline (PBS)	Thermo Scientific, 14-190-250
Fetal Bovine Serum (FBS)	R&D Systems, S12895
Penicillin/Streptomycin (P/S)	Thermo Scientific, 10378016
Roswell Park Memorial Institute (RPMI)-1640	Thermo Scientific, 11-875-093
mirVana miR negative control mimic	Thermo Scientific, 4464059
mirVana-miR-181c-5p mimic	Thermo Scientific, 4464067, Assay ID: MC10181
mmu-PRKRA silencer	Thermo Scientific, AM-16708
Neon Electroporation System	Thermo Scientific, MPK10096
Trypsin	Thermo Scientific, 25-200-056
miScript inhibitor negative control	Qiagen, 1027272

Reagent	Company and Catalog Number
anti-hsa-miR-181c inhibitor	Qiagen, MIN0000674, Product no: 219300
PACT siRNA	Qiagen, SI00054761
All-star negative control scrambled siRNA	Qiagen, 1027281

2.1.3. Antibodies

Antibodies used in this study and their working conditions are summarized in Table 2.3

Table 2.3. Antibodies and Working Conditions

Antibody	Company	Catalog Number	Working Condition
pIRE1 (phsopho-S724)	Abcam	ab124945	o/n 4°C
IRE1	Cell Signaling	3294	o/n 4°C
Thiophosphate Ester Antibody	Abcam	ab133473	o/n 4°C
β-Actin-Horse Radish Peroxidase	Santa Cruz	47778	1 hr RT
PACT	Abcam	ab31967	o/n 4°C
PACT	Proteintech	10771-1-AP	o/n 4°C
OXPHOS Rodent Antibody Cocktail	Abcam	ab110413	o/n 4°C
PGC1α	Abcam	ab54481	o/n 4°C
Normal Rabbit IgG	Cell Signaling	2729S	1 hr RT
TFAM	Proteintech	22586-1-AP	o/n 4°C
TOM70	Proteintech	14528-1-AP	o/n 4°C
GRP75	Antibodies Inc.	75-127	o/n 4°C

NRF1	Santa Cruz	sc-33771	o/n 4°C
UCP1	Santa Cruz	sc-6528	o/n 4°C
Secondary-IgG-Mouse	SeraCare	5220-0341	1 hr RT
Secondary-IgG-Rabbit	SeraCare	5220-0337	1 hr RT

2.1.4. Solutions

Solutions used in this study are summarized in Table 2.4.

Table 2.4. Solutions

Buffer	**Composition**
10X SDS Running Buffer	30g Tris Base, 144g Glycine, 10gr SDS, 1L dH_2O
10X Transfer Buffer	30g Tris Base, 144g Glycine, 1L dH_2O
Blocking solution (5% (w/v) milk or BSA)	2.5 g Bovine Serum Albumin or milk is dissolved in 50 ml 1X TBS-T.
10X TBS	80 g NaCl 24.2 g Trizma Base adjust pH 7.6 with 1N HCl add dH_2O to 1 L
1X-TBS-T	450 ml ddH_2O, 50 ml TBS, 500 µl Tween-20
10X PBS	80 g NaCl, 2 g KCl and 15.2 g sodium phosphate dibasic dehydrate to 1L dH_2O, pH to 7.4
HBS Buffer for Electroporation (Instead of R Buffer)	21 mM commercial HEPES (pH; 7.05), 137 mM NaCl,5 mM KCl, 0.7 mM Na_2HPO_4, 6 mM Glucose. Filter and keep at 4°C.
15 % Resolving Gel	2.5 ml 1.5 M Tris-HCl, pH: 8.8 3.54 ml dH_2O 3.75 ml 40% Acrylamide mix 100 µl 10% SDS

Buffer	Composition
	100 µl 10% Ammonium persulfate 10 µl TEMED
10% Resolving Gel	2.5 ml 1.5 M Tris-HCl, pH: 8.8 4.8 ml dH_2O 2.5 ml 40% Acrylamide mix 100 µl 10% SDS 100 µl 10% Ammonium persulfate 10 µl TEMED
12 % Resolving Gel	2.5 ml 1.5 M Tris-HCl, pH: 8.8 4.29 ml dH_2O 3 ml 40% Acrylamide mix 100 µl 10% SDS 100 µl 10% Ammonium persulfate 10 µl TEMED
9 % Resolving Gel	2.5 ml 1.5 M Tris-HCl, pH: 8.8 5.3 ml dH_2O 2 ml 40% Acrylamide mix 100 µl 10% SDS 100 µl 10% Ammonium persulfate 10 µl TEMED
8 % Resolving Gel	2 ml 1.5 M Tris-HCl, pH: 8.8 4.2 ml dH_2O 1.6 ml 40% Acrylamide mix 80 µl 10% SDS 80 µl 10% Ammonium persulfate 8 µl TEMED
5 % Stacking Gel	2.5 ml 1.5 M Tris-HCl, pH: 8.8 6.29 ml dH_2O 1 ml 40% Acrylamide mix 100 µl 10% SDS 100 µl 10% Ammonium persulfate 10 µl TEMED

Buffer	Composition
0.5 M Tris-HCl (pH: 6.8)	30.3 g Tris Base 800 ml ddH_2O adjust pH to 6.8 with 1 N HCl add dH_2O to 500 ml
1.5 M Tris-HCl (pH: 8.8)	90.8 g Tris Base 800 ml ddH_2O adjust pH to 8.8 with 1 N HCl add dH_2O to 500 ml
HBSS	8 g NaCl 400 mg KCl 140 mg $CaCl_2$ 100 mg $MgSO_4$-7H_2O 100 mg $MgCl_2$-6H_2O 60 mg Na_2HPO_4-2H_2O 60 mg KH_2PO_4 1g Glucose 350 mg $NaHCO_3$
6X Laemmli SDS Loading Buffer (50 ml)	6 g SDS 23,5 ml glycerol 0.01% bromophenol blue 6 ml 0.5 M Tris HCl, pH: 6,8 10,5 ml dH2O 10% 2-mercaptoethanol
Phospholysis Buffer	50 mM HEPES (pH: 7.9), 100 mM NaCl, 4 mM Tetra Sodium pyrophosphate ($Na_4P_2O_7$), 10 mM EDTA, 10 mM NaF, 1% Triton, *Add Phosphatase Inhibitor Cocktail 3 and Protease Inhibitor Cocktail (10µM/ ml) before use.*
Alkaline Lysis Buffer	25 mM NaOH 0.2 mM $Na_2EDTA.2H_2O$ pH 12 (do not adjust)
Neutralization Buffer	40 mM Tris-HCL (242.28 g) pH 12 (do not adjust)

Buffer	Composition
TAE buffer (50X)	242 g tris base in double-distilled H_2O 57.1 ml glacial acetic acid 100 ml 0.5 M EDTA solution (pH 8.0) Adjust volume to 1 L

2.1.5. Primers

Primers are listed in Table 2.5.

Table 2.5. Primers

Hsa/Mmu_PACT_F:	5'-CAGCGGGACCTTCAGTTTG-3'
Hsa/Mmu_PACT_R:	5'-GCACATCGGATCTTTCACATTCA-3'
Mmu_Pgc1α_F:	5'-TATGGAGTGACATAGAGTGTGCT-3'
Mmu_Pgc1α_R:	5'-CCACTTCAATCCACCCAGAAAG-3'
Mmu_Tfam_F:	5'- ATTCCGAAGTGTTTTTCCAGCA-3'
Mmu_Tfam_R:	5'- TCTGAAAGTTTTGCATCTGGGT-3'
Mmu_Ucp1_F:	5'-CACCTTCCCGCTGGACACT -3'
Mmu_Ucp1_R:	5'-CCCTAGGACACCTTTATACCTAATGG-3'
Mmu_Gapdh_F:	5'-ATTCAACGGCACAGTCAAGG-3'
Mmu_Gapdh_R:	5'-TGGATGCAGGGATGATGTTC -3'
Hsa_GAPDH_F:	5'- GGAGCGAGATCCCTCCAAAAT-3'
Hsa_GAPDH_R:	5'- GGCTGTTGTCATACTTCTCATGG -3'
Hsa_mt Min Arc_F:	5'-CTAAATAGCCCACACGTTCCC-3'

Hsa mt Min Arc_R:	5’-AGAGCTCCCGTGAGTGGTTA-3’
Hsa_mt Maj Arc_F:	5’-CTGTTCCCCAACCTTTTCCT-3’
Hsa_mt Maj Arc_R:	5’-CCATGATTGTGAGGGGTAGG-3’
Hsa_B2M_F:	5’-TGGGTAGCTCTAAACAATGTATTCA-3’
Hsa_B2M_R:	5’CATGTACTAACAAATGTCTAAAATGGT-3’
Mmu_Cox1_F:	5’-TCGCCATCATATTCGTAGGAG-3’
Mmu_Cox1_R:	5’-GTAGCGTCGTGGTATTCCTGA-3’
Mmu_Nd4_F:	5’-TTATTACCCGATGAGGGAACC-3’
Mmu_Nd4_R:	5’-GAGGGCAATTAGCAGTGGAAT-3’
Mmu_ApoB_F:	5’-CGTGGGCTCCAGCATTCTA-3’
Mmu_ApoB_R:	5’-TCACCAGTCATTTCTGCCTTTG-3’

2.1.6. Plasmids and Cell Lines

Prkra$^{-/-}$ and Prkra$^{+/+}$ (wild type; WT) mouse embryonic fibroblasts (MEFs) and pCMV-PACT-3X Flag plasmid were a kind gift from Dr. Ganes Sen (Cleveland Clinic, Department of Inflammation and Immunity, Cleveland) (190). Human embryonic kidney (HEK293T) cells were from American Type Culture Collection (ATCC) (CRL-3216).

2.1.7. Transgenic mice

Prkra$^{-/-}$ mice sperm was obtained from Jackson Laboratory, deposited from Dr. Ganes Sen’s laboratory. Prkra$^{+/-}$ mice or wild type littermates were used in isolation of brown adipose tissue for primary brown adipocyte cell culture and for injection of CL316,243.

2.2. Methods

2.2.1. Study Design

In vitro experiments were done in triplicates with at least three independent repeats on separate times. Quantitative real time polymerase chain reaction (qRT-PCR) analysis was performed in triplicate/quadruplicates and replicated at least in three independent experiments.

For in vivo experiments, the only elimination criteria were health related (such as more than 20% weight loss, fighting and injury) and in compliance with the approved IACUC protocol.

2.2.2. Cell Culture and Transfections

MEFs and HEK293T cells were grown in DMEM supplemented with 10% FBS and 1% L-glutamine in a humidified, 5% carbon dioxide incubator at 37ºC.

Isolation of Peritoneal Macrophages: C57BL/6 mice were injected with %4 Thioglycollate (Sigma, 70157) and peritoneal macrophages were collected 5 days after injection as described earlier (191).

Primary BAT and iWAT culture and differentiation: The stromal vascular fraction from BAT and iWAT of 6-8 weeks old mice were obtained by collagenase digestion, as previously described (192). Briefly, the digested tissue centrifuged at 700g for 10 minutes. The pellet was resuspended in Culture Medium (10% FBS, 1% Pen-Strep DMEM) and filtered through a 70-μm cell strainer (BD BioSciences; 352350). Cells were centrifuged again at 700g for 10 min and plated in the same medium. After reaching confluence (day 0) cells were placed in the differentiation induction medium (DMEM with 10% FBS, 1% Pen-Strep, 5 μg/ml insulin (Sigma-Aldrich; I-0516),1 nM triiodo-L-thyronine (T3; Sigma-Aldrich; T-2877), 2 μg/ml dexamethasone (Sigma-Aldrich; D-1756), 0.125 μM indomethacin (Sigma-Aldrich; I-7378), 0.5 mM IBMX (Sigma-Aldrich; I-5879), and 1 μM

rosiglitazone (Sigma-Aldrich ;R-2408)). On day 2, cells were placed in the maintenance medium (DMEM with 10% FBS, 5 µg/ml insulin, and 1 nM T3) and were used on days 6-7 upon complete maturation.

Plasmid Transfection: Plasmids were transfected with PEI into 80% confluent cells.

Silencer RNA (siRNA), miRNA (mimic or inhibitor) electroporations: HEK293T or MEF cells were electroporated with PACT siRNA (100 nM) or all-star negative control scrambled siRNA (100 nM), mirVana-miR-181c-5p mimic (100 nM), scrambled miR (100 nM), miR-181c-5p antagomiRs (100 nM) and scrambled antagomiR (100 nM) using the Neon electroporator (Thermo Scientific) and manufacturer-provided electroporation conditions for different cell types, as described earlier (186). 24 or 48 hours after electroporation, cells were treated with 500 µM PA.

λ phosphatase treatment: Cell lysates were incubated with λ phosphatase (New England BioLabs; P0753S) at 30°C for 30 min. After incubation, SDS loading buffer was added, and the samples were boiled at 95°C for 5 minutes to analyze proteins.

2.2.3. Inhibitor Treatments

When indicated, 10 µM of KIRA-6, 5 µM of AMG-18 or 100 µM of 4µ8c were used to inhibit IRE1 kinase or RNase activity, respectively.

2.2.4. Palmitate (PA)-BSA Complex Preparation and Treatment

PA was dissolved in absolute ethanol to get a stock concentration of 500 mM and stored at −80°C. Stock PA was dissolved in %1 fatty acid-free bovine serum albumin (BSA) and RPMI medium, and heated at 55°C for 15 minutes to achieve a suspension (final working concentration was 500 µM) (193).

2.2.5. Animals

All procedures were approved by the Institutional Animal Care and Use Committee (IACUC) of Cedars-Sinai Medical Center. Mice were housed at 22°C with a 12 hr light/12 hr dark cycle and fed with regular Chow diet. Sperm of Prkra$^{-/-}$ mice was purchased from Jackson Laboratories and mice were redrived at the Cedars-Sinai Medical Center Animal Models Core Facility. Age matched C57BL/6J littermates were used as controls.

2.2.6. Toe Numbering and Genotyping for Prkra$^{-/-}$ mice

Pups were numbered by cutting toes at day 8 of age. Toes were incubated in 95ºC with Alkaline Lysis Buffer for 1 hour and neutralized with equal volumes of Neutralization Buffer to extract DNA. PCR was performed with cycling conditions and primers stated below.

Table 2.6. Primers and PCR Details for Genotyping

Cycling conditions	4 min 95 ºC 30sec 95 ºC 30sec 60 ºC 30cycles 40sec 72 ºC 4 min 72 ºC	
Primers	PRKRA 5' PRKRA 3' PRKRA neo	tct ctt cag att ccg tca act ttc aca ttc atc aca agc ctc aacac gcc gaa tat cat ggt gga aaa
PCR mix	1 µL of each primer+5 µL of Kapa Mastermix+2 µL of DNA	

2.2.7. RNA Isolation and qRT-PCR

Total cellular RNA was isolated by TRIsure Reagent and reverse transcribed by using RevertAid First strand cDNA synthesis kit to complementary deoxyribonucleic acid

(cDNA), according to manufacturer's protocol. cDNAs were amplified using specific primers and the Power-Up-SYBR green. miScript II RT kit (Qiagen; 2128160) was used for miR conversion to cDNA. miScript primer assay for mature miR-181c-5p (MS00032382), premiR-181c (MP00004424) and RNU6-2 (MS00033740) were from Qiagen. miR expression analysis was performed using miScript Quantitec SYBR green kit (Qiagen; 204143). Gene expression was quantified using the relative threshold ΔΔCt method: ΔΔCt=(primer efficiency)^(−ΔΔCt), where ΔΔCt means ΔCt (target gene) −ΔCt (reference gene), as previously described (194).

2.2.8. Protein Lysates, SDS/PAGE Electrophoresis, Transfer and Western Blotting

Cell were lysed in Phospho-Lysis Buffer (PLB) (50 mM 4-(2-hydroxyethyl)-1-piperazineethanesulfonic acid (HEPES) pH:7, 100 mM NaCl, 10 mM Ethylenediaminetetraacetic acid (EDTA),10 mM sodium fluoride (NaF), 4 mM Tetra sodium pyrophosphate (NaPP), 1% TritonX-100, 1x phosphatase inhibitor mixture, 1x protease inhibitor mixture). Lysates were cleared with brief centrifugation for 10 minutes at 8000 g, normalized and boiled at 95°C after addition of 5x sodium dodecyl sulfate (SDS) loading dye. Proteins were then loaded to SDS/PAGE gels and transferred to PVDF membranes. Blocking and primary/secondary antibody incubation were carried out in 5% (w/v) dry milk or BSA (in tris-buffered saline buffer with 0.1% Tween-20 (v/v)). Membranes were developed in ECL prime reagent (Amersham; RPN2236) and images were captured with ChemiDoc Imager (BioRad). Blots shown are representative of three or more experiments.

2.2.9. Immuno-precipitation

Protein G Magnetic Beads (Bio-Rad; 1614023) were blocked with 2% BSA-PBS for 1 hour at 4°C and coated with specific antibodies for IRE1, PACT or rabbit immunoglobulin-G

(IgG) (control antibody) while rotating overnight. The antibody-coated beads were washed with PLB three times before incubating with protein lysates from HEK293T cells overnight. The antibody-conjugated beads were then washed three times to remove unbound protein and boiled with SDS Buffer at 95°C for 5 minutes prior to loading onto SDS/PAGE gels.

2.2.10. IRE1 Kinase Assay

250 ng of recombinant active IRE1 and PACT proteins were incubated in IRE1 kinase buffer (SignalChem; K01-09) at 30°C for 45 minutes with 100 µM ATP-γ-S. Samples were then incubated at 24°C for 1 hour with p-Nitrobenzyl mesylate to alkylate the kinase substrate, as described (195). Finally, samples were boiled in SDS loading buffer at 95°C prior to loading onto SDS/PAGE gel.

2.2.11. Site Directed Mutagenesis

3X-Flag tagged WT PACT plasmid was used as template for site directed mutagenesis PCR and Phusion High-Fidelity DNA Polymerase (M0530S) was used to introduce mutations to the target sites. Reaction buffer composition is summarized in Table 2.7 and PCR conditions are described in Table 2.8.

Table 2.7. Site Directed Mutagenesis Reaction Buffer

Reagent	For 50 µl	Final Concentration
Nuclease-free water	to 50 µl	
5X Phusion HF or GC Buffer	10 µl	1X
10 mM dNTPs	1 µl	200 µM
10 µM Forward Primer	2.5 µl	0.5 µM
10 µM Reverse Primer	2.5 µl	0.5 µM

Template DNA	variable	< 250 ng
DMSO (optional)	(1.5 µl)	3%
Phusion DNA Polymerase	0.5 µl	1.0 units/50 µl PCR

Table 2.8. PCR cycle conditions

Step	**Temperature**	**Time**
Initial Denaturation	98°C	30 seconds
25-35 Cycles	98°C 45-72°C 72°C	5-10 seconds 10-30 seconds 15-30 seconds per kb
Final Extension	72°C	5-10 minutes
Hold	4-10°C	

2.2.12. Phospho-Proteomics Analysis

Proteins were immunoprecipitated after an *in vitro* kinase reaction using 6 µg of recombinant hPRKRA (Novus Biologicals; H00008575-P01) and hERN1 (Signalchem; E31-11G) proteins via the methanol-chloroform precipitation methods, as described (196). Pellets were dried and dissolved in 8 M urea/100 mM triethylammonium bicarbonate (TEAB) (Thermo Scientific; 90114), pH 8.5. Proteins were reduced with 5 mM tris (2-carboxyethyl) phosphine hydrochloride (Thermo Scientific; T2556) and alkylated with 10 mM chloroacetamide (Sigma Aldrich; 22790). Proteins were digested at 37°C in 0.8 M urea/100 mM TEAB, pH 8.5, sequentially with 500 ng Trypsin (Promega; V5111) for 17 hours, followed by 500 ng Endoproteinase GluC (NEB; P8100S) for 4.5 hours. Digestion was quenched with formic acid (5% final concentration). The digest was injected directly onto a 20 cm, 100 µm ID column packed with BEH 1.7 µm C18 resin (Waters; 186005225). Samples were separated at a flow rate of 400 nl/minutes on an nLC 1000 (Thermo; LC120). Buffer A and B were 0.1% formic acid in 5% acetonitrile and 0.1% formic acid in 80% acetonitrile, respectively. A gradient of 1–25% B over 110 minutes, an increase to 40% B over next 20 min, an increase to 90% B over another 10 minutes and a hold at 90% B for

the final 10 minutes was used for a total run time of 140 minutes. The column was re-equilibrated with 20 µl of buffer A prior to the injection of sample. Peptides were eluted directly from the tip of the column and nano-sprayed into the mass spectrometer by application of 2.8 kV voltage at back of the column. The Orbitrap Fusion Lumos (Thermo) was operated in data dependent mode. Full MS1 scans were collected in the Orbitrap at 120K resolution with a mass range of 400 to 1500 m/z and an AGC target of 4e5. The cycle time was set to 3 s, and within these 3 s, the most abundant ions per scan were selected for CID MS/MS in the ion trap with an AGC target of 2e4 and minimum intensity of 5000. Maximum fill times were set to 50 ms and 35 ms for MS and MS/MS scans, respectively. Quadrupole isolation at 1.6 m/z was used, monoisotopic precursor selection was enabled, charge states of 2–7 were selected and dynamic exclusion was used with an exclusion duration of 5 s. Samples were also analyzed with HCD fragmentation (35 NCE) and detection at 7500 resolution.

Protein and peptide identification were done with Integrated Proteomics Pipeline – IP2 (Integrated Proteomics Applications). Tandem mass spectra were extracted from raw files using RawConverter (197) and searched with ProLuCID (198) against a concatenated database comprising of amino acid sequences from vendors for hPRKRA, hERN1 and Endoproteinase GluC, sf9 cell proteome compiled from RNAseq data (https://bioshare.bioinformatics. Ucdavis .edu/bioshare/view/sf9prot/#) and UniProt reference proteome of Escherichia coli K12 (UP000000625). The search space included all fully-tryptic and half-tryptic peptide candidates. Carbamidomethylation (+57.02146) was considered a static modification on cysteine, and phosphorylation (+79.966331) was considered a differential modification on serine/threonine/tyrosine. Data was searched with 50 ppm precursor ion tolerance and 500 ppm fragment ion tolerance. Identified proteins were filtered to using DTASelect (199) and utilizing a target-decoy database search strategy to control the false discovery rate at 1%, at the spectrum level (200). A minimum of 1 peptide per protein and 1 tryptic end per peptide were required and precursor delta mass cut-off was fixed at 10 ppm. Localization scores were assigned to identified sites of phosphorylation using A-Score (201).

2.2.13. SeaHorse Mito Stress Test

MEFs were cultured in X^{Fe} 96-well cell culture microplates (Agilent; 103730-100) at a density of 1×10^4 cells per well in 200 µL of appropriate growth medium and incubated for 24 hours at 37°C under 5% CO_2 atmosphere. One day before starting the assay, XF sensor cartridges were hydrated by adding 180 µL of X^{Fe} Calibrant buffer to each well in the XF utility plate, the XF sensor cartridges were placed on top of the utility plate and incubated at 37°C incubator without CO_2 overnight. Media in the cell culture plate was removed on the day of the assay and each well was washed once with Seahorse X^{Fe} Assay Medium (1% L-glutamine, 1% sodium pyruvate, 1.8 mg/ml D-glucose, pH: 7.4, in Sea Horse XF DMEM Medium (Agilent; 103575-100)). 180 µL fresh SeaHorse assay medium was added onto each well and the plate was incubated at 37°C incubator without CO_2, while the three inhibitors are loaded to the cartridge and the X^{Fe} 96-well plate. The inhibitors used in Mito Stress Test Kit (Agilent; 103015-100) to measure OCR were ATP synthase inhibitor oligomycin (1 µM), mitochondrial uncoupler Carbonyl cyanide-4 (trifluoromethoxy) phenylhydrazone (FCCP, 1 µM) and a mixture of Complex I inhibitor Rotenone and Complex III inhibitor Antimycin A (1 µM). These three compounds were injected consecutively and OCR values with different parameters of respiration were measured with Mito Stress Test Kit.

2.2.14. SeaHorse Mitochondrial Fuel Flex Test

Capacity and dependency for fatty acid oxidation, glutamine, and pyruvate were measured with SeaHorse Fuel Flex Kit (Agilent; 103260-100) via injection of Etomoxir (2 µM), Bis-2-(5-phenylacetamido-1,3,4-thiadiazol-2-yl) ethyl sulfide (BPTES) (3 µM) and UK5099 (4 µM), respectively. Oxygen consumption rate (OCR) was measured using a Seahorse $X^{Fe}96$. Capacity and dependency on these pathways were calculated by using SeaHorse fuel flex report generator.

2.2.15. MitoTracker Staining

MitoTracker Green FM (Invitrogen; M7514) was used to stain mitochondria according to the manufacturer's protocols. Cells were fixed with 4% paraformaldehyde (PFA), mounted onto slides with Fluoroshield Mounting Medium with DAPI (Abcam; ab104139), visualized with Leica TCS SP5 X Confocal Microscope, and images were analyzed in ImageJ software.

2.2.16. mtROS Measurement

Mitochondrial ROS was assessed by incubating the cells with 5μM mitoSOX red (Invitrogen; M36008), followed by flow cytometry analysis. ROS levels were quantified as the mean fluorescence intensity (MFI) using BD Fortessa (BD Biosciences) and FACSDiva software with compensation controls acquired on the same day.

2.2.17. Assessment of mtDNA Copy Number

Cells were scraped into the DNA Lysis Buffer (10mM NaCl, 20mM Tris pH:6, 1mM EDTA, 10% SDS) and incubated at 37°C for 2 hours. UltraPure Phenol:Chloroform:Isoamyl Alcohol (Thermo Scientific; 15-593-031) was added to induce phase separation (at 12000 g for 15 min). The DNA containing, transparent upper phase was collected into a new tube, mixed with chloroform and centrifuged (at 12000 g for 5 minutes). The clear upper phase was collected to a new tube and DNA was precipitated by the addition of absolute ethanol containing sodium acetate (1/10 volume) followed by centrifugation (at 12000 g for 20 minutes). The precipitated DNA was dissolved in water. DNA (0.2 μg) was amplified using nuclear- or mitochondria-encoded genes-specific primers and the Power-Up-SYBR green (Applied Biosystems; A25742). mtDNA: nucDNA

ratios were calculated by normalizing results of mitochondria-encoded gene to nuclear-encoded gene.

2.2.18. Mitochondrial Enrichment

Cell were homogenized in mitochondrial isolation buffer (250mM sucrose, 1mM EDTA, 10mM HEPES, pH 7.4) containing inhibitors 1x phosphatase inhibitor cocktail 3 and 1x protease inhibitor cocktail by running through 27.5 g needle three times. Nucleus and unbroken cells were eliminated by low-speed spin (600 g, 4°C, 5 min). A small portion of the supernatant was saved (cell lysate; CL) and the rest was centrifuged (7,000 g, 4°C, 15 min) to obtain the final mitochondria-enriched pellet and supernatant (cytosol; Cyto). The mitochondria-enriched pellet was resuspended in isolation buffer and centrifuged (7,000 g, 4°C, 5 min) as a final wash. The pellet was resuspended in cold PLB with inhibitors. Protein concentrations are measured with DC Protein Assay Kit II (Bio-Rad; 500-0112). Normalized samples are boiled in SDS loading dye at 95°C for 5 minutes before loading on SDS/PAGE gels. After separation according to protein molecular weights on these gels, samples were transferred to nitrocellulose membranes. Membranes are then stained with Ponceau S. solution (Sigma-Aldrich; P7170-1L), washed with distilled water and imaged, as equal loading control.

2.2.19. CL-316,243 Treatment

For *in vivo* experiments, CL-316,243 (1 mg/kg body weight) or a vehicle control sterile saline was injected intraperitoneally once a day for 6 days. Mice were sacrificed 24 hours after the last injection. Adipose tissue depots, iWAT and BAT were harvested for protein, DNA, RNA, and histological analyses.

2.2.20. Metabolic Cages

Mice were single housed in the Phenomaster System (TSE Systems) for a total of 3 days with a 24-hour acclimation period. During the 48 hours of data collection, airflow, temperature, oxygen and carbon dioxide content, oxygen uptake (VO_2), carbon dioxide production (VCO_2), food, water intake and locomotor activity were measured simultaneously. Energy expenditure and respiratory exchange ratio were calculated automatically from the VO_2 and VCO_2. Data were collected with the instrument software and exported to Excel.

2.2.21. EchoMRI

Whole body composition of mice was detected via the EchoMRI system (EchoMRI, LLC), for fat and lean mass. Animal was placed in a clear plastic holder without anesthesia. The holder was then inserted into the tubular space of the EchoMRI system for the animal to be scanned.

2.2.22. Histological Analysis

Brown adipose tissues were fixed for 24 hours at room temperature (RT) in PBS containing 4% paraformaldehyde. Following sucrose gradient to cryopreserve the tissues, they were embedded in optimal cutting temperature (OCT) Compound. Tissue sections (8 μm) were used for hematoxylin and eosin (H&E) staining.

2.2.23. *In vitro* DICER or IRE1 cleavage assay

Pre-miR-181c or pre-miR-2137 was custom synthesized by IDT DNA technologies. DICER or IRE1 cleavage reaction was performed in cleavage assay buffer (20mM Tris–HCl (pH 6.5), 1.5mM $MgCl_2$, 25mM NaCl, 1mM dithiothreitol and 1% glycerol) with DICER (0.2 ug) or PACT (0.2 ug) or IRE1 (0.2 ug) and synthetic pre-miR (10 uM) at 37°C for 4 hours. Reaction was stopped by adding an equal volume of RNA loading dye (NEB) and heating at 70°C for 5 minutes followed by resolving on 15% urea-acrylamide gel. Gel was stained with SYBR Gold and imaged using ChemiDoc imager (BioRad).

2.2.24. miRNA profiling by microarray

BMDMs were treated with 500μM PA or vehicle control for 6 h and total RNA was isolated using miRNeasy RNA isolation kit (Qiagen,217004). RNA was quantified on Nanodrop 2000 (Invitrogen) and 2μg used for the microarray analysis, which was carried out by LC Sciences (Texas, USA). Mouse miRbase 22 (March 2018) database was used in this analysis.

2.2.25. Statistics

Data were analyzed in GraphPad Prism 8 (GraphPad Software, Inc.). Results are reported as mean ± SEM. Statistical significance was determined with Student's t test with Welch's correction for two groups and one-way ANOVA (Tukey's multiple comparison test) for multiple groups. $P < 0.05$ was considered as * significant.

3. CHAPTER 3. RESULTS

3.1. PACT is an IRE1 kinase substrate

3.1.1. Inhibiting IRE1 kinase domain but not RNase domain impacts PACT protein levels

ER stress has been shown to induce PACT phosphorylation (on serine (S) 18 and 287) by unidentified kinases. (106-108). During RISC nucleation, PACT can localize to the ER membranes, where IRE1 is also anchored (88). Published IRE1 interactome data shows PACT interacts with IRE1 in both ER stress and no stress conditions (150). I hypothesized that IRE1 could be an ER stress-induced kinase that phosphorylates PACT. To investigate this, IRE1 kinase activity was induced in human cells (HEK293T) with the ER stress inducers, thapsigargin (TG; a Ca^{2+}-ATPase inhibitor) or palmitate (PA; a saturated fatty acid) (15, 202-204). Both ER stressors simultaneously induced IRE1 kinase activity (IRE1 autophosphorylation) and PACT protein (as detected by Western blotting) (Fig.3.1A). PACT protein signal induction occurred quickly (in one hour) after the ER stressor treatment, suggesting ER stress induced a post-translational modification of PACT that could be recognized by the total PACT antibody in Western blots. Indeed, λ-phosphatase (PPase) treatment of the cellular protein lysate, prevented the ER stress-induced PACT intensity change in Western blots (205). Moreover, treatment of the cells with an inhibitor of IRE1 kinase activity, KIRA-6, prevented PA-induced PACT protein signal (Fig.3.1B). In confirmation, a second IRE1 kinase-specific inhibitor, AMG-18, also prevented PA-induced PACT protein signal (Fig.3.1C) (206, 207). This data shows that the observed-phosphatase sensitive PACT post-translational modification is also dependent on IRE1 kinase activity.

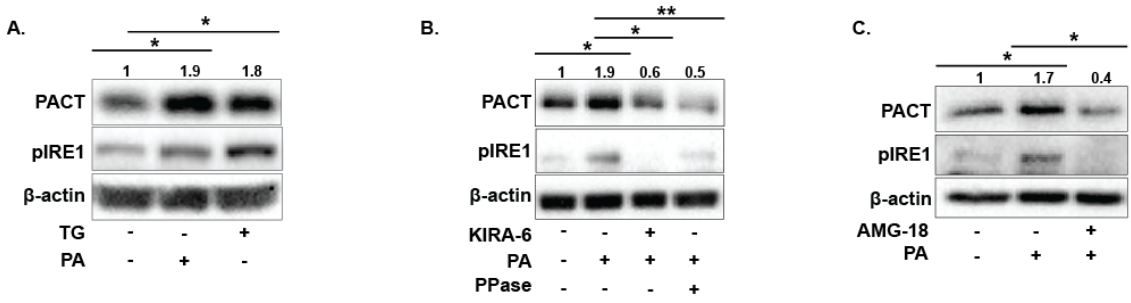

Figure 3.1 PACT's phosphorylation is IRE1 kinase activity dependent. (A) HEK293T cells were treated with PA (500μM; 3 hours) or TG (300nM; 2 hours). Protein lysates were analyzed by western blotting using specific antibodies for PACT, pIRE1 and β-actin (n=3). **(B)** HEK293T cells were pre-treated (1 hour) with vehicle (DMSO) or KIRA-6 (10μM) followed by PA (500μM; 3hours) treatment. Protein lysates, treated with λ phosphatase (PPase) or not, were analyzed by western blotting using specific antibodies for PACT, pIRE1 and β-actin (n=3). **(C)** HEK293T cells were pre-treated (1 hour) either with vehicle (DMSO) or AMG-18 (5 μM) followed by PA (500 μM; 3 hours) treatment. Protein lysates were analyzed by Western blotting using specific antibodies for PACT, pIRE1 and β-actin (n=3). Data are mean ± SEM. Unpaired *t*-test with Welch's correction or one-way ANOVA. *P≤ 0.05, **P≤ 0.01, ***P≤ 0.001.

In contrast, the observed PACT induction was not altered by an IRE1 RNase activity-specific inhibitor, 4μ8C (208, 209) (Fig.3.2 A-B). No changes were detected in Prkra mRNA (encoding PACT protein) expression with any of the IRE1 inhibitor treatments (Fig.3.2 C). Collectively, these findings show that ER stress-induced PACT phosphorylation occurs in an IRE1 kinase-dependent manner.

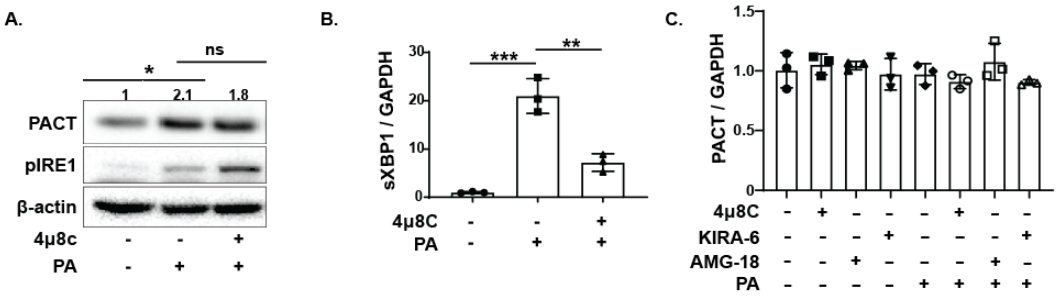

Figure 3.2 PACT's phosphorylation is not dependent on IRE1 RNase activity and mRNA levels are not affected by IRE1. (A) HEK293T cells were pre-treated (1 hour) with vehicle (DMSO) or 4μ8C (100 μM) followed by PA (500 μM; 3 hours) treatment. Protein lysates were analyzed by Western blotting using specific antibodies for PACT, pIRE1 and β-actin (n=3). **(B)** sXBP1 and GAPDH mRNA was measured by qRT-PCR from the RNA lysate of samples in Fig. 1D (n=3). **(C)** HEK293T cells were pre-treated (1 hour) with KIRA-6 (10 μM), AMG-18 (5 μM) or 4μ8C (100 μM) followed by PA (500μM) treatment for 9 hours. Total RNA extract was analyzed by qRT-PCR for PACT and GAPDH mRNA (n=3). Data are mean ± SEM. Unpaired *t*-test with Welch's correction or one-way ANOVA. *P≤ 0.05, **P≤ 0.01, ***P≤ 0.001.

To confirm IRE1 kinase-dependent regulation of PACT phosphorylation *in vivo*, wild type (C57BL/6J) mice were injected with an ER stress-inducer, tunicamycin (TUN; inhibitor of protein glycosylation), to induce IRE1 kinase activity and with one of the IRE1 kinase inhibitors or vehicle (210). The *in vivo* effective concentrations, duration and delivery method for these small molecule inhibitors of IRE1 were reported earlier (205, 206, 211, 212). TUN simultaneously induced IRE1 kinase activity and PACT protein signal in Western blots conducted using the proteins lysates obtained from the treated mice's peritoneal macrophages. Both IRE1 kinase inhibitors suppressed TUN-induced IRE1 autophosphorylation and PACT protein signal increase in these macrophages (Fig.3.3A). These findings demonstrate that IRE1 kinase activity is required for ER stress-induced PACT phosphorylation *in vivo*.

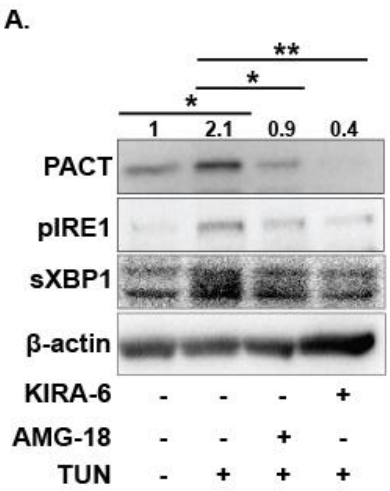

Figure 3.3 PACT's phosphorylation is not dependent on IRE1 in vivo. (A) C57BL/6 mice were injected with vehicle (DMSO), AMG-18 (30 mg/kg; 8 hours) or KIRA-6 (5 mg/kg; 8 hours), followed by TUN injection (1 mg/kg; 8 hours). Protein lysates of thioglycolate-elicited peritoneal macrophages were analyzed by Western blotting using specific antibodies for PACT, pIRE1, sXBP1 and β-actin (n=3). Data are mean ± SEM. Unpaired *t*-test with Welch's correction or one-way ANOVA. *P≤ 0.05, **P≤ 0.01, ***P≤ 0.001.

3.1.2. IRE1 interacts with and phosphorylates PACT

I next investigated whether IRE1 and PACT physically interact as indicated by the interactome data (150). I immunoprecipitated endogenous PACT or IRE1 using antibodies specific for these proteins. These results show that IRE1 and PACT co-immunoprecipitates in ER stress as well as in no stress conditions, confirming IRE1 and PACT physically interact with each other (Fig.3.4A). To assess whether IRE1 kinase is responsible for PACT phosphorylation, I performed an *in vitro* kinase assay using recombinant, active IRE1 and PACT proteins that were incubated in kinase buffer containing ATP-γ-S. When used by kinases, ATP-γ-S thio-phosphorylates the substrates. Following the kinase reaction, an alkylation step induced by incubating with p-Nitrobenzyl mesylate (PNBM) was carried out to yield thiophosphate esters (ThioP) on the substrate. These ThioP modifications can

be recognized by a thiophosphate-specific antibody in Western blots (195). Results from this experiment showed that IRE1 thio-phosphorylated itself and PACT (Fig.3.4B).

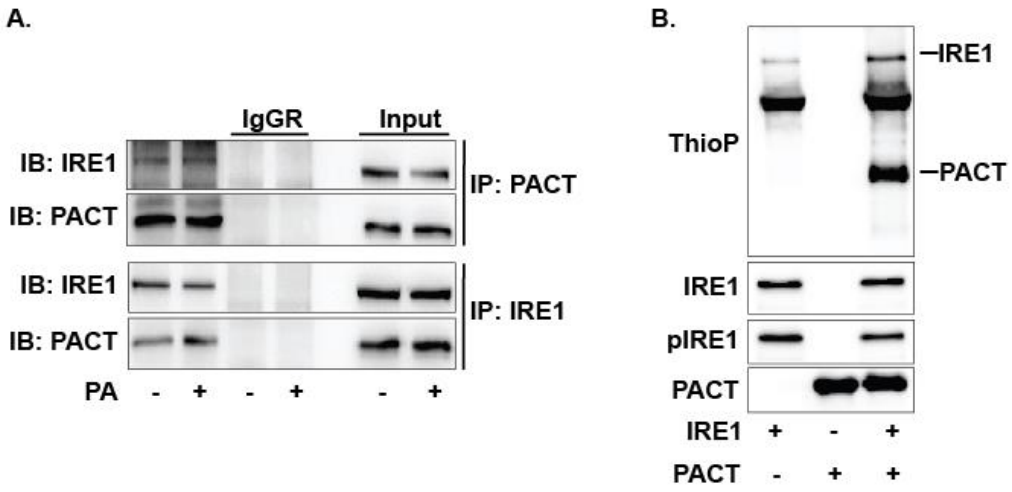

Figure 3.4 PACT's phosphorylation is not dependent on IRE1 in vivo. (A) HEK293T cells were treated with PA (500 μM) for 3 hours. Specific antibodies for PACT (upper panel), IRE1 (lower panel) or IgG (control) were used to immunoprecipitate respective proteins and analyzed by western blotting using antibodies for PACT, pIRE1 and β-actin (n=3). **(B)** *In vitro* kinase assay: recombinant PACT (34 kDa) and active IRE1 kinase (100 kDa) were incubated in kinase buffer with ATP-γ-S (100 μM) (n=3). Data are mean ± SEM. Unpaired *t*-test with Welch's correction or one-way ANOVA. *P≤ 0.05, **P≤ 0.01, ***P≤ 0.001.

To determine the specific amino acids phosphorylated by IRE1, I performed the kinase reaction using recombinant IRE1 and PACT proteins and subjected to liquid chromatography-mass spectrometry (LC-MS/MS)-based analysis. This analysis revealed seven potential IRE1 kinase-mediated phosphorylation sites on PACT at serine (S2, S4, S18, S104 and S202) and threonine (T20, T160) (Fig.3.5A-B). Among these, Serine 18 (S18) is conserved in all mammals and was previously reported to be regulated by ER-stress (108). For this reason, I decided to pick S18 and T20 as the most likely IRE1 regulated phosphorylation sites on PACT, considering they are in close proximity and most

probably phosphorylated together. Overall, these findings demonstrate that PACT is a novel substrate of IRE1 kinase.

A.

AA	Sequence	z	XCorr	DeltaCN	[M+H]+	A-Score
*pS*2	GSHMGSM*pS*QSR	2	2.811	0.2873	1244.46	24.24
	GSHMGSM*pS*QSR	2	3.001	0.3837	1244.4591	12.65
*pS*4	GSHMGSMSQ*pS*R	2	2.771	0.2814	1244.4568	43.03
	GSHMGSMSQ*pS*R	2	2.727	0.3115	1244.4581	42.65
➤ *pS*18	HRAEAPPLERED*pS*GTFSLGK	3	3.264	0.2772	2277.0654	8.52
	HRAEAPPLERED*pS*GTFSLGK	3	3.655	0.4125	2277.0693	14.65
	HRAEAPPLERED*pS*GTFSLGK	3	3.395	0.2926	2277.069	18.34
	HRAEAPPLERED*pS*GTFSLGK	4	3.193	0.2484	2277.0667	1.06
	HRAEAPPLERED*pS*GTFSLGK	4	3.83	0.3979	2277.0813	5.97
	HRAEAPPLERED*pS*GTFSLGK	4	3.946	0.3128	2277.0806	9.57
	AEAPPLERED*pS*GTFSLGK	2	5.204	0.4834	1983.9182	30.7
	AEAPPLERED*pS*GTFSLGK	2	4.702	0.4248	1983.9186	24.75
	AEAPPLERED*pS*GTFSLGK	3	3.602	0.3533	1983.9185	31.51
	AEAPPLERED*pS*GTFSLGK	3	3.352	0.3909	1983.9097	34.98
*pT*20	HRAEAPPLEREDSG*pT*FSLGK	4	3.383	0.2929	2277.0803	11.72
	AEAPPLEREDSG*pT*FSLGK	2	4.885	0.4843	1983.9098	42.65
	AEAPPLEREDSG*pT*FSLGK	3	3.101	0.2866	1983.92	18.34
*pS*104	ANA*pS*ICFAVPDPLMPDPSKQPK	3	3.367	0.3055	2463.1616	43.52
*pT*160	EY*pT*TICR	2	1.916	0.3063	1022.4078	13.24
*pS*202	FSNISPENHI*pS*LTNVVGHSLGCTWHSLR	4	5.327	0.3373	3242.5222	7.32
	FSNISPENHI*pS*LTNVVGHSLGCTWHSLR	4	3.075	0.3366	3242.544	8.64

B.

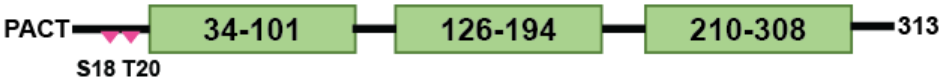

Figure 3.5 PACT is phosphorylated on S18 and T20 by IRE1. (A) Kinase assay was followed with alkylation with PNMB and analyzed by Western blotting using specific antibodies for ThioP, PACT, IRE1 and pIRE1, whereas in **(B)** Kinase reaction was directly analyzed by LC-MS/MS. Of the 7 sites identified, S18 and T20 were selected for further mutagenesis studies as explained in results.

3.2. PACT is a suppressor of mitobiogenesis

3.2.1. PACT regulates mitochondrial mass in vitro

Next question was what is the biological consequence of IRE1-induced PACT phosphorylation could be? PACT-PKR signaling has been extensively characterized in innate immune response to viruses, yet the ubiquitously expressed PACT's non-immune functions are unknown (104, 105, 107, 109, 213). PACT also associates with Dicer and alter post-transcriptional gene expression (214). Interestingly, PACT protein and mRNA expression are reduced several folds upon cold-induced activation of brown adipose tissue (BAT) in mice (137, 138). BAT activation is accompanied with dramatical gene expression changes governing mitochondrial bioenergetics and mitobiogenesis (134, 215-217). For this reason, I wondered whether PACT plays a role in mitochondrial biology. I observed that PACT-deficient (Prkra$^{-/-}$) mouse embryonic fibroblasts (MEF) displayed significant increased mitochondrial mass (as observed with MitoTracker Green stain) in comparison to wild type (Prkra$^{+/+}$) MEFs. Reconstitution with wild type (WT)-PACT protein reduced mitochondrial mass in Prkra$^{-/-}$ MEF, showing mitochondrial mass was regulated by PACT (Fig.3.6A). Mitochondrial mass was also induced upon silencer RNA (siRNA)-mediated PACT knock down in human cells (Fig.3.6B). These findings demonstrate that PACT regulates cellular mitochondria mass.

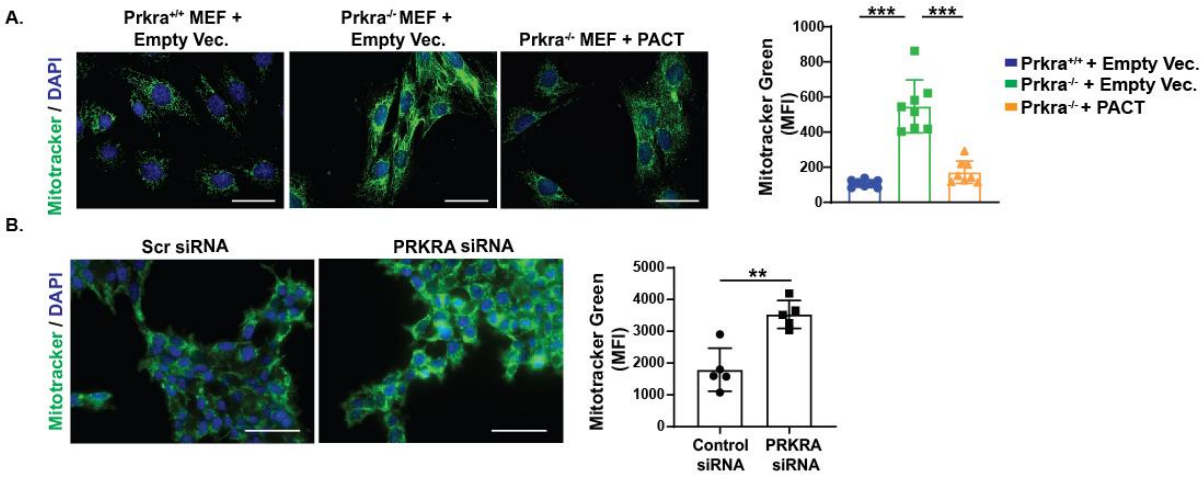

Figure 3.6 Mitochondrial mass is regulated by PACT in vitro. (A-B) Mitochondrial mass was determined from MitoTracker Green-stained cells (quantified by measuring mean fluorescence intensity (MFI) with ImageJ from at least 200 cells; representative image shown (n=8). Scale bar: 50 μm): **(A)** $Prkra^{+/+}$, $Prkra^{-/-}$ or $Prkra^{-/-}$ MEFs reconstituted with WT-PACT, **(B)** HEK293T cells transfected with either scrambled (control) or Prkra siRNA (n=5). Data are mean ± SEM. Unpaired *t*-test with Welch's correction or one-way ANOVA. *P≤ 0.05, **P≤ 0.01, ***P≤ 0.001.

3.2.2. PACT is involved in human I/R injury related mitobiogenesis

An example of enhanced mitobiogenesis occurs in human hearts upon ischemia-reperfusion (I/R) injury. Mitobiogenesis is induced in the atrial tissue that was obtained from patients who went through cardiopulmonary bypass (157). I examined these human atrial biopsy samples (taken before (A) and after (B) cardiopulmonary bypass) for PACT protein expression. Confirming previous results, mitobiogenesis was induced after I/R injury (B samples) as evident by the increase in PGC1α, TFAM, NRF1, Translocase of outer mitochondrial membrane 70 (TOM70) and electron transport chain (ETC) proteins (Complex I (CI) subunit NADH:Ubiquinone Oxidoreductase Subunit B8 (NDUFB8), CII succinate dehydrogenase complex iron sulfur subunit B (SDHB), CIII ubiquinol-cytochrome C reductase core protein 2 (UQCRC2), CIV mitochondrially encoded cytochrome C oxidase I (MTCO1) and Complex V ATP synthase alpha-subunit (ATP5A)), which is accompanied by a significant downregulation of PACT protein (Fig.3.7A). This data shows that PACT protein downregulation is associated with increased mitobiogenesis in human cardiac tissue *in vivo*.

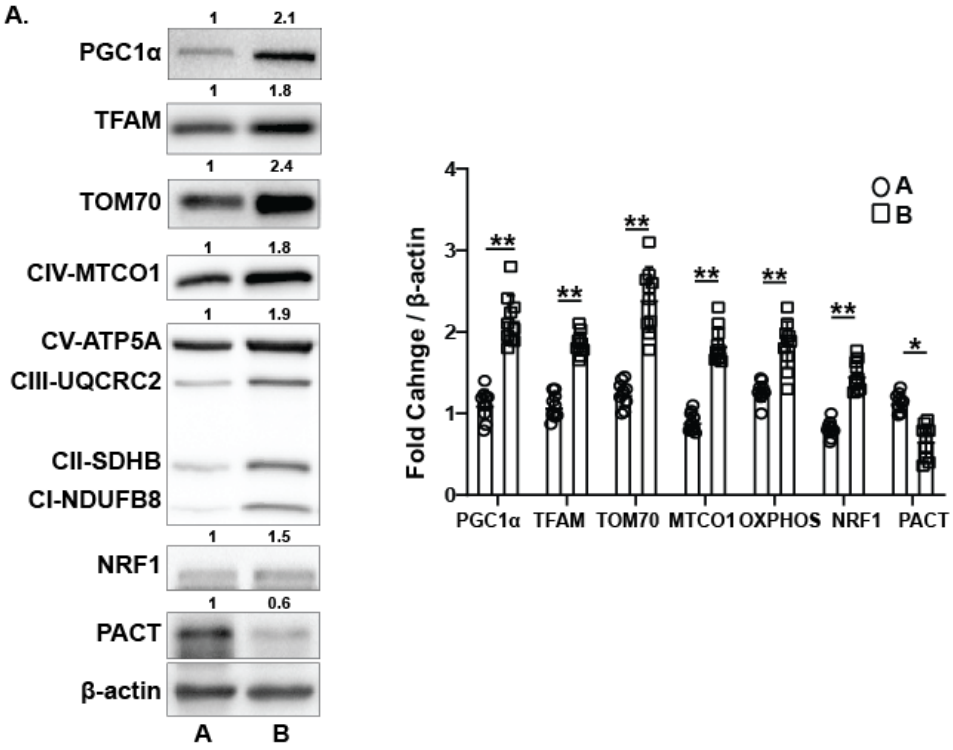

Figure 3.7 PACT is involved in upregulation of mitobiogenesis in human I/R condition. (A) Paired right atrial heart biopsies taken before (A) and after (B) surgery from patients who underwent cardiopulmonary bypass. Protein lysates were analyzed by Western blotting using specific antibodies for PGC1α, TFAM, TOM70, an antibody cocktail against ETC proteins, NRF1, PACT and β-actin (n=10). Data are mean ± SEM. Unpaired *t*-test with Welch's correction or one-way ANOVA. *P≤ 0.05, **P≤ 0.01, ***P≤ 0.001.

3.2.3. PACT blocks mitochondrial biogenesis in mouse and human cells

Next, I reconstituted Prkra$^{-/-}$ MEFs with WT-PACT and observed PACT expression significantly suppressed PGC1α, NRF1, TFAM, and MTCO1 proteins in no stress and ER stress conditions (Fig.3.8A). To investigate the consequences of IRE1-mediated PACT phosphorylation on mitobiogenesis regulation, I generated alanine mutations of ER stress-regulated S18 amino acid residue and the neighboring Threonine 20 (T20) on PACT protein (Mut-PACT; S18A, T20A). Unlike the mitobiogenesis inhibitory effect of WT-PACT reconstitution in Prkra$^{-/-}$ MEF, Mut-PACT reconstitution did not suppress mitochondrial proteins or mtDNA copy number (Fig.3.8A-B). PACT reconstitution also reduced Tfam and Pgc1α mRNA (Fig.3.8C-D).

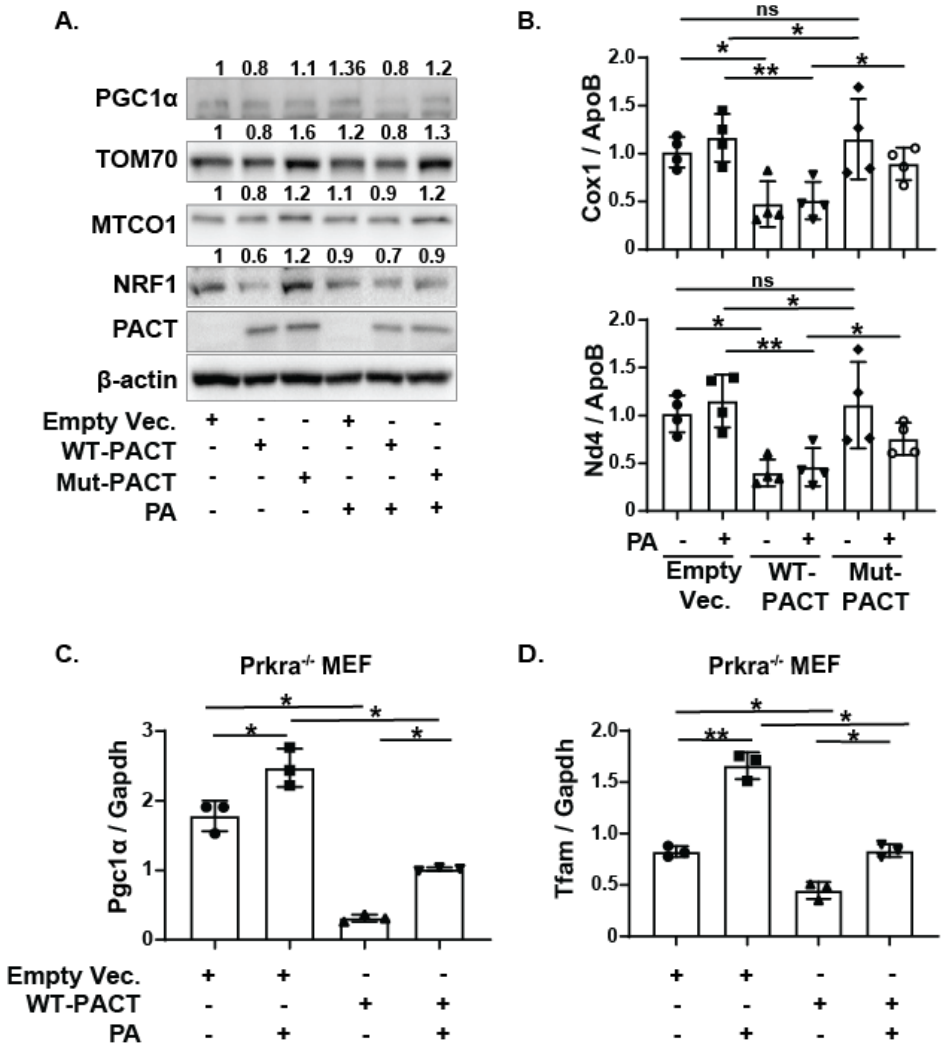

Figure 3.8 PACT is a suppressor of mitobiogenesis in mouse cells. (A-B) Prkra$^{-/-}$ MEFs were transfected either with empty control vector (Empty Vec.), WT-PACT or Mut-PACT) and treated with PA (500 μM) for 3 hours. **(A)** Protein lysates were analyzed by Western blotting using specific antibodies for PGC1α, TOM70, antibody cocktail against ETC proteins, NRF1, PACT and β-actin (n=3). **(B)** Total genomic DNA was isolated and mtDNA: nucDNA ratio (NADH-ubiquinone oxidoreductase chain 4 (Nd4) and Cytochrome c oxidase I (Cox1) for mtDNA and Apolipoprotein B (ApoB) for nucDNA) was analyzed by qRT-PCR (n=4). **(C-D)** Prkra$^{-/-}$ MEFs were transfected with either empty vector or WT-PACT and treated with PA (500 μM; 3 hours). RNA extracts were analyzed by qRT-PCR for Pgc1α, Tfam and Gapdh mRNA. Data are mean ± SEM. Unpaired *t*-test with Welch's correction or one-way ANOVA. *P≤ 0.05, **P≤ 0.01, ***P≤ 0.001.

Similarly, PACT overexpression in human cells (HEK293T) reduced mitochondrial proteins and mtDNA copy number (Fig.3.9A-B). On the other hand, siRNA-mediated PACT knockdown in HEK293T cells induced mitochondrial proteins and mtDNA copy number (Fig.3.9C-D). These finding demonstrates the critical role of IRE1-mediated phosphorylation of PACT in mitobiogenesis.

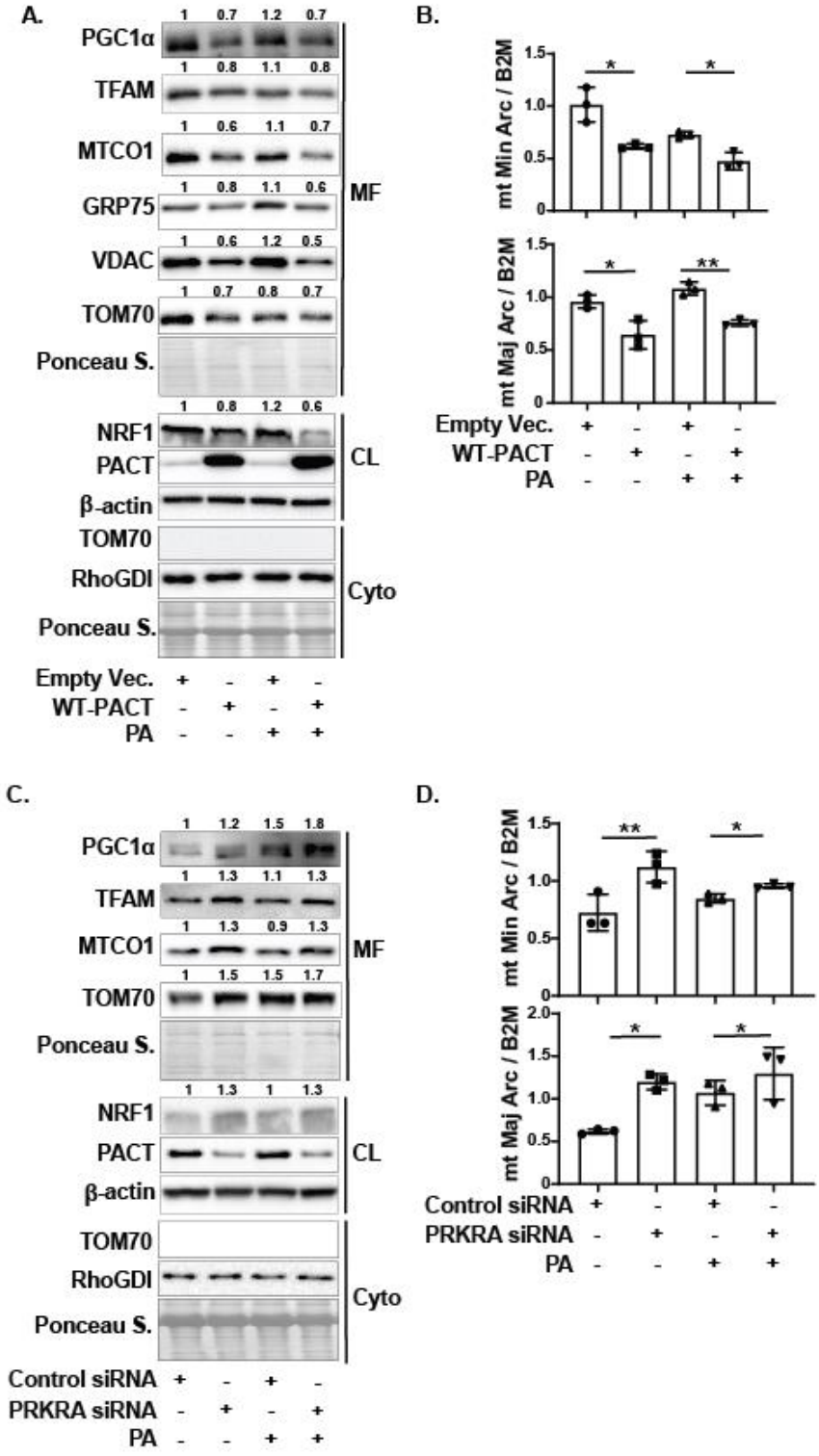
A.
PGC1α
TFAM
MTCO1
GRP75
VDAC
TOM70
Ponceau S.
MF
NRF1
PACT
β-actin
CL
TOM70
RhoGDI
Ponceau S.
Cyto
Empty Vec.
WT-PACT
PA
B.
mt Min Arc / B2M
mt Maj Arc / B2M
Empty Vec.
WT-PACT
PA
C.
PGC1α
TFAM
MTCO1
TOM70
Ponceau S.
MF
NRF1
PACT
β-actin
CL
TOM70
RhoGDI
Ponceau S.
Cyto
Control siRNA
PRKRA siRNA
PA
D.
mt Min Arc / B2M
mt Maj Arc / B2M
Control siRNA
PRKRA siRNA
PA

Figure 3.9 PACT is a suppressor of mitobiogenesis in human cells. (A) HEK293 cells were transfected with empty vector or WT-PACT and treated with PA (500 μM; 3 hours). Mitochondria enriched fraction (MF), total cell lysate (CL) and cytosolic fraction (Cyto) protein lysates were analyzed by Western blotting using specific antibodies for PGC1α, TFAM, MTCO1, GRP75, VDAC, TOM70, NRF1, PACT, RhoGDI and β-actin (n=3). **(B)** Total genomic DNA was isolated from the same experimental set-up in panel A, and mtDNA: nucDNA ratio was analyzed by qRT-PCR (mtMajArc, mtMinArc for mtDNA and B2M for nucDNA) (n=3). **(C)** HEK293T cells were transfected with PACT siRNA and treated with PA (500 μM; 3 hours). MF, CL and Cyto fraction proteins lysates were analyzed from by Western blotting using specific antibodies for PGC1α, TFAM, MTCO1, TOM70, NRF1, PACT, RhoGDI and β-actin (n=3). **(D)** Total genomic DNA was isolated from the same experimental set-up in Fig. S2H, and mtDNA; nucDNA ratio was analyzed by qRT-PCR (mtMajArc, mtMinArc for mtDNA and B2M for nucDNA) in HEK293T cells (n=3). Data are mean ± SEM. Unpaired *t*-test with Welch's correction or one-way ANOVA. *P≤ 0.05, **P≤ 0.01, ***P≤ 0.001.

3.2.4. PACT has a role in the regulation of mitochondrial fusion and fission

To understand whether PACT's impact on mitochondria is limited to mitochondrial biogenesis, I next sought to determine how silencing or overexpressing PACT affects mitochondrial dynamics in terms of fusion and fission. For this purpose, I checked the protein levels of two major mitochondrial fusion markers OPA1 and MFN2, as well as fission marker DRP1. Silencing PACT significantly increased protein levels of both MFN2 and OPA1, which stimulate fusion. Interestingly, silencing PACT also significantly increased phospho-DRP1 (pDRP1) on serine 616, which is an activatory phosphorylation on DRP1 to stimulate mitochondrial fission (218). (Figure 3.10 A-B). Supporting these results, overexpression of WT-PACT had a trend of impacting MFN2, OPA1 and pDRP1 levels negatively, though not significant (Figure 3.10 C-D). Overall, these results suggest that PACT might also be a blocker of mitochondrial fusion and fission.

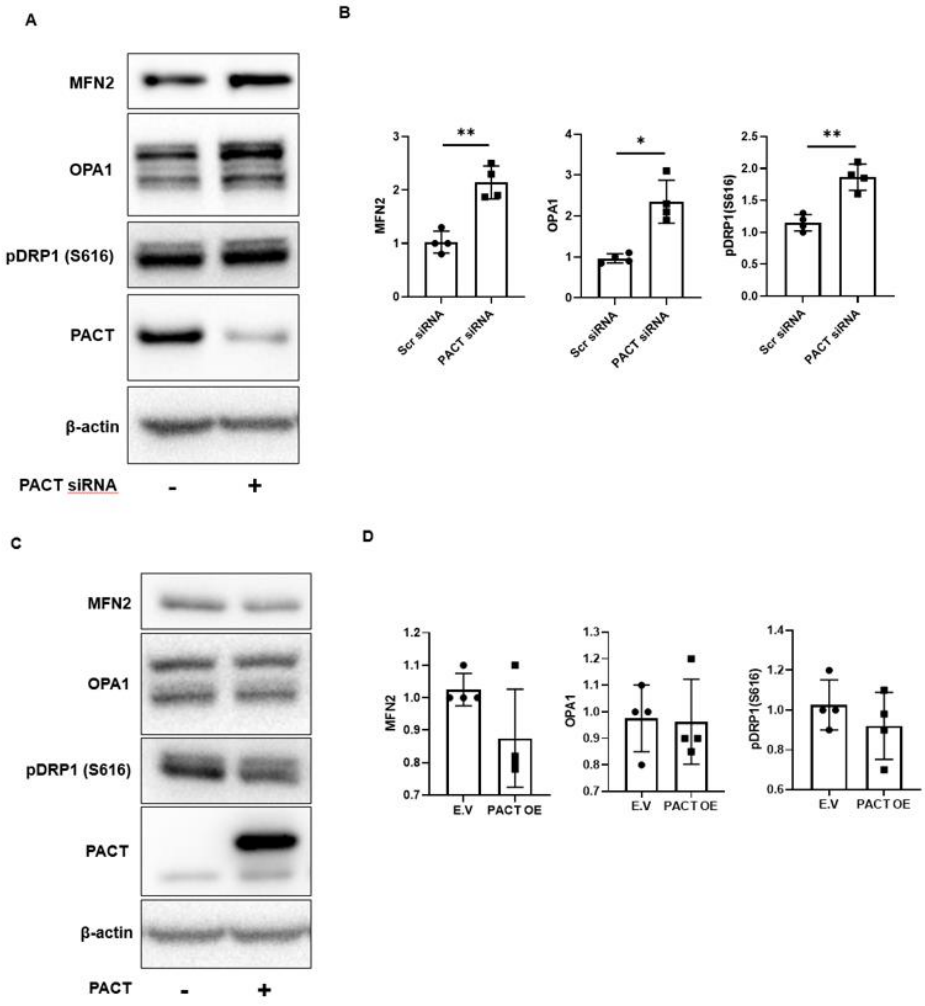

Figure 3.10 PACT has an impact on mitochondrial fusion and fission. (A-B) HEK293T cells were transfected with PACT siRNA and whole cell lysates were analyzed by Western blotting using specific antibodies for MFN2, OPA1, pDRP1 (S616), PACT and β-actin and normalized to β-actin (n=4). **(C-D)** HEK293 cells were transfected with empty vector or WT-PACT and whole cell lysates were analyzed by Western blotting using specific antibodies for MFN2, OPA1, pDRP1 (S616), PACT and β-actin and normalized to β-actin (n=4). Data are mean ± SEM. Unpaired *t*-test with Welch's correction or one-way ANOVA. *P≤ 0.05, **P≤ 0.01, ***P≤ 0.001.

3.3. PACT regulates mitochondrial energetics

3.3.1. PACT is a regulator of mitochondrial oxygen consumption

To understand how PACT affects mitochondrial energetics, I first characterized mitochondrial oxygen consumption rates (OCR) in Prkra$^{-/-}$ and Prkra$^{+/+}$ MEFs. I observed significantly higher OCR in Prkra$^{-/-}$ MEFs in the mitochondrial stress test, and this phenotype was reversed when Prkra$^{-/-}$ MEFs were reconstituted with WT-PACT (Fig.3.11A). Simultaneous extra-cellular acidification rate (ECAR) measurements showed high basal glycolytic activity in Prkra$^{-/-}$ MEFs (Fig.3.11B). Prkra$^{-/-}$ MEFs displayed significantly higher ATP production, maximal respiration as well as basal respiration, and these parameters were reversed back to Prkra$^{+/+}$ MEF levels upon reconstitution of Prkra$^{-/-}$ MEFs with WT-PACT (Fig.3.11C-E). Bioenergetic map of these cells revealed Prkra$^{-/-}$ MEFs are highly energetic compared to Prkra$^{+/+}$ MEFs, which was again reversed with WT-PACT reconstitution (Fig. 3.11F). These results confirm that PACT suppresses mitochondrial respiration and energetics.

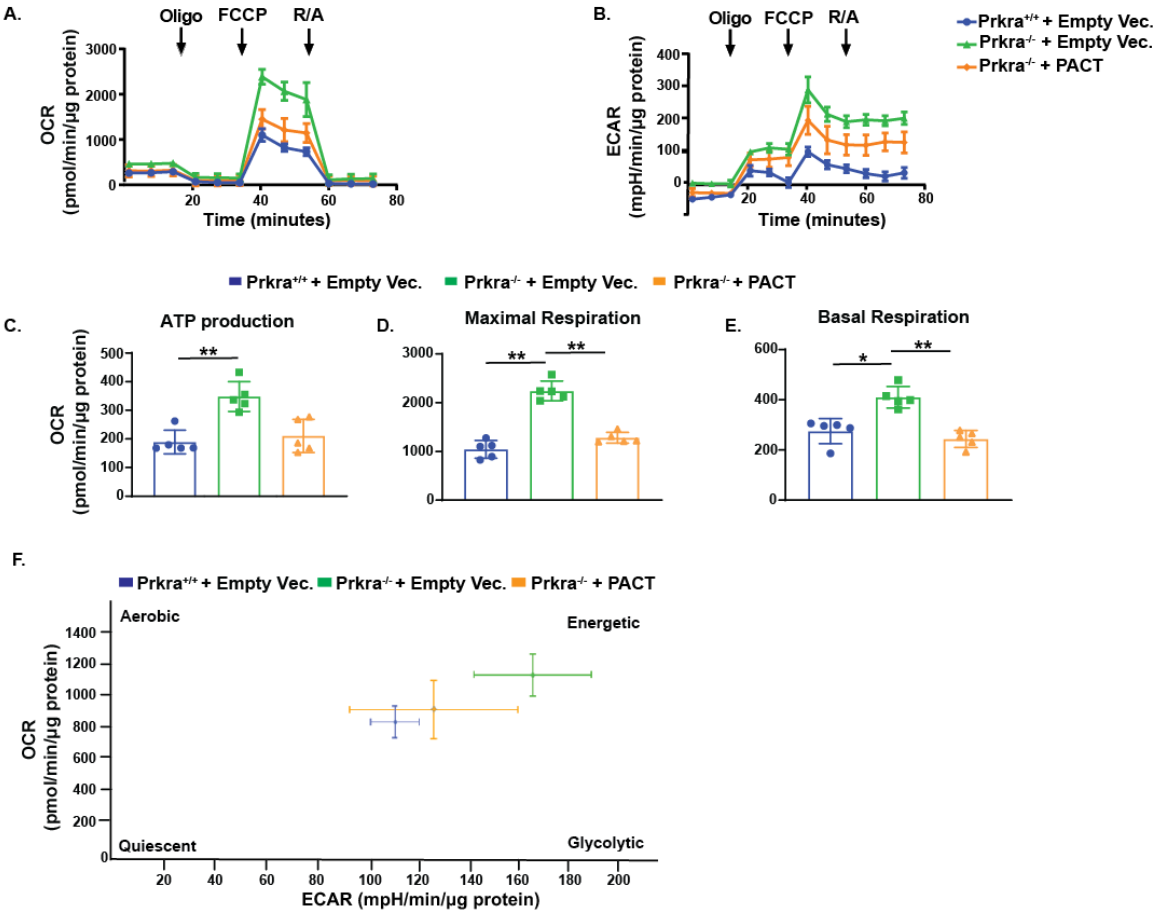

Figure 3.11 PACT is a regulator of mitochondrial oxygen consumption and ATP production. (A-E) Mitochondrial respiration was analyzed by Seahorse Mito Stress test in Prkra$^{+/+}$ or Prkra$^{-/-}$ MEFs by measuring **(A)** oxygen consumption rate (OCR) **(B)** extracellular acidification rate ECAR, and **(C)** ATP production after oligomycin (Oligo; 1 µM) injection. Oligomycin: ATP synthase inhibitor; FCCP: mitochondrial uncoupler; R/A: rotenone and antimycin A mix (inhibitors for ETC complex I and III, respectively). **(D)** Maximal respiration (as the highest OCR after FCCP injection; 1 µM). **(E)** Basal Respiration (as OCR before oligomycin injection. Arrows indicate time for drug injections (n=5). **(F)** Energy map after Mito Stress Test for Prkra$^{+/+}$, Prkra$^{-/-}$ MEFs and Prkra$^{-/-}$ MEFs reconstituted with WT-PACT treated with 3 hours PA (500 µM). Cells were categorized according to their bioenergetics, where high OCR and ECAR corresponds to an energetic state and low OCR and ECAR indicates quiescence. Data are mean ± SEM. Unpaired *t*-test with Welch's correction or one-way ANOVA. *P≤ 0.05, **P≤ 0.01, ***P≤ 0.001.

3.3.2. PACT is a regulator of mitochondrial oxygen consumption in human cells

The hypothesis on PACT's impact on mitochondrial respiration holds true also in a human cell line. In HEK293 cells transfected with PACT siRNA, OCR and related respiratory parameters are significantly downregulated as seen from basal respiration, maximal respiration and ATP production(Fig. 3.12A-B). In support of these findings, in HEK293 cells transfected with WT-PACT same parameters of OCR are significantly decreased. (Fig. 3.12C-D).

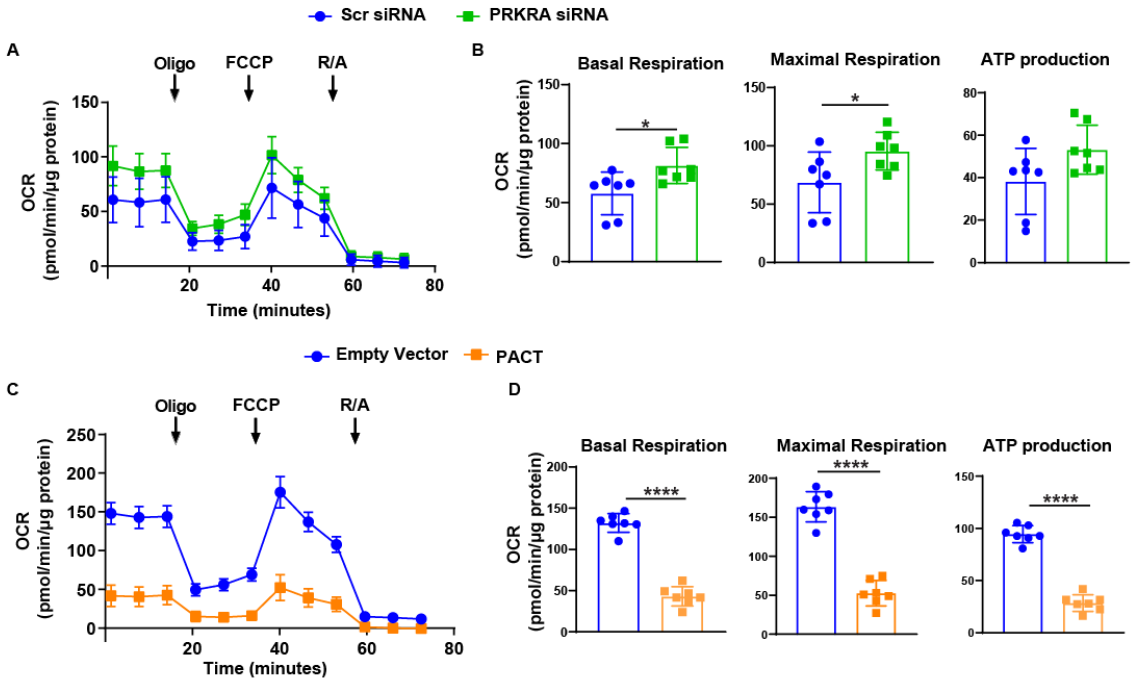

Figure 3.12 PACT is a regulator of mitochondrial oxygen consumption in human cells. **(A)** Mitochondrial respiration was analyzed by Seahorse Mito Stress test in HEK293-T cells transfected with 100nM PACT siRNA for 24 hours from OCR **(B)** oxygen consumption rate (OCR), maximal respiration (as the highest OCR after FCCP injection; 1 µM) and ATP production after oligomycin (Oligo; 1 µM) injection. Oligomycin: ATP synthase inhibitor; FCCP: mitochondrial uncoupler; R/A: rotenone and antimycin A mix

(inhibitors for ETC complex I and III, respectively). **(C)** Mitochondrial respiration was analyzed by Seahorse Mito Stress test in HEK293-T cells transfected with WT-PACT for 24 hours from OCR **(D)** oxygen consumption rate (OCR), maximal respiration (as the highest OCR after FCCP injection; 1 µM) and ATP production after oligomycin (Oligo; 1 µM) injection. Oligomycin: ATP synthase inhibitor; FCCP: mitochondrial uncoupler; R/A: rotenone and antimycin A mix (inhibitors for ETC complex I and III, respectively). Data are mean ± SEM. Unpaired *t*-test with Welch's correction or one-way ANOVA. *P≤ 0.05, **P≤ 0.01, ***P≤ 0.001.

3.3.3. Mitochondrial substrate utilization is altered by PACT

Next step was to analyze substrate dependency and oxidation capacity of these cells (using the Mito Fuel Flex Test). PACT-deficiency did not alter dependency on glucose, fatty acids or glutamine. Interestingly, reconstitution of Prkra$^{-/-}$ MEFs with WT-PACT, increased dependency of these cells for all substrates (Fig.3.13A). This could be a compensatory response to the impaired OCR and low ATP production that occurs as a consequence of WT-PACT reconstitution (Fig.3.11C-E). Oxidation capacity for all types of substrates was significantly higher in Prkra$^{-/-}$ MEFs in comparison to Prkra$^{+/+}$ MEFs, which was reversed upon reconstitution with WT-PACT (Fig.3.11B).

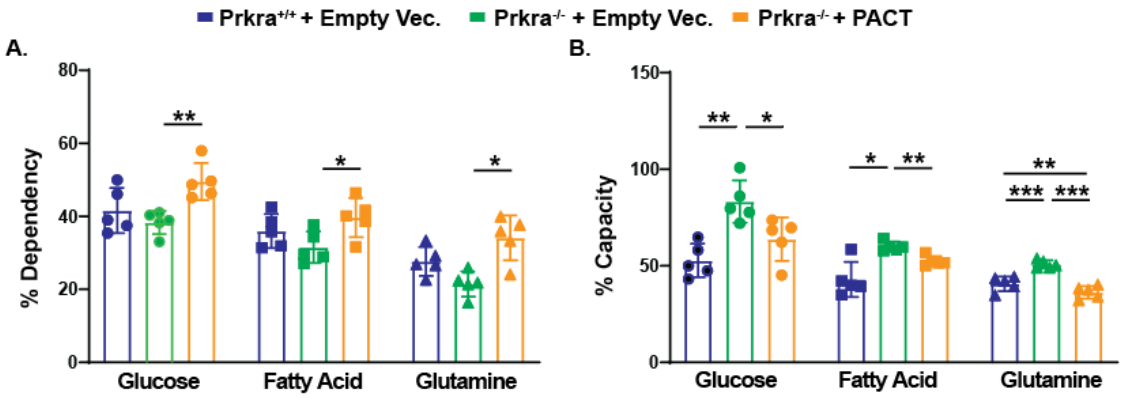

Figure 3.13 PACT knock-out or reconstitution changes mitochondrial substrate utilization. (A-B) Mitochondrial fuel oxidation measurements of Prkra$^{+/+}$, Prkra$^{-/-}$ and

Prkra$^{-/-}$ MEFs reconstituted with WT-PACT to determine **(A)** dependency on and **(B)** capacity to oxidize glucose, glutamine or fatty acids during mitochondrial respiration (n=5).

3.3.4. Mitochondrial MTCO1 protein levels are dependent on PACT

The higher OCR and substrate oxidation capacity of Prkra$^{-/-}$ MEFs was accompanied by higher levels of ETC complex proteins, which were also suppressed upon reconstitution with WT-PACT. Of note, MTCO1 was the most affected ETC subunit overall (Fig.3.14A). siRNA-medicated PACT knockdown in HEK293T cells similarly induced ETC proteins, especially MTCO1 expression, in both no stress and ER stress conditions (Fig. 3.14B). These collective results demonstrate that PACT loss of function leads to higher mitochondrial OCR with more oxidation capacity.

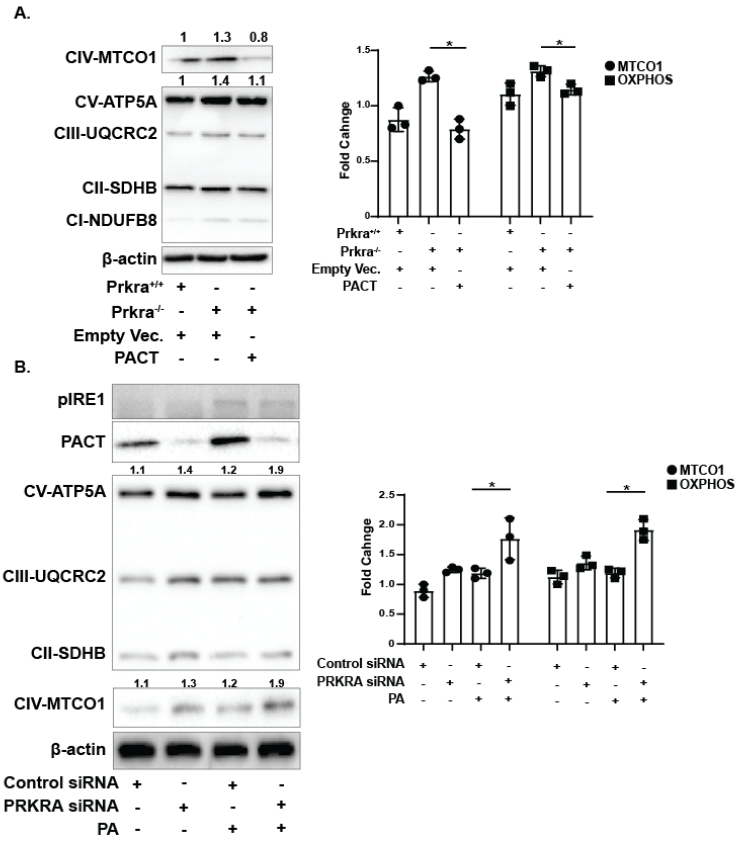

Figure 3.14 PACT regulates ETC protein levels. (A) Prkra$^{+/+}$ MEFs, Prkra$^{-/-}$ MEFs or Prkra$^{-/-}$ MEFs reconstituted with either empty vector or WT-PACT and protein lysates were analyzed by Western blotting using antibody cocktail against ETC proteins (n=3). The quantification of band intensities for MTCO1 and total ETC complex are relative β-actin. **(B)** Control or PRKRA siRNA were transfected into HEK293T cells. Protein lysates were analyzed by Western blotting using antibodies specific for pIRE1, PACT, ETC and β-actin (n=3). The quantification of band intensities for MTCO1 and total ETC are relative to β-actin. Data are mean ± SEM. Unpaired *t*-test with Welch's correction or one-way ANOVA. *P≤ 0.05, **P≤ 0.01, ***P≤ 0.001.

3.3.5. Phospho-mutant PACT does not regulate mitochondrial oxygen consumption

Finally, I investigated the consequences of IRE1-mediated PACT phosphorylation on mitochondrial energetics. While WT-PACT significantly reduced OCR in Prkra$^{-/-}$ MEF, Mut-PACT did not (Fig.3.15A). This finding emphasizes the importance of IRE1-mediated PACT phosphorylation in the regulation of mitochondrial oxidation capacity.

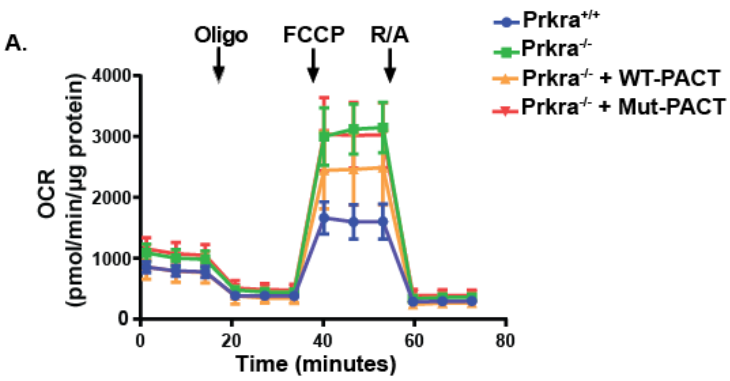

Figure 3.15 Mut-PACT cannot regulate mitochondrial OCR. (A) Prkra$^{+/+}$ MEFs, Prkra$^{-/-}$ MEFs or Prkra$^{-/-}$ MEFs reconstituted with either empty vector or WT-PACT and mitochondrial respiration was analyzed by Seahorse Mitochondrial Stress test by measuring OCR. Arrows indicate time for drug injections (n=5).

3.3.6. Loss of PACT downregulates mitochondrial reactive oxygen species production

My previous results showed that mitochondrial oxygen consumption increased in parallel to the increase in mitochondrial mass in PACT-deficient cells. The increase in mitochondrial respiration in PACT-deficient is coupled to more ATP production. Furthermore, the mitochondria in Prkra$^{-/-}$ MEFs are highly efficient in utilizing all types of substrates to produce ATP and do not display preference for a particular type of fuel. A consequence of this enhanced respiration could be a build-up of reactive oxygens species (ROS), but instead mitochondrial ROS production was reduced in Prkra$^{-/-}$ MEFs and this could be reversed by PACT reconstitution (Fig. 3.16A). This could be related to PACT's impact on the anti-oxidant system enzymes. These findings support a model where PACT suppression releases a post-transcriptional block on mitobiogenesis, upon which cells and tissues can generate more mitochondria and expand their respiratory capacity and ATP production.

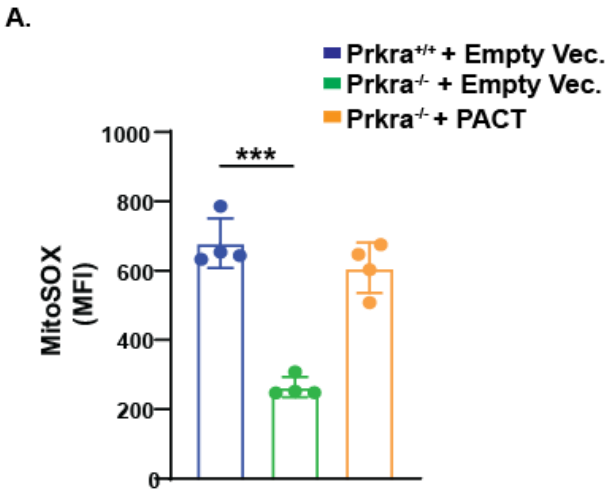

Figure 3.16 Knocking-out PACT decreases mtROS production. (A) Flow cytometry measurements for mitochondrial ROS stained with mitoSOX Red mitochondrial

superoxide indicator from Prkra$^{+/+}$, Prkra$^{-/-}$ MEFs and Prkra$^{-/-}$ MEFs reconstituted with PACT. Data are mean ± SEM. One-way ANOVA. *P≤ 0.05, **P≤ 0.01, ***P≤ 0.001.

3.3.7. PACT does not regulate mitochondrial or cytosolic ROS metabolizing enzymes

To further investigate the mechanism behind PACT's impact on ROS production, I checked ROS metabolizing enzymes. Superoxide Dismutase 1 (SOD1) and 2 (SOD2) are cytosolic and mitochondrial enzymes, respectively, that catalyze superoxide radicals into hydrogen peroxide (82). Protein levels of these enzymes were not significantly changed upon silencing or overexpression of PACT (Figure 3.17 A-D). Catalase and Peroxiredoxin3 (PRDX3) enzymes are responsible for the reaction of reducing hydrogen peroxide into water in cytosol or peroxisomes (82). The protein levels of these enzymes were also not significantly affected by silencing or overexpression of PACT (Figure 3.17 A-D). These results indicate that PACT does not control the expression levels of ROS metabolizing enzymes and this might be relevant to PACT's role in remodeling ETC proteins to function more efficiently via forming super-complexes by forming oligomers, thus producing less ROS, while consuming more oxygen.

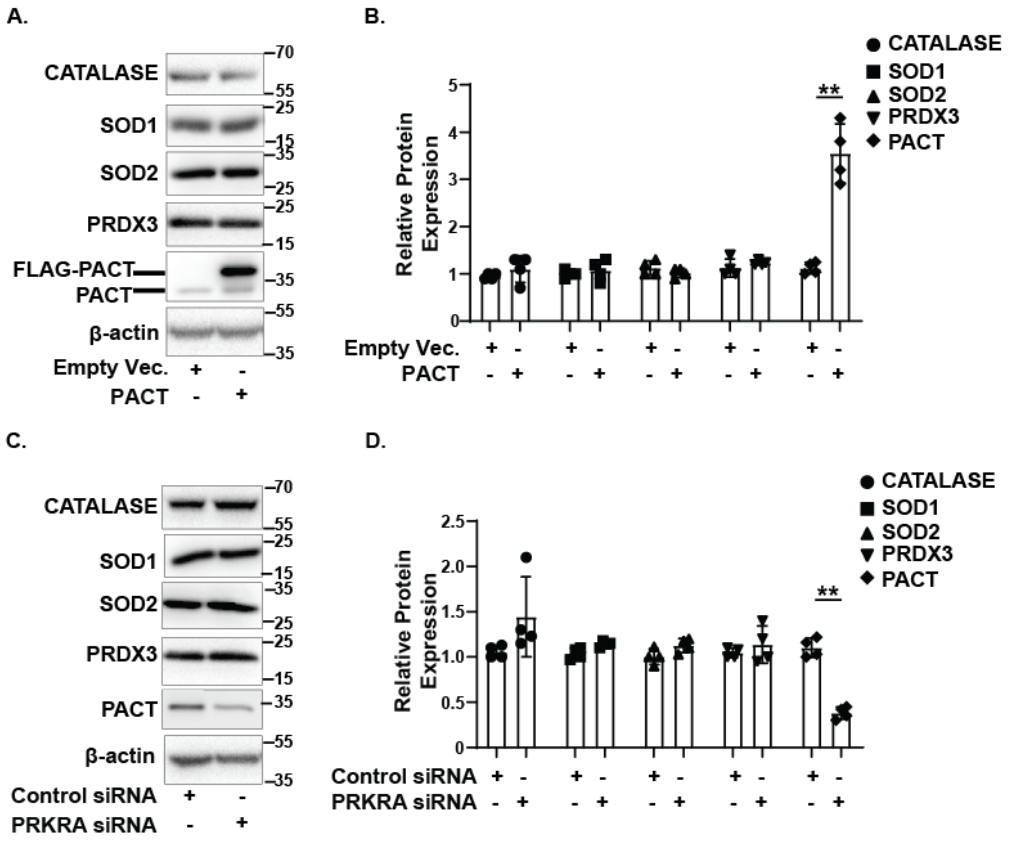

Figure 3.17 PACT does not affect cytosolic or mitochondrial ROS metabolizing enzymes. (A-B) HEK293-T cells transfected with 100 nM PACT siRNA for 24 hours. Protein levels of Catalase, SOD1 & 2, PRDX3, PACT and β-actin were analyzed by western blotting using specific antibodies and quantified against β-actin. **(C-D)** HEK293-T cells transfected with WT-PACT for 24 hours. Protein levels of Catalase, SOD1 & 2, PRDX3, PACT and β-actin were analyzed by western blotting using specific antibodies and quantified against β-actin. Data are mean ± SEM. Unpaired *t*-test with Welch's correction. *P≤ 0.05, **P≤ 0.01, ***P≤ 0.001.

3.3.8. PACT is not involved in mitophagy pathway

Maintaining mitochondrial homeostasis is an interplay between clearing old/damaged mitochondria and producing new/functional mitochondria. Adapter-mediated mitophagy is facilitated by phosphatase and tensin homolog (PTEN)-induced putative kinase 1 (PINK1), as well as E3 ubiquitin ligase Parkinson juvenile disease protein 2 (Parkin), where it

ubiquitinates the target. Damage to mitochondria or a reduction in the mitochondrial membrane potential triggers PINK1 to stabilize to the mitochondria and consequently recruitment of Parkin, which ubiquitinates the outer mitochondrial proteins. Ubiquitinated targets are recognized via autophagy adapters p62 and OPTINEURIN to enable their recognition and degradation by LC3 mediated autophagosome. Therefore, the role of PACT in Parkin-dependent mitophagy was also investigated. Here, I observed no significant changes in the recruitment of Parkin or p62 to mitochondria, degradation of OPTINEURIN or a change in levels of LC3A/B, in cells either overexpressing or deficient for PACT. Moreover, PACT had no impact on mitochondrial uncoupler carbonyl cyanide m-chlorophenylhydrazone (CCCP) induced mitophagy or the autophagic flux (Fig. 3.18A-D). This finding supports that PACT is not involved in the removal of mitochondria but controls new mitochondria production.

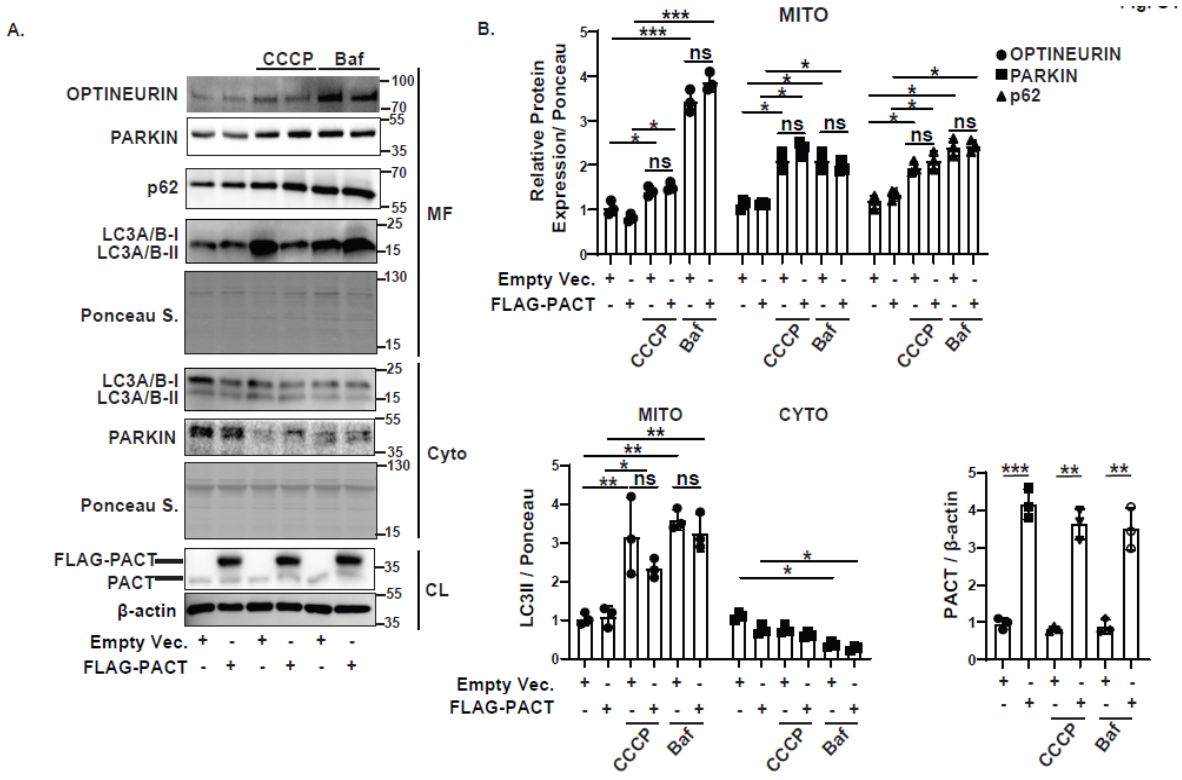

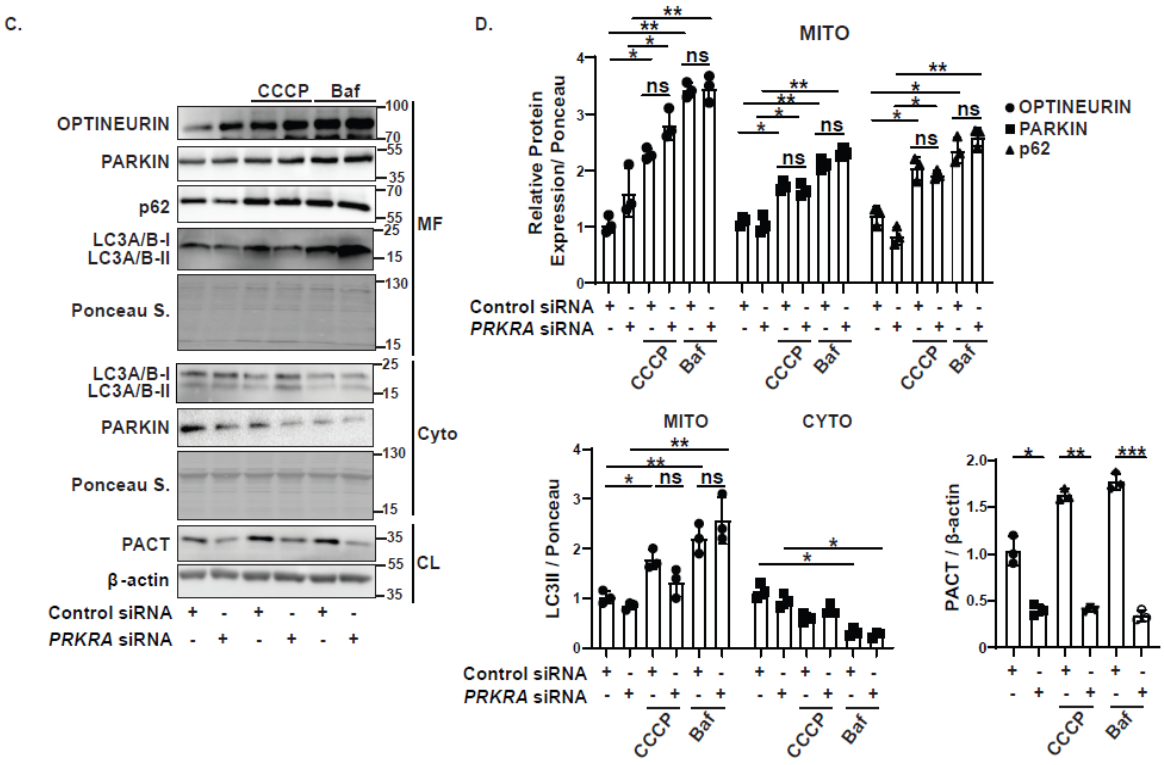

Figure 3.18 PACT does not regulate mitophagy. (A) Protein lysates from HEK293T cells that were transfected with empty vector (Empty Vec.) or FLAG-PACT plasmid and treated with CCCP (10µM; 16 hrs) or Bafilomycin A1 (Baf) (50nM; 16 hrs) were analyzed by Western blotting using specific antibodies for Optineurin, Parkin, p62, LC3A/B, PACT and β-actin (n=3). **(B)** Quantification of the band intensities in (A): Optineurin, Parkin, p62 and LC3-II relative to Ponceau S. and PACT relative to β-actin (n=3). **(C)** Protein lysates from HEK293T cells that were transfected with 100 nM Scrambled or *PRKRA* siRNA and treated with CCCP (10µM; 16 hrs) or Bafilomycin A1 (50nM; 16 hrs) were analyzed by Western blotting using specific antibodies for Optineurin, Parkin, p62, LC3A/B, PACT and β-actin (n=3) **(D)** Quantification of band intensities in (C): Optineurin, Parkin, p62 and LC3-II relative to Ponceau S. and PACT relative to β-actin (n=3).Unpaired *t*-test with Welch's correction. *P≤ 0.05, **P≤ 0.01, ***P≤ 0.001, ns: not significant. MF: Mitochondrial fraction, CL: Cell lysate.

3.4. PACT suppresses mitobiogenesis through miR-181c

3.4.1. PACT regulates maturation of miR-181c

Next step was to investigate how PACT regulates mitobiogenesis. Through its association with RISC, PACT can regulate the maturation of specific miRs (214). Prior results of this thesis showed that PACT regulates the expression of PGC1α, TFAM, NRF1 and MTCO1 proteins. My analysis of the 3'UTR of these PACT targets pointed out that miR181c could targets Tfam, Nrf1, Mtco1, Cox11 and 15 as well as a Pgc1α upstream regulator, Sirt1 (Fig.3.19A). Multiple studies have shown that miR-181 family members (miR-181a/b/c/d), which share the same seed sequence, regulate mitochondria through targeting MTCO1 and SIRT1 (123, 124, 127, 128, 219). Therefore, I turned my attention to miR-181 family as a potential mediator of PACT's role in mitobiogenesis regulation. In $Prkra^{-/-}$ MEFs, WT-PACT reconstitution significantly induced mature miR-181c levels (Fig.3.19B). Pre-miR-181c was significantly reduced by WT-PACT reconstitution, suggesting PACT regulates mature miR-181c maturation (Fig.3.19C). Other miR-181 family members were not significantly regulated in both no stress and ER stress conditions (Fig.3.19D). Similarly, siRNA-mediated PACT knock-down in HEK293T cells reduced miR-181c expression while increasing pre-miR-181c levels (Fig.3.19E-G). I next investigated the consequences of IRE1-mediated PACT phosphorylation on miR-181c expression. Whereas reconstitution of $Prkra^{-/-}$ MEFs with WT-PACT significantly induced miR-181c levels, reconstitution with Mut-PACT did not. This result demonstrates IRE1-mediated PACT phosphorylation induces miR-181c expression in cells (Fig.3.19H).

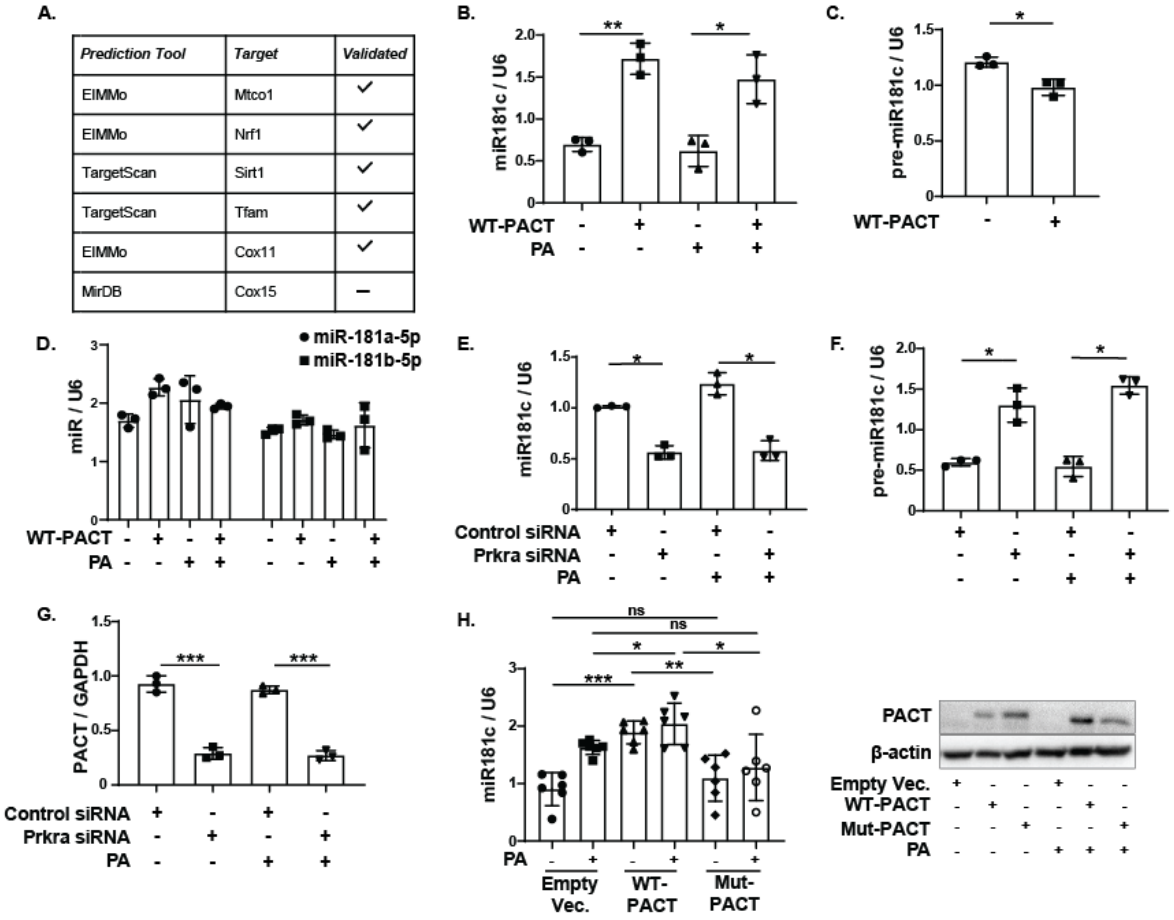

Figure 3.19 WT-PACT but not Mut-PACT regulates maturation of miR-181c. (A) List of mitochondrial targets of miR-181. **(B-C)** Prkra $^{-/-}$ MEFs transfected with empty vector or WT-PACT and treated with PA (500 μM; 3 hours). RNA extracts were analyzed by qRT-PCR to determine **(B)** miR-181c and RNA, U6 small nuclear RNA (U6) and **(C)** pre-miR-181c and U6 RNA expression (n=4). **(D)** Prkra$^{-/-}$ MEFs reconstituted with WT-PACT were treated with PA (500 μM; 3 hours). Total RNA was analyzed by qRT-PCR for miR-181a, miR-181b, and U6 by qRT-PCR (n=3).**(E-F)** HEK293T cells were transfected with Prkra or control siRNA and treated with PA (500 μM; 3 hours). RNA extracts were analyzed by qRT-PCR for **(E)** miR-181c and U6 RNA and **(F)** pre-miR-181c and U6 RNA expression (n=3). **(G)** PRKRA and GAPDH expression (n=3). **(H)** Prkra $^{-/-}$ MEFs were transfected with empty vector (Empty Vec.), WT-PACT or Mut-PACT and treated with PA (500 μM; 3 hours). Total RNA extract was analyzed with qRT-PCR for miR-181c and U6 RNA expression and PACT levels are analyzed by Western Blotting to confirm transfection (n=6). Data are mean ± SEM. Unpaired *t*-test with Welch's correction or one-way ANOVA. *P≤ 0.05, **P≤ 0.01, ***P≤ 0.001.

To test the effect of PACT on premiR-181c processing by DICER, I performed an *in vitro* DICER cleavage assay. In this reaction, product miR-181c levels were higher when PACT was in the reaction compared to DICER only condition, confirming that DICER requires PACT to optimally facilitate the maturation of premiR-181c (Fig.3.20A). Altogether, these results show that PACT expression controls cellular levels of miR-181c, a miRNA implicated in mitobiogenesis regulation.

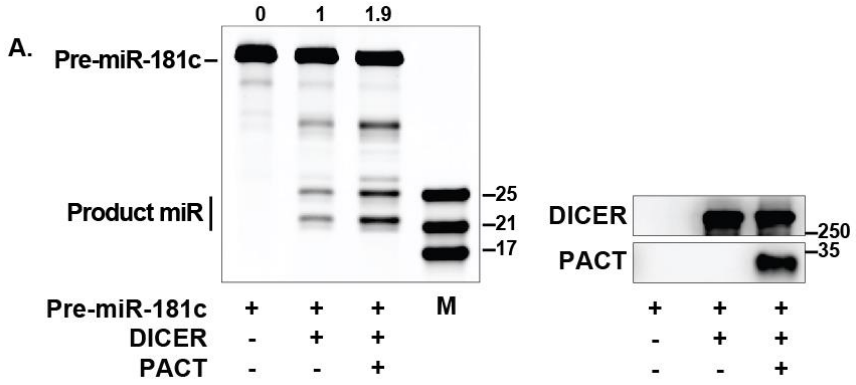

Figure 3.20 PACT impacts DICER cleavage of pre-miR-181c. (A) Left panel: DICER cleavage assay performed using synthetic pre-miR-181c (10 uM) as substrate with recombinant DICER or PACT (0.2 ug) at 37°C for 4 hours. Samples are separated in 15% Urea-PAGE and detected with SYBR gold staining. M indicates microRNA marker. Average band intensity for the mature miR product is indicated at top. Right panel: 5 uL of same samples were spared to confirm DICER and PACT levels by Western blotting (n=3).

3.4.2. miR-181c is also a suppressor of mitobiogenesis

Since PACT regulates miR-181c levels, I next sought confirmation that miR-181c can suppress mitobiogenesis. Transfection of miR-181c mimic into HEK293T cells decreased the expression of mitobiogenesis regulators, PGC1α, TFAM, NRF1, MTCO1 and SIRT1, while simultaneously reducing mtDNA copy number (Fig.3.21A-B). Additionally, miR-181c mimic decreased mitochondrial OCR (Fig.3.21C). On the other hand, inhibiting miR-181c with an antagomiR transfected into WT MEF cells resulted in higher PGC1α, TFAM, MTCO1, NRF1 and SIRT1 protein and mRNA levels while simultaneously induction in mtDNA copy number (Fig.3.21D-E). miR-181c antagomiR also increased OCR (Fig.3.21F).

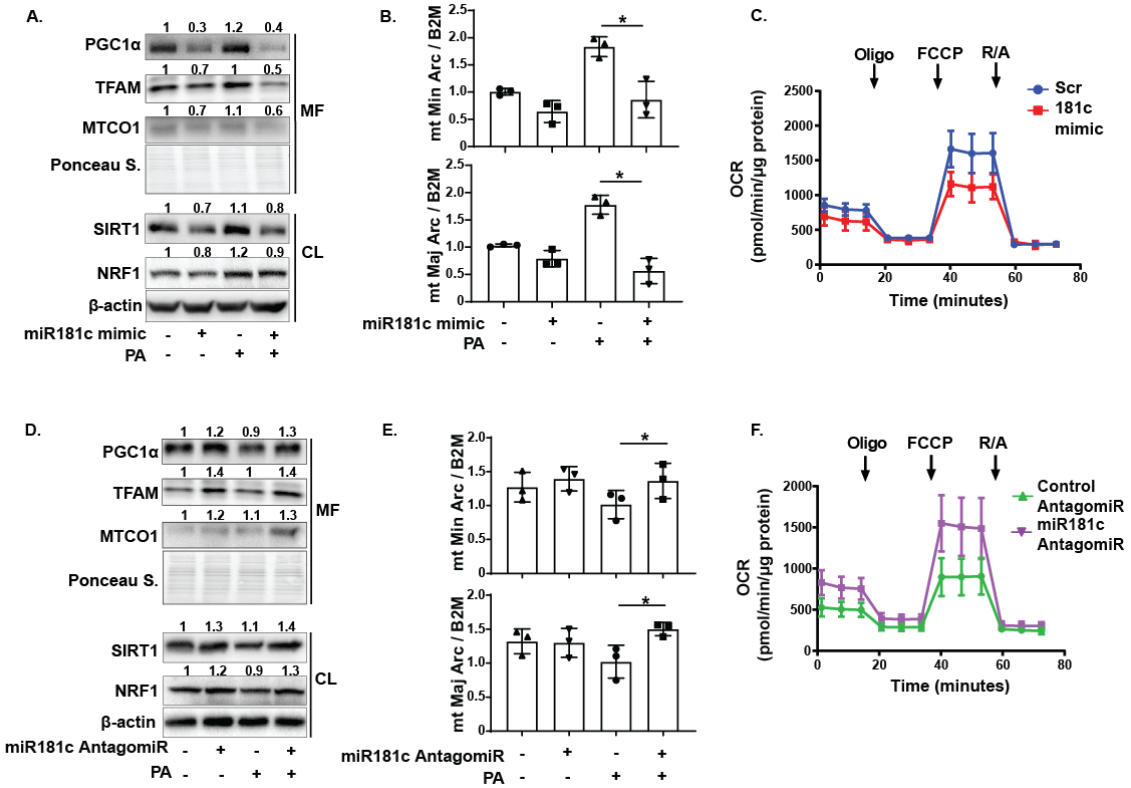

Figure 3.21 miR-181c blocks mitochondrial biogenesis and oxygen consumption. (A-B) HEK293T cells were transfected with miR-181c mimic (100 nM) and treated with PA (500 µM; 3 hours) (n=3). **(A)** The mitochondria enriched fraction (MF) and total cell lysates

(CL) proteins were analyzed by Western blotting using specific antibodies for PGC1α, TFAM, antibody cocktail against ETC proteins, SIRT1, NRF1 and β-actin. **(B)** Total genomic DNA was analyzed by qRT-PCR to determine mtDNA: nucDNA ratio (mitochondrial Major Arc (mt MajArc) and mitochondrial minor Minor Arc (mtMinArc) for mtDNA and Beta-2-Microglobulin (B2M) for nucDNA) (n=3). **(C)** $Prkra^{+/+}$ MEFs were transfected with miR-181c-5p mimic (100 nM) and mitochondrial respiration was analyzed by Seahorse Mitochondrial Stress test. Arrows indicate time for drug injections (n=5). **(D-F)** HEK293T cells were transfected with miR-181c AntagomiR (100 nM) and treated with PA (500μM; 3 hours). **(D)** MF and CL protein lysates were analyzed by Western blotting using specific antibodies for PGC1α, TFAM, antibody cocktail against ETC proteins, SIRT1, NRF1 and β-actin (n=3). **(E)** Total genomic DNA was analyzed by qRT-PCR to determine mtDNA: nucDNA ratio (mt Maj Arc, mtMinArc for mtDNA and B2M for nucDNA) (n=3). **(F)** Mitochondrial respiration was analyzed by Seahorse Mito Stress test. Arrows indicate time for drug injections (n=5). Data are mean ± SEM. Unpaired *t*-test with Welch's correction or one-way ANOVA. *P≤ 0.05, **P≤ 0.01, ***P≤ 0.001.

Finally, miR-181c mimic transfection into $Prkra^{-/-}$ MEFs significantly reduced mtDNA copy number, which is induced by PACT deficiency in these cells (Fig.3.22A-C). These findings confirm that PACT-miR181c axis inhibits mitobiogenesis in mouse and human cells.

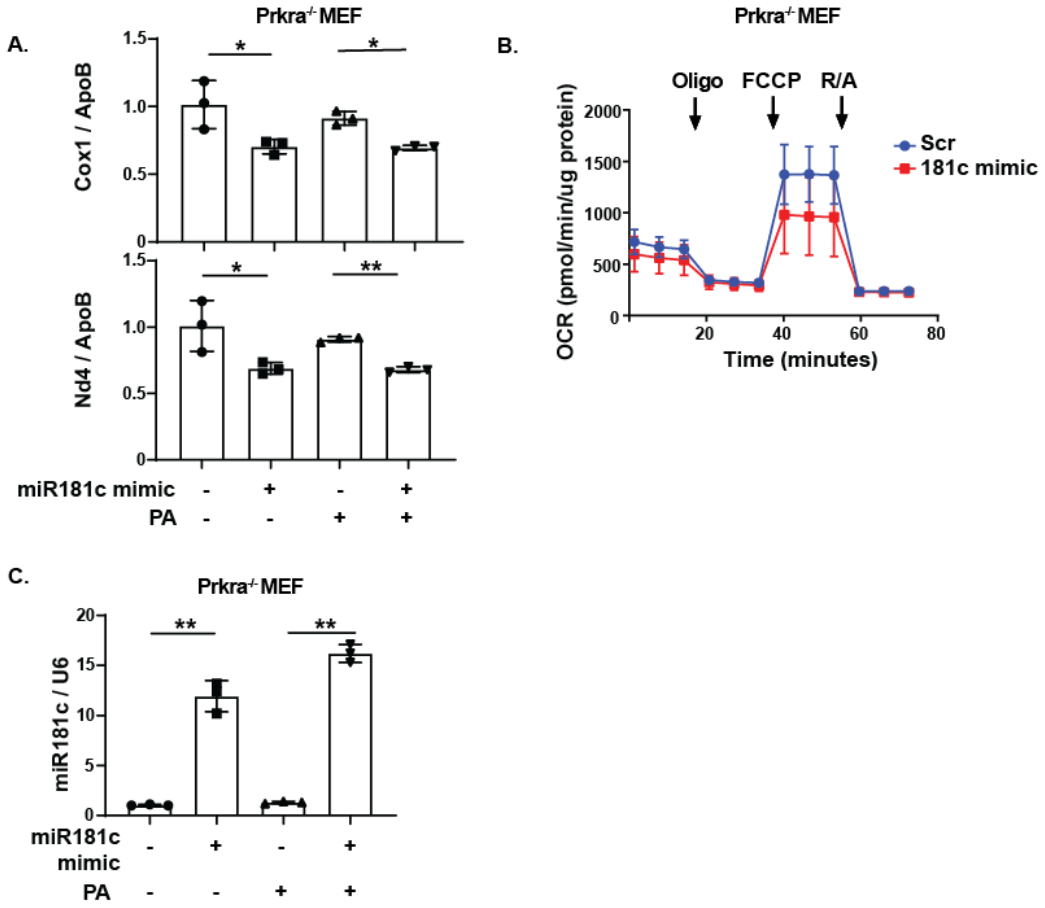

Figure 3.22 miR-181c blocks mitochondrial biogenesis and oxygen consumption. (**A)** miR-181c mimic (100 nM) transfected Prkra$^{-/-}$ MEF cells that were treated with PA (500 µM; 3 hours) and mtDNA:nucDNA ratio was analyzed by qRT-PCR from total genomic DNA (Cox1 and Nd4 for mtDNA and ApoB for nucDNA) (n=3). **(B)** Mitochondrial respiration was analyzed by Seahorse Mito Stress test from same experimental set in panel A. Arrows indicate time for drug injections (n=5). **(C)** miR-181c mimic (100 nM) transfected Prkra$^{-/-}$ MEF cells that were treated with PA (500 µM; 3 hours) and miR-181c and U6 levels were analyzed by qRT-PCR from total RNA (n=3). Data are mean ± SEM. Unpaired *t*-test with Welch's correction or one-way ANOVA. *P≤ 0.05, **P≤ 0.01, ***P≤ 0.001.

3.5. Loss of PACT augments β_3-AR agonist-induced brown adipose mitobiogenesis

3.5.1. PACT is crucial for differentiated brown adipose cell mitobiogenesis and oxygen consumption

My findings show that PACT is a suppressor of mitobiogenesis and energetics in mouse and human cells. I next sought experimental evidence showing PACT can regulate mitobiogenesis *in vivo*. Since previous publications show adaptive response to cold stimulus results in a significant decrease in PACT expression in BAT, I decided to investigate the consequences of PACT-deficiency on mitobiogenesis during BAT activation (137, 138). I used a well-established pharmacologic approach to activate BAT with β_3-AR agonist, CL316,243 (217, 220). First, I compared the mitochondria from differentiated brown adipocytes collected from $Prkra^{+/-}$ and $Prkra^{+/+}$ mice. The partial loss of PACT enhanced the expression of proteins that control mitobiogenesis and increased mtDNA copy number (Fig.3.23A-C). Brown adipocytes from $Prkra^{+/-}$ mice were also respiring more efficiently and showed more induction in oxygen consumption after CL316,243 injection in the mitochondria stress test, when compared to brown adipocytes from $Prkra^{+/+}$ mice (Fig.3.23D-E). These findings show that partial PACT loss-of-function in brown adipocytes leads to an induction in mitobiogenesis parallel with increased mitochondrial respiration.

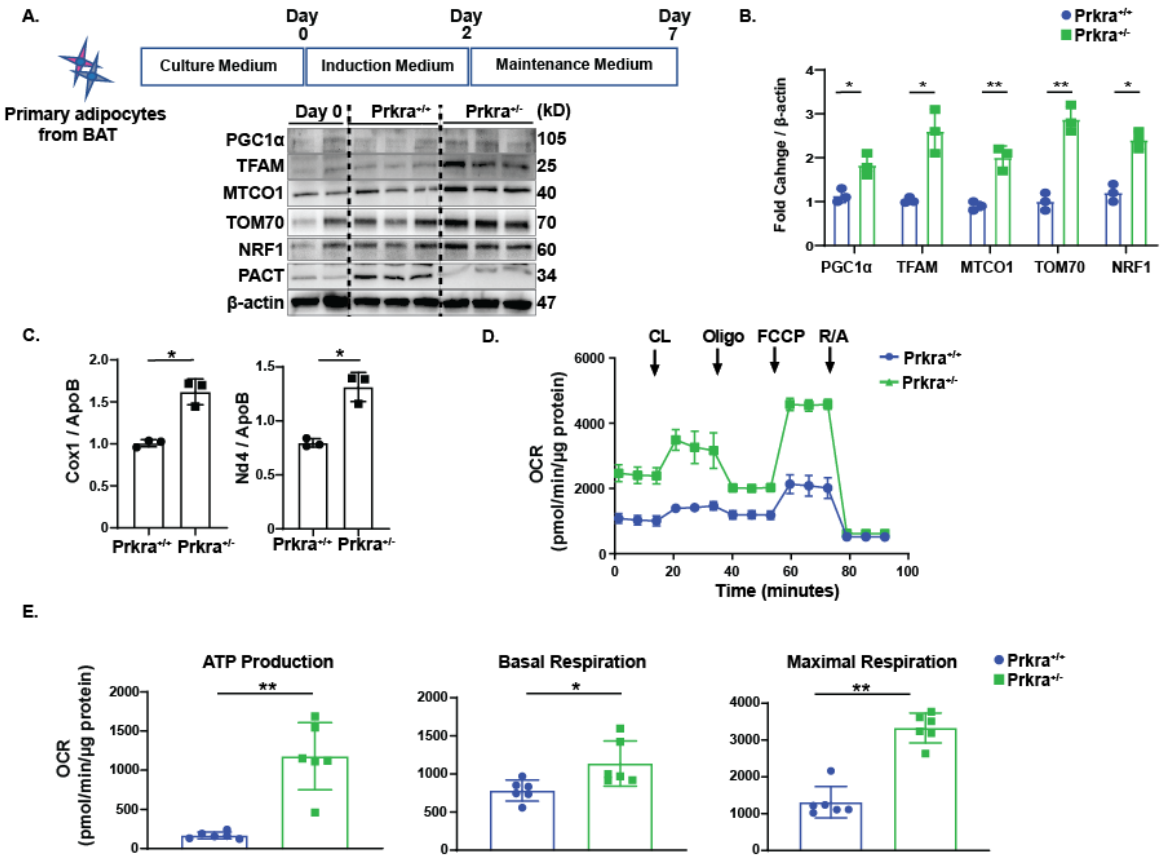

Figure 3.23 PACT is important for brown adipocyte mitobiogenesis and respiration. **(A)** Schematic representation of primary brown adipocyte differentiation protocol (upper panel). Mitochondrial protein levels were analyzed from protein lysates of undifferentiated (Day 0) or differentiated Prkra$^{+/+}$ or Prkra$^{+/-}$ brown adipocytes by Western blotting using specific antibodies for PGC1α, TFAM, antibody cocktail against ETC proteins, TOM70, NRF1 and β-actin (n=3). **(B)** The quantification of band intensities for PGC1α, TFAM, MTCO1, TOM70 and NRF1 relative to β-actin for panel A. **(C)** The genomic DNA obtained from differentiated brown adipocytes in (A) was analyzed by qRT-PCR for mtDNA: nucDNA ratio (n=3). **(D)** Mitochondrial respiration was analyzed by Seahorse Mitochondrial Stress test in differentiated Prkra$^{+/+}$ or Prkra$^{+/-}$ brown adipocytes (n=6). **(E)** Related to panel D: ATP production after oligomycin (Oligo; 1 µM) injection, Maximal respiration (as the highest OCR after FCCP injection; 1 µM) and Basal Respiration (as OCR before oligomycin injection) calculated from Prkra$^{+/+}$ or Prkra$^{+/-}$ brown adipocytes (n=5). Data are mean ± SEM. Unpaired *t*-test with Welch's correction or one-way ANOVA. *P≤ 0.05, **P≤ 0.01, ***P≤ 0.001.

3.5.2. In-vivo brown adipose tissue activation and related mitobiogenesis is more pronounced in Prkra$^{+/-}$ mice

To induce brown adipose activation and mitobiogenesis *in vivo*, I used 1mg/kg/day CL316,243 injection for 6 days. BAT isolated from these mice revealed that CL316,243-induced mitobiogenesis and UCP1 protein levels were more pronounced in Prkra$^{+/-}$ mice in comparison to Prkra$^{+/+}$ mice (Fig.3.24A). The mtDNA copy number was also significantly higher in Prkra$^{+/-}$ BAT (Fig.3.24B). Consistent with the observed PACT-dependent regulation of miR-181c expression, miR-181c levels were significantly downregulated in Prkra$^{+/-}$ BAT when compared to Prkra$^{+/+}$ BAT (Fig.3.24C). The histological analysis of BAT did not reveal any morphological differences between the genotypes (Fig.3.24D).

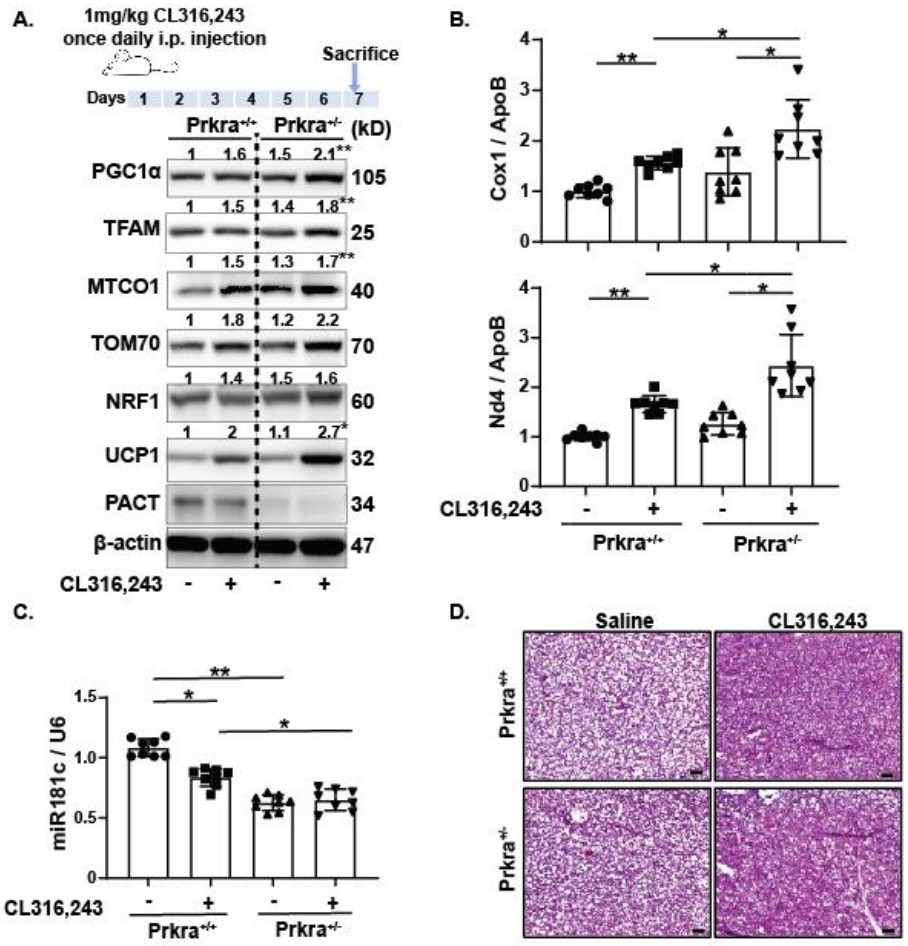

Figure 3.24 PACT is involved in brown adipose tissue mitobiogenesis. (A) Prkra$^{+/+}$ or Prkra$^{+/-}$ mice were injected with CL316,243 (1mg/kg/day) for 6 days and sacrificed 24 hours after the final injection (n=8). BAT protein lysates were analyzed by Western blotting using specific antibodies for PGC1α, TFAM, antibody cocktail against ETC proteins, TOM70, NRF1, UCP1 and β-actin. **(B)** mtDNA: nucDNA ratio was analyzed by qRT-PCR from total genomic DNA. **(C)** Total BAT RNA extracts were analzyed by qRT-PCR for miR-181c and U6 levels. **(D)** Representative H&E stained images of BAT (n=8) (Scale bar = 50 μm). Data are mean ± SEM. Unpaired *t*-test with Welch's correction or one-way ANOVA. *P≤ 0.05, **P≤ 0.01, ***P≤ 0.001.

3.5.3. Energy expenditure of Prkra$^{+/-}$ mice is higher compared to Prkra$^{+/+}$ mice

To assess the metabolism of these mice, I performed indirect calorimetry test on Prkra$^{+/-}$ and Prkra$^{+/+}$ mice placed in metabolic cages. I measured energy expenditure, oxygen consumption and respiratory exchange ratio (RER) for a duration of 48 hours. Prkra$^{+/-}$ mice showed significantly higher energy expenditure, during both light and dark cycles of the day. This was also reflected in the increased oxygen consumption and RER (Fig.3.25A-C), Together, these data show that mitobiogenesis upregulation due to the partial loss of PACT protein is paired with higher metabolic rates in these animals. Furthermore, RER was significantly higher in Prkra$^{+/-}$ mice during the dark cycle, which indicates Prkra$^{+/-}$ mice rely more on carbohydrate metabolism rather than fat utilization (Fig.3.25D). Importantly, these mice did not differ in their food and water intake, physical activity, or lean and fat mass (Fig.3.25D-F). Collectively, these results show that PACT plays a critical role in β_3-AR-stimulated BAT activation and subsequent increase in energy expenditure *in vivo*.

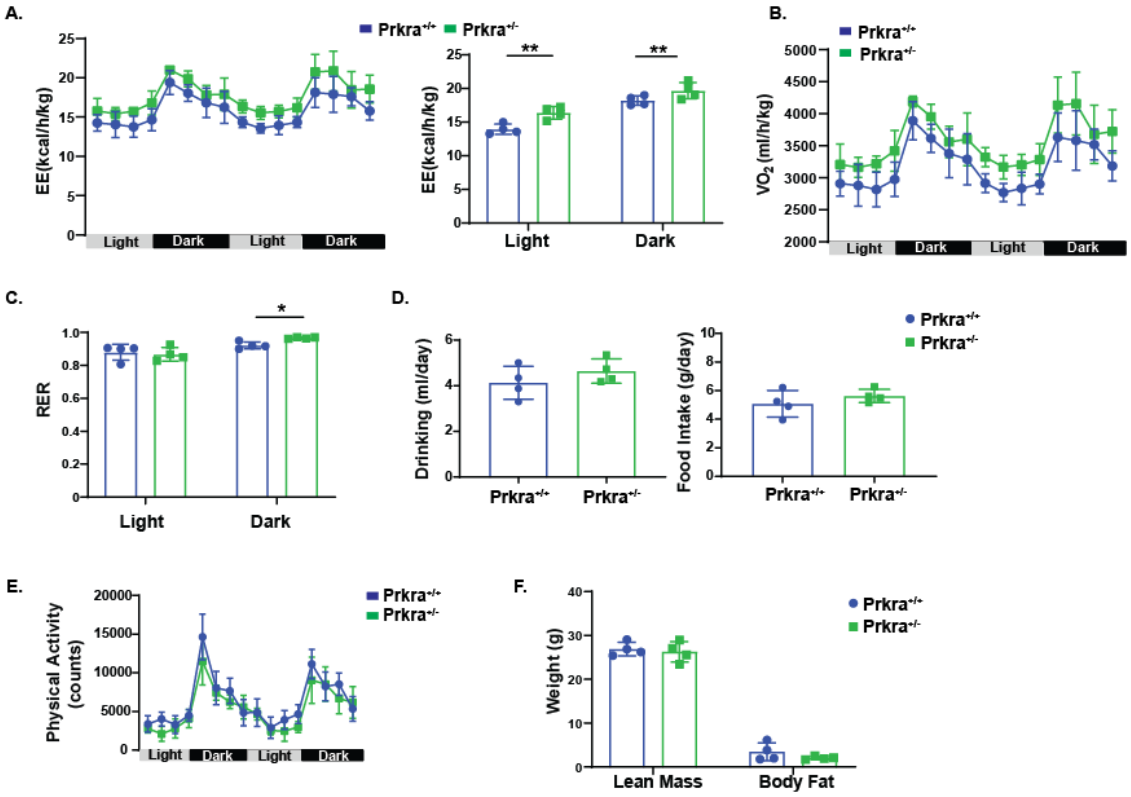

Figure 3.25 Partial PACT loss increases energy expenditure and oxygen consumption in mice. (A-C) Metabolic parameters of Prkra$^{+/+}$ or Prkra$^{+/-}$ animals (n=4): **(A)** Energy expenditure (EE), **(B)** oxygen consumption (VO_2) and **(C)** Respiratory exchange ratio (RER). (**D**) The water and food intake, **(E)** physical activity**, (F)** lean and fat mass of mice in Fig.4 (n=4). Data are mean ± SEM. Unpaired *t*-test with Welch's correction or one-way ANOVA. *P≤ 0.05, **P≤ 0.01, ***P≤ 0.001.

3.5.4. PACT is not involved in iWAT activation and mitobiogenesis

Exploration of PACT's impact on mitochondria in inguinal white adipose tissue (iWAT) was also important, as this tissue has the capacity of expanding their mitochondria (beigeing) under cold or β_3-AR stimulation (217). In both iWAT-derived, differentiated adipocytes and the iWAT from CL316,243 injected mice, there was no significant differences in mitobiogenesis (Fig.3.26A-B). Collectively, these findings show that PACT's regulatory role in β_3-AR-stimulated mitobiogenesis is specific to BAT.

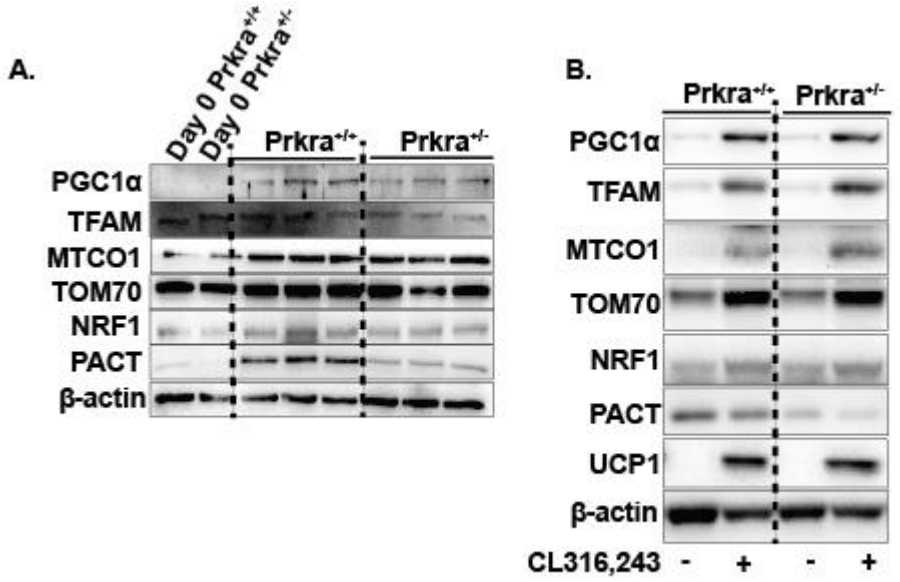

Figure 3.26 PACT is not involved in iWAT mitobiogenesis. (A) Total cell protein lysate of undifferentiated (Day 0) or differentiated iWAT adipocytes from Prkra$^{+/+}$ or Prkra$^{+/-}$ mice were analyzed by Western blotting using specific antibodies for PGC1α, TFAM, OXPHOS, TOM70, NRF1, PACT and β-actin (n=3). (**B)** The total protein lysates from iWAT of Prkra$^{+/+}$ or Prkra$^{+/-}$ animals that were injected with saline or CL316,243 (1mg/kg/day) were analyzed by Western blotting using antibodies specific for PGC1α, TFAM, OXPHOS, TOM70, NRF1, PACT, UCP1 and β-actin (n=8). Data are mean ± SEM. Unpaired *t*-test with Welch's correction or one-way ANOVA. *P≤ 0.05, **P≤ 0.01, ***P≤ 0.001.

3.6. Ablation of IRE1 alone is not sufficient to upregulate mitobiogenesis

I also investigated whether IRE1 is directly involved in regulation of mitochondrial biogenesis or mtDNA copy number. To achieve this, IRE1's kinase activity was inhibited with AMG-18 or RNase activity was inhibited with 4μ8C. Inhibition of either activity did not significantly regulate PGC1α, TFAM or TOM70 protein levels, as well as mtDNA copy number (Fig3.27A-B). Supporting these results, genetic deletion of IRE1 with siRNA also did not result in a significant change in PGC1α, TOM70 or ETC subunit protein levels (Fig3.27C). These findings rule out a direct involvement of IRE1 in regulating mitochondrial dynamics itself, but more likely through its kinase substrates and downstream signaling.

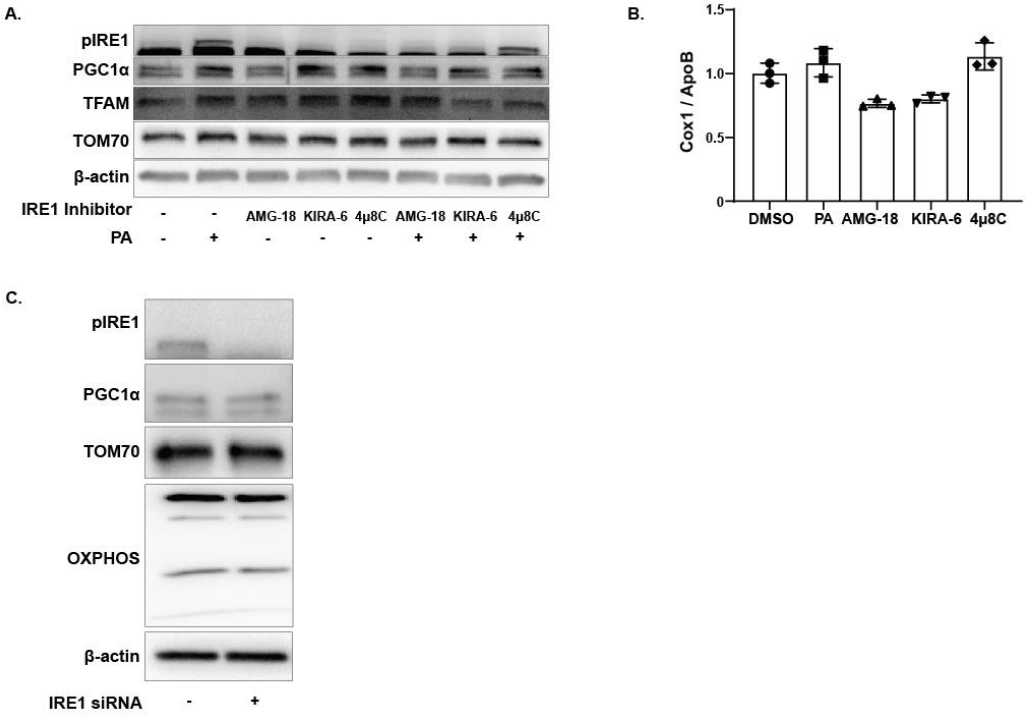

Figure 3.27 Ablation of IRE1 or its kinase activity is not sufficient to induce mitobiogenesis. (A-B) WT MEF cells were pre-treated (1 hour) with vehicle (DMSO), KIRA-6 (10 μM) or AMG-18 (5 μM) followed by PA (500μM; 3 hours). **(A)** The protein lysates were analyzed by Western blotting using specific antibodies for pIRE1, PGC1α, TFAM, TOM70 and β-actin (n=3). **(B)** The total genomic DNA was analyzed by qRT-PCR for mtDNA: nucDNA ratio (Cox1 for mtDNA and ApoB for nucDNA) (n=3). **(C)** MEF cells treated with IRE1 siRNA (100 nM) for 24 hours. Protein lysates were analyzed by Western blotting using specific antibodies against pIRE1, PGC1α, TOM70, antibody cocktail against ETC proteins and β-actin (n=3). Data are mean ± SEM. Unpaired *t*-test with Welch's correction or one-way ANOVA. *P≤ 0.05, **P≤ 0.01, ***P≤ 0.001.

3.7. IRE1- dependent miR expression changes during ER-stress

RNA isolated from these BMDMs was analyzed for changes in miRNAs' differential expression using a microarray platform and the PA upregulated miRNAs in $IRE1^{+/+}$ are shown along with their corresponding levels in $IRE^{-/-}$ cells (Fig.3.28A). Based on this analysis, miR-2137 was the highest, induced miRNA by PA in $IRE1^{+/+}$ BMDMs. A smaller, but not significant, induction of miR-2137 was observed in the $IRE1^{-/-}$ BMDMs. IRE1-dependent upregulation of miR-2137 by PA in these cells by qRT–PCR was further confirmed (Fig.3.28B). These results show that IRE1 RNase activation leads to a significant increase in miR2137 expression in BMDMs.

A.

Micro RNA up-regulated by palmitate treatment		
	$IRE1^{+/+}$	$IRE1^{-/-}$
miRNA	Fold Change (Log2)	Fold Change (Log2)
mmu-miR-2137	2.08	NS
mmu-miR-12197-3p	1.3	1.5
mmu-miR-6937-5p	1.16	NS
mmu-miR-762	1.15	NS
mmu-miR-5126	0.86	NS
mmu-miR-3963	0.55	NS
mmu-miR-7a-5p	0.51	NS
mmu-miR-7b-5p	0.44	NS
mmu-miR-23-3p	0.12	NS

B.

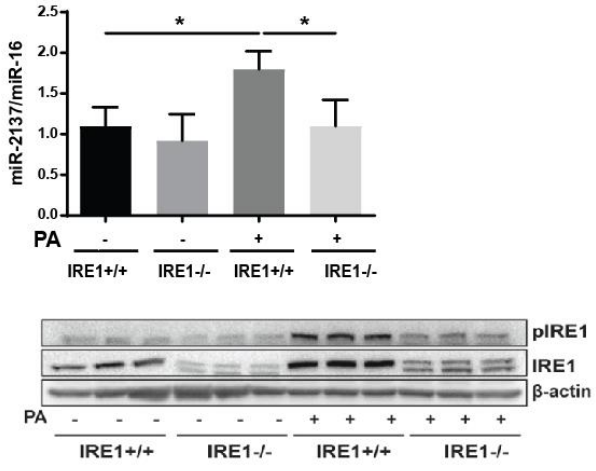

Figure 3.28 IRE1-dependent changes in miRNA expression in ER-stress. (A-B) $IRE1^{-/-}$ and $IRE1^{+/+}$ BMDMs were treated with PA (500 µM) or vehicle for 6 h prior to RNA isolation for miRNA analysis using a microarray platform. **(A)** Table showing fold change (log2) of statistically significant (P-value < 0.050) top PA-upregulated miRNAs in $IRE1^{+/+}$ and $IRE1^{-/-}$ cells. NS indicates microRNAs that did not show statistically significant difference. Fold change was calculated by comparing mean intensity values of microarray signal for vehicle treatment with PA treatment (n = 3). **(B)** Top panel: RNA lysates from the same experiment were analyzed by qRT–PCR for miR-2137 expression. Bottom panel: Protein lysates from the same experiment were analyzed by Western blotting for pIRE1 and IRE1 levels. All data are mean ± SEM (n = 3); unpaired t-test with Welch's correction; *P ≤ 0.05).

Upon observing co-regulation of miR-2137 and IRE1 RNase activity by lipids, next step was to investigate whether IRE1 is directly involved in the regulation of miR-2137 expression. For this, cells were transfected with a silencer RNA (siRNA) specific for IRE1 and treated with PA (6 or 9 h). Suppression of IRE1 expression significantly reduced PA-induced miR-2137 expression (Fig.3.29A). Additionally, the IRE1 RNase inhibitor, 4µ8c, significantly reduced both PA-induced miR-2137 expression (Fig3.29B).

These findings led to the intriguing possibility that IRE1's RNase activity may be directly involved in the cleavage of pre-miR-2137 and promote its maturation to miR-2137. This question was approached by designing an in vitro cleavage experiment using recombinant IRE1 and synthetic pre-miR-2137 in RNase cleavage buffer. In this reaction, only the active form of recombinant IRE1 cleaved pre-miR-2137, resulting in an RNA fragment that corresponds to the mature-sized miR-2137 (Fig.3.29C). These findings show IRE1 can directly cleave pre-miR-2137 and produce a mature-sized miR-2137 product.

IRE1 RNase activity's impact on miR-2137 regulation was further confirmed by using $IRE1^{-/-}$ MEFs. PA treatment led to a smaller increase in miR-2137 levels in the $IRE^{-/-}$ MEFs, suggesting other factors also contribute to miR-2137 expression in fibroblasts. However, reconstitution with wild type (WT) IRE1, but not with an RNase-dead IRE1 (K907A) mutant, drove miR-2137 expression to a significantly higher level (Fig.3.29D). These results show that IRE1 amplifies ER-stress-induced miR-2137 expression in both BMDMs and MEFs. Furthermore, these data demonstrate that a functional IRE1 RNase domain is critical for miR-2137 induction by ER stress.

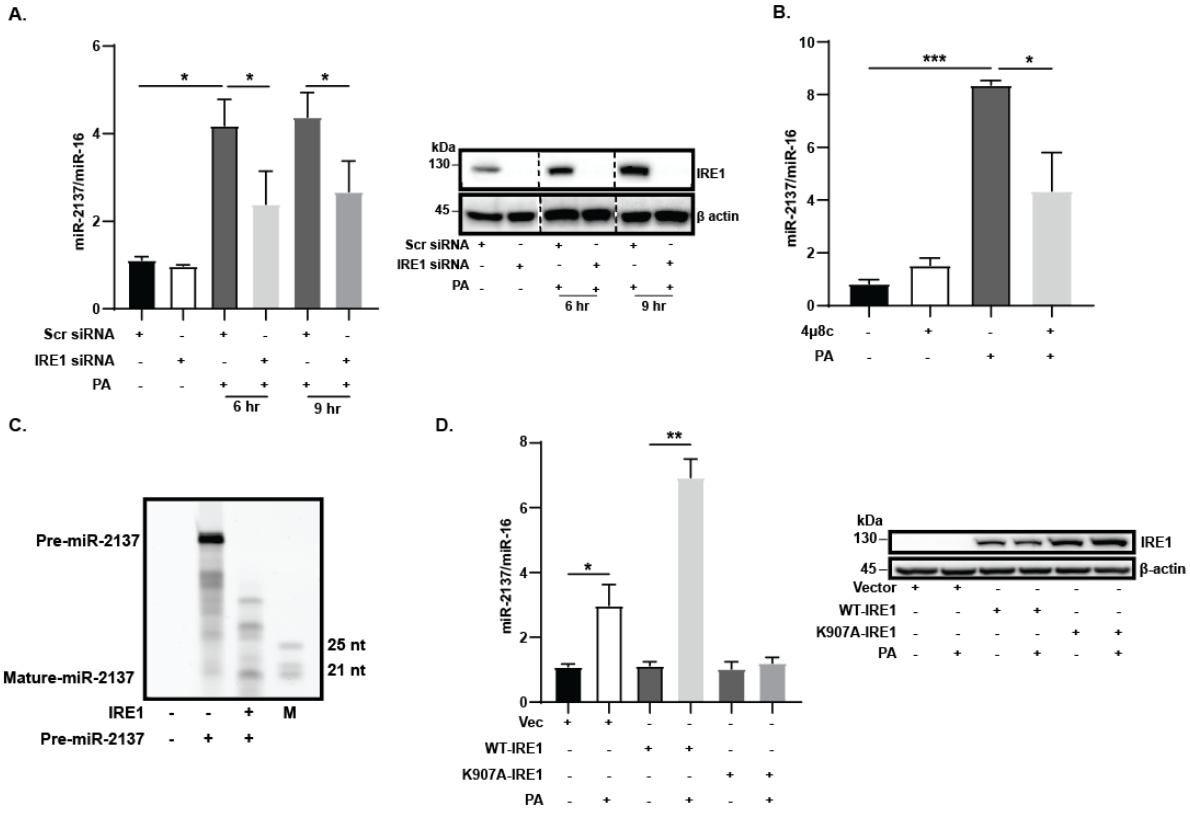

Figure 3.29 miR-2137 is regulated by IRE1 RNase activity. (A) Left panel: BMDMs were transfected with scrambled (Scr) or IRE1-specific siRNA (40 nM) and treated with palmitate (PA, 500 µM) or vehicle for 6 and 9 h. RNA lysates were analyzed by qRT–PCR for miR-2137 expression (n = 3). Right panel: Protein lysates from the same experiment analyzed by Western blotting for IRE1 levels (n=3). **(B)** BMDMs were treated with PA (500 µM) and 4µ8c (100 µM) or vehicle for 9 h. RNA lysates were analyzed by qRT–PCR for miR-2137 expression (n = 3). **(C)** IRE1 cleavage assay performed using synthetic pre-miR-2137 (50 nM) as substrate with active, recombinant IRE1 (100 ng) at 37°C for 2 h, followed by sample separation in Urea-PAGE and detection with SYBR gold staining. M indicates microRNA marker. **(D)** IRE1$^{-/-}$ MEFs were transfected with vector (control), WT-IRE1 or K907A-IRE1 (RNase-dead mutant) plasmids for 24 h, followed by PA (500 µM) treatment for 9 h. RNA lysates were analyzed by qRT–PCR for miR-2137 expression (n = 3). All data are mean ± SEM (n = 3); unpaired t-test with Welch's correction; *P ≤ 0.05).

CHAPTER 4. DISCUSSION

Mitochondria and ER cooperate and communicate (by exchanging calcium, reactive oxygen species, lipids and other metabolites) through membrane contact sites (221). In this study, I report a novel mode of inter-organelle communication between the ER and mitochondria independent of these contact sites. This novel mode of ER-to-mitochondria communication utilizes a small non-coding RNA, miR-181c, which is induced in response to IRE1-mediated PACT phosphorylation. These findings demonstrate that IRE1-mediated PACT phosphorylation, in part by controlling miR-181c expression, suppresses mitobiogenesis, mitochondrial respiration and ATP production. Moreover, this thesis work provides strong evidence supporting PACT is an inhibitor of mitobiogenesis in both mice and humans.

First, my findings demonstrate PACT is a novel substrate of IRE1 kinase. PACT is one of the many RNAbps that were implicated as interaction partners of IRE1 (150). Earlier studies that showed PACT gets phosphorylated on S18 and S287 upon ER stress have implicated PACT in UPR signaling. The ER stress-induced PACT phosphorylation was shown to lead to its dissociation from TRBP in the RISC (104, 105, 109). The kinase responsible for ER-stress induced phosphorylation of PACT had remained unknown. In this study, I was able to demonstrate that PACT and IRE1 kinase physically interact and IRE1 kinase can phosphorylate PACT on S18 and T20. Moreover, the data shows that IRE1 kinase activity is required for ER stress-induced PACT phosphorylation *in vivo*.

Second, findings of this thesis reveal an unprecedented role for IRE1 in regulating the mitochondrial life cycle through activating a PACT-mediated brake on mitobiogenesis. Prior studies have shown that the ER embraces mitochondria at membrane contact sites where mitochondrial division (fission) and fusion occurs (51, 222), demonstrating ER's involvement in mitochondrial dynamics. The dynamic changes in mitochondria shape through frequent fission and fusion is known to also support the generation of new

mitochondria through mitobiogenesis (223). Mitobiogenesis is a highly convoluted process, that requires mtDNA replication, and new mitochondrial protein synthesis and import (224, 225). Maintaining mitochondrial homeostasis is an interplay between clearing old and damaged mitochondria together with producing new and functional mitochondria (226). Findings of this thesis show that suppression of PACT expression removes a block on mitobiogenesis (as evident by the increase in the expression of key mitobiogenesis regulators, mtDNA copy number and mitochondrial mass) in both ER stressed and non-stressed cells. In PACT-deficient cells, mitochondrial oxygen consumption increased in parallel to the increase in mitochondrial mass. The increased mitochondrial respiration in PACT-deficient cells was coupled to increased ATP production, suggesting a much efficient functioning of electron transport chain complex subunits. Intriguingly, the mitochondria in Prkra$^{-/-}$ MEFs were very efficient in utilizing all available substrates to produce ATP, yet they did not display preference for a particular fuel type. These data show that PACT depletion enhanced mitochondrial energetics. Furthermore, supporting the functionality of IRE1-mediated PACT phosphorylation, mutating both IRE1-phospohorylation sites abolished PACT's control over mitochondrial replication. Therefore, these findings delineate a novel IRE1-PACT axis in the regulation of mitochondrial biogenesis.

Third, data of my work showed that PACT exerts its effect on mitochondria through regulating the expression of miR-181c. Several miR-181 family members were previously shown to target Sirt1 and Nrf1 and regulate mitobiogenesis, and Mtco1 and regulate mitochondrial oxygen consumption and ROS production (123, 124, 127, 128, 219). The miR-181 family has been implicated in mitochondrial disease, where inhibition of miR181a/b was shown to protect against mitochondria-induced neurodegeneration (127). In this study, I was able to show that PACT specifically induces the expression of miR-181c, likely through RISC-associated PACT's involvement at the maturation step of this miRNA. Similar to PACT, the inhibition of miR-181c expression increased mitobiogenesis, whereas its overexpression suppressed mitobiogenesis. Therefore, the impact of PACT can be, in part, explained by PACT-regulated miR-181c expression. The manipulation of miR-181c expression is not as potent as PACT on mitobiogenesis,

implying that more miRNAs or other PACT-regulated factors could be involved in the regulation of mitobiogenesis. Future comprehensive analysis of all miRNAs regulated by PACT will be useful to understand the full range of PACT's targets and role in mitochondrial biology.

Notably, while mutating IRE1-mediated phosphorylation of PACT ablates its ability to block mitobiogenesis, genetic depletion of IRE1 nor inhibition of its kinase activity alters mitobiogenesis (Fig.3.27). This indicates that there are redundant pathways (converging on PACT, miR181c expression, or further downstream in the mitobiogenesis program) can compensate for the lack of PACT phosphorylation by IRE1 kinase. For example, PERK mediates the induction of heme oxygenase-1 (HO-1) to transmit ER stress to the mitochondria and promotes mtDNA replication through NRF2 induction in macrophages (227). Additionally, PERK is phosphorylated and activated upon cold exposure (independent of ER stress) during brown adipocyte differentiation and promotes mitochondrial biogenesis (228). Future investigation regarding the redundancies of the three UPR arms in regulating mitobiogenesis can provide clarification. In summary, my data suggest that the existing small molecule strategies to modulate IRE1 kinase activity will not alter mitobiogenesis and that antisense technology to suppress PACT expression may be a better strategy to attempt to induce mitobiogenesis.

Fourth, my findings show that PACT-deficiency can induce mitobiogenesis *in vivo*, in the BAT tissue upon β_3-AR agonist-induced activation. In addition, a strong correlation of reduced PACT expression with mitobiogenesis induction in human cardiac tissue was observed (upon ischemia/reperfusion injury), which suggests that PACT's role as a suppressor of mitobiogenesis is conserved from mice to humans. Moreover, these *in vivo* results imply that PACT-regulated mitobiogenesis brake can come into effect in both physiological and pathological situations. Whether the same or different miRNAs mediate PACT's function in these tissues and contexts is not known. Future studies will be needed to clarify PACT's role in cardiac ischemia/reperfusion injury. Importantly, PACT's role in the pathophysiology in young onset, dystonia-parkinsonism disorder (dystonia 16) patients,

who bear mutations in the human PACT gene, is still unknown (229, 230). The mechanistic insight into PACT's role in mitobiogenesis regulation could explain the PACT-mediated defects in dystonias and other diseases that impact the mitochondrial energetics while simultaneously providing a novel therapeutic target to prevent such metabolic disturbances.

Findings of this thesis also showed an unprecedented, direct role for IRE1 RNase activity in the generation of miR-2137. In the canonical miRNA biogenesis pathway, pre-miRNA is cleaved in the cytoplasm by Dicer, which interacts with Ago2, TRBP and PACT in the RNA-induced silencing complex (RISC) (115, 231). While IRE1 does not associate with Dicer or Ago2, several other RNA binding proteins found in the RISC complex were shown to be in physical interaction with IRE1 in both non-stress and ER stress conditions, such as PACT (150). IRE1's direct involvement on miR maturation might be another explanation of why inhibition of kinase activity does not regulate mitobiogenesis, whether its kinase substrate PACT is a suppressor of this pathway. Data in this thesis showed that IRE1 might be implicated in miR cleavage and maturation, therefore can possible impact numerous miRs that are involved in mitobiogenesis regulation that have opposing effects. Future studies will be necessary to unearth the details of IRE1's complex interactions with these RNA binding proteins found in the miRNA biogenesis machinery and the consequences on miR biogenesis or miR-mediated expression changes in cells.

In summary, the findings of this thesis illuminate a novel, RNA-mediated inter-organelle communication that blocks mitobiogenesis. My findings strongly support that the IRE1-PACT-miR181c axis-induced mitobiogenesis brake operates in diverse tissues from mice to humans in both physiological and pathological contexts.

CHAPTER 5. FUTURE PERSPECTIVES

Throughout this project, I have shown that IRE1 phosphorylation of PACT is a mechanism to regulate maturation of miR-181c, that in turn causes a translational break on mitobiogenesis and this pathway is relevant to brown adipose tissue activation. Upon this observation, it is important to investigate the effects of IRE1 kinase activity and other possible kinase substrate's impact on brown adipose mitobiogenesis both *in vivo* and *in vitro*. Further, it is also crucial prove that PACT's regulation on mitobiogenesis is specific to brown adipose tissue but not other adipose tissue types. For this, a brown adipose specific PACT knock-out mice model should be stimulated with either CL-316,243 treatment or cold exposure to investigate mitobiogenesis and browning in BAT and iWAT. Since PACT is a RISC binding protein and is known to regulate miRNA maturation, exploration of all possible miRNA targets of PACT could be important to fully decipher the role of PACT in BAT activation and mitobiogenesis. From the same BAT specific PACT knock-out animals a miRNA sequencing would reveal multiple pathways downstream of IRE1-PACT interaction. Similarly, reconstitution of WT and Mut-PACT to BAT specific PACT knock-out animals would also prove that IRE1 phosphorylation on PACT is the key mechanism on regulating BAT activation *in vivo*.

To understand the exact mechanism behind PACT's regulation on mtROS release, a more comprehensive study should be done on ROS regulating enzymes. All possible enzymes that are catalyzing and reducing ETC byproducts should be screened where PACT is overexpressed or silenced. In my thesis, I have checked a few of such enzymes, however, there are various peroxisomal and mitochondrial antioxidant systems and pathways that scavenge intracellular ROS. Furthermore, one possible explanation of higher OCR and lower mtROS production is mitochondrial super-complex formation for ETC subunits. Complexes I and III and IV are known to form hetero- and homo-dimers to produce more ATP by requiring less electron transfer and consequently less ROS (232). Therefore, it

might be possible that PACT, through regulation of certain miRNAs, might be regulating mitochondrial super-complex formation.

Moreover, lipid stress activates UPR and via ER resident kinase and endoribonuclease IRE1. IRE1 has been previously studied in the context of inflammation, insulin resistance and atherosclerosis (186, 233). It is now known that IRE1 has a crucial role in regulation of atherogenic genes as well as macrophage polarization and these were all related to IRE1's RNase activity (186, 233). In this thesis study, I showed that PACT is a novel kinase substrate of IRE1, and IRE1-PACT axis regulated mitobiogenesis. Previous studies have also shown that high fat diet drives a decrease in genes that orchestrate mitobiogenesis and ROS metabolism during atherosclerotic plaque formation (234, 235). During atherosclerosis progression, ROS and mtDNA damage is increased, whereas mitochondrial energetics is suppressed. Intervention to suppress the elevated ROS production and mitochondrial dysfunction can result in alleviation of atherosclerosis (236). Moreover, literature also shows that ER-mitochondria communication is crucial for the clearance of dead macrophages in the atherosclerotic plaque area through mitochondrial fission (237). Overall, mitochondrial dysfunction is closely related to atherosclerosis progression (234-236). Since ER stress and activation of downstream signaling, as well as suppression of mitobiogenesis both contribute to atherosclerosis, it is highly important to study IRE1-PACT-miR181c signaling in the context of atherosclerosis and hyperlipidemia. Furthermore, screening all the differentially expressed miRNA targets of PACT in high fat diet induced atherosclerotic plaques will be highly relevant to discover novel pathways of disease progression. Investigation of these miRNAs will be crucial for finding therapeutically targeting atherosclerosis. This investigation will be clinically important also because many more molecular mechanisms regulating organelle stress will be revealed that can be relevant for treating diabetes, obesity, and fatty liver diseases in humans (238, 239).

BIBLIOGRAPHY

1. Walter P, and Ron D. The unfolded protein response: from stress pathway to homeostatic regulation. *Science.* 2011;334(6059):1081-6.
2. Schwarz DS, and Blower MD. The endoplasmic reticulum: structure, function and response to cellular signaling. *Cell Mol Life Sci.* 2016;73(1):79-94.
3. Araki K, and Nagata K. Protein folding and quality control in the ER. *Cold Spring Harb Perspect Biol.* 2012;4(8):a015438.
4. Fagone P, and Jackowski S. Membrane phospholipid synthesis and endoplasmic reticulum function. *J Lipid Res.* 2009;50 Suppl(Suppl):S311-6.
5. Krols M, Bultynck G, and Janssens S. ER-Mitochondria contact sites: A new regulator of cellular calcium flux comes into play. *J Cell Biol.* 2016;214(4):367-70.
6. Cárdenas C, Miller RA, Smith I, Bui T, Molgó J, Müller M, et al. Essential regulation of cell bioenergetics by constitutive InsP3 receptor Ca2+ transfer to mitochondria. *Cell.* 2010;142(2):270-83.
7. Booth DM, Enyedi B, Geiszt M, Várnai P, and Hajnóczky G. Redox Nanodomains Are Induced by and Control Calcium Signaling at the ER-Mitochondrial Interface. *Mol Cell.* 2016;63(2):240-8.
8. Rizzuto R, Marchi S, Bonora M, Aguiari P, Bononi A, De Stefani D, et al. Ca(2+) transfer from the ER to mitochondria: when, how and why. *Biochim Biophys Acta.* 2009;1787(11):1342-51.
9. Taouji S, Wolf S, and Chevet E. Oligomerization in endoplasmic reticulum stress signaling. *Prog Mol Biol Transl Sci.* 2013;117:465-84.
10. Hetz C. The unfolded protein response: controlling cell fate decisions under ER stress and beyond. *Nat Rev Mol Cell Biol.* 2012;13(2):89-102.
11. Volmer R, van der Ploeg K, and Ron D. Membrane lipid saturation activates endoplasmic reticulum unfolded protein response transducers through their transmembrane domains. *Proc Natl Acad Sci U S A.* 2013;110(12):4628-33.
12. Çimen I, Kocatürk B, Koyuncu S, Tufanlı Ö, Onat UI, Yıldırım AD, et al. Prevention of atherosclerosis by bioactive palmitoleate through suppression of organelle stress and inflammasome activation. *Sci Transl Med.* 2016;8(358):358ra126.
13. Cox JS, Shamu CE, and Walter P. Transcriptional induction of genes encoding endoplasmic reticulum resident proteins requires a transmembrane protein kinase. *Cell.* 1993;73(6):1197-206.
14. Mori K, Ma W, Gething MJ, and Sambrook J. A transmembrane protein with a cdc2+/CDC28-related kinase activity is required for signaling from the ER to the nucleus. *Cell.* 1993;74(4):743-56.
15. Urano F, Wang X, Bertolotti A, Zhang Y, Chung P, Harding HP, et al. Coupling of stress in the ER to activation of JNK protein kinases by transmembrane protein kinase IRE1. *Science.* 2000;287(5453):664-6.

16. Hamid SM, Citir M, Terzi EM, Cimen I, Yildirim Z, Dogan AE, et al. Inositol-requiring enzyme-1 regulates phosphoinositide signaling lipids and macrophage growth. *EMBO Rep.* 2020:e51462.
17. Harrison SR, Scambler T, Oubussad L, Wong C, Wittmann M, McDermott MF, et al. Inositol-Requiring Enzyme 1-Mediated Downregulation of MicroRNA (miR)-146a and miR-155 in Primary Dermal Fibroblasts across Three TNFRSF1A Mutations Results in Hyperresponsiveness to Lipopolysaccharide. *Front Immunol.* 2018;9:173.
18. Wang JM, Qiu Y, Yang Z, Kim H, Qian Q, Sun Q, et al. IRE1α prevents hepatic steatosis by processing and promoting the degradation of select microRNAs. *Sci Signal.* 2018;11(530).
19. Li Q, Liu T, Yang S, and Zhang Z. Upregulation of miR-34a by Inhibition of IRE1α Has Protective Effect against Aβ-Induced Injury in SH-SY5Y Cells by Targeting Caspase-2. *Oxid Med Cell Longev.* 2019;2019:2140427.
20. Rashid HO, Kim HK, Junjappa R, Kim HR, and Chae HJ. Endoplasmic reticulum stress in the regulation of liver diseases: Involvement of Regulated IRE1α and β-dependent decay and miRNA. *J Gastroenterol Hepatol.* 2017;32(5):981-91.
21. Huang S, Xing Y, and Liu Y. Emerging roles for the ER stress sensor IRE1α in metabolic regulation and disease. *J Biol Chem.* 2019;294(49):18726-41.
22. Carthew RW, and Sontheimer EJ. Origins and Mechanisms of miRNAs and siRNAs. *Cell.* 2009;136(4):642-55.
23. Harding HP, Zhang Y, Bertolotti A, Zeng H, and Ron D. Perk is essential for translational regulation and cell survival during the unfolded protein response. *Mol Cell.* 2000;5(5):897-904.
24. Liu Z, Lv Y, Zhao N, Guan G, and Wang J. Protein kinase R-like ER kinase and its role in endoplasmic reticulum stress-decided cell fate. *Cell Death Dis.* 2015;6(7):e1822.
25. Haze K, Yoshida H, Yanagi H, Yura T, and Mori K. Mammalian transcription factor ATF6 is synthesized as a transmembrane protein and activated by proteolysis in response to endoplasmic reticulum stress. *Mol Biol Cell.* 1999;10(11):3787-99.
26. Yoshida H, Matsui T, Yamamoto A, Okada T, and Mori K. XBP1 mRNA is induced by ATF6 and spliced by IRE1 in response to ER stress to produce a highly active transcription factor. *Cell.* 2001;107(7):881-91.
27. McBride HM, Neuspiel M, and Wasiak S. Mitochondria: more than just a powerhouse. *Curr Biol.* 2006;16(14):R551-60.
28. Kamer KJ, and Mootha VK. The molecular era of the mitochondrial calcium uniporter. *Nat Rev Mol Cell Biol.* 2015;16(9):545-53.
29. Nikoletopoulou V, Markaki M, Palikaras K, and Tavernarakis N. Crosstalk between apoptosis, necrosis and autophagy. *Biochim Biophys Acta.* 2013;1833(12):3448-59.
30. Rambold AS, and Pearce EL. Mitochondrial Dynamics at the Interface of Immune Cell Metabolism and Function. *Trends Immunol.* 2018;39(1):6-18.
31. Yan C, Duanmu X, Zeng L, Liu B, and Song Z. Mitochondrial DNA: Distribution, Mutations, and Elimination. *Cells.* 2019;8(4).

32. Liesa M, Palacín M, and Zorzano A. Mitochondrial dynamics in mammalian health and disease. *Physiol Rev.* 2009;89(3):799-845.
33. Wai T, and Langer T. Mitochondrial Dynamics and Metabolic Regulation. *Trends Endocrinol Metab.* 2016;27(2):105-17.
34. Zemirli N, Morel E, and Molino D. Mitochondrial Dynamics in Basal and Stressful Conditions. *Int J Mol Sci.* 2018;19(2).
35. Otera H, Ishihara N, and Mihara K. New insights into the function and regulation of mitochondrial fission. *Biochim Biophys Acta.* 2013;1833(5):1256-68.
36. Mishra P, and Chan DC. Metabolic regulation of mitochondrial dynamics. *J Cell Biol.* 2016;212(4):379-87.
37. Rambold AS, Kostelecky B, Elia N, and Lippincott-Schwartz J. Tubular network formation protects mitochondria from autophagosomal degradation during nutrient starvation. *Proc Natl Acad Sci U S A.* 2011;108(25):10190-5.
38. Kraus F, and Ryan MT. The constriction and scission machineries involved in mitochondrial fission. *J Cell Sci.* 2017;130(18):2953-60.
39. Pernas L, and Scorrano L. Mito-Morphosis: Mitochondrial Fusion, Fission, and Cristae Remodeling as Key Mediators of Cellular Function. *Annu Rev Physiol.* 2016;78:505-31.
40. Garbern JC, and Lee RT. Mitochondria and metabolic transitions in cardiomyocytes: lessons from development for stem cell-derived cardiomyocytes. *Stem Cell Res Ther.* 2021;12(1):177.
41. Hoppins S, and Nunnari J. Cell Biology. Mitochondrial dynamics and apoptosis--the ER connection. *Science.* 2012;337(6098):1052-4.
42. Kornmann B, Currie E, Collins SR, Schuldiner M, Nunnari J, Weissman JS, et al. An ER-mitochondria tethering complex revealed by a synthetic biology screen. *Science.* 2009;325(5939):477-81.
43. Chen H, Detmer SA, Ewald AJ, Griffin EE, Fraser SE, and Chan DC. Mitofusins Mfn1 and Mfn2 coordinately regulate mitochondrial fusion and are essential for embryonic development. *J Cell Biol.* 2003;160(2):189-200.
44. Mori T, Hayashi T, Hayashi E, and Su TP. Sigma-1 receptor chaperone at the ER-mitochondrion interface mediates the mitochondrion-ER-nucleus signaling for cellular survival. *PLoS One.* 2013;8(10):e76941.
45. Verfaillie T, Rubio N, Garg AD, Bultynck G, Rizzuto R, Decuypere JP, et al. PERK is required at the ER-mitochondrial contact sites to convey apoptosis after ROS-based ER stress. *Cell Death Differ.* 2012;19(11):1880-91.
46. Duchen MR. Roles of mitochondria in health and disease. *Diabetes.* 2004;53 Suppl 1:S96-102.
47. Szabadkai G, Simoni AM, Bianchi K, De Stefani D, Leo S, Wieckowski MR, et al. Mitochondrial dynamics and Ca2+ signaling. *Biochim Biophys Acta.* 2006;1763(5-6):442-9.
48. Hayashi T, and Su TP. Sigma-1 receptor chaperones at the ER-mitochondrion interface regulate Ca(2+) signaling and cell survival. *Cell.* 2007;131(3):596-610.
49. Nutt LK, Pataer A, Pahler J, Fang B, Roth J, McConkey DJ, et al. Bax and Bak promote apoptosis by modulating endoplasmic reticular and mitochondrial Ca2+ stores. *J Biol Chem.* 2002;277(11):9219-25.

50. Youle RJ, and van der Bliek AM. Mitochondrial fission, fusion, and stress. *Science.* 2012;337(6098):1062-5.
51. Friedman JR, Lackner LL, West M, DiBenedetto JR, Nunnari J, and Voeltz GK. ER tubules mark sites of mitochondrial division. *Science.* 2011;334(6054):358-62.
52. de Brito OM, and Scorrano L. Mitofusin 2 tethers endoplasmic reticulum to mitochondria. *Nature.* 2008;456(7222):605-10.
53. Frezza C, Cipolat S, Martins de Brito O, Micaroni M, Beznoussenko GV, Rudka T, et al. OPA1 controls apoptotic cristae remodeling independently from mitochondrial fusion. *Cell.* 2006;126(1):177-89.
54. Meeusen S, DeVay R, Block J, Cassidy-Stone A, Wayson S, McCaffery JM, et al. Mitochondrial inner-membrane fusion and crista maintenance requires the dynamin-related GTPase Mgm1. *Cell.* 2006;127(2):383-95.
55. Bravo R, Vicencio JM, Parra V, Troncoso R, Munoz JP, Bui M, et al. Increased ER-mitochondrial coupling promotes mitochondrial respiration and bioenergetics during early phases of ER stress. *J Cell Sci.* 2011;124(Pt 13):2143-52.
56. Carreras-Sureda A, Jaña F, Urra H, Durand S, Mortenson DE, Sagredo A, et al. Non-canonical function of IRE1α determines mitochondria-associated endoplasmic reticulum composition to control calcium transfer and bioenergetics. *Nat Cell Biol.* 2019;21(6):755-67.
57. Gao P, Yan Z, and Zhu Z. Mitochondria-Associated Endoplasmic Reticulum Membranes in Cardiovascular Diseases. *Front Cell Dev Biol.* 2020;8:604240.
58. Gottlieb RA, and Bernstein D. Mitochondrial remodeling: Rearranging, recycling, and reprogramming. *Cell Calcium.* 2016;60(2):88-101.
59. Civitarese AE, Carling S, Heilbronn LK, Hulver MH, Ukropcova B, Deutsch WA, et al. Calorie restriction increases muscle mitochondrial biogenesis in healthy humans. *PLoS Med.* 2007;4(3):e76.
60. Klingenspor M. Cold-induced recruitment of brown adipose tissue thermogenesis. *Exp Physiol.* 2003;88(1):141-8.
61. Holloszy JO. Biochemical adaptations in muscle. Effects of exercise on mitochondrial oxygen uptake and respiratory enzyme activity in skeletal muscle. *J Biol Chem.* 1967;242(9):2278-82.
62. Garesse R, and Vallejo CG. Animal mitochondrial biogenesis and function: a regulatory cross-talk between two genomes. *Gene.* 2001;263(1-2):1-16.
63. Kelly DP, and Scarpulla RC. Transcriptional regulatory circuits controlling mitochondrial biogenesis and function. *Genes Dev.* 2004;18(4):357-68.
64. Vega RB, Huss JM, and Kelly DP. The coactivator PGC-1 cooperates with peroxisome proliferator-activated receptor alpha in transcriptional control of nuclear genes encoding mitochondrial fatty acid oxidation enzymes. *Mol Cell Biol.* 2000;20(5):1868-76.
65. Cameron RB, Beeson CC, and Schnellmann RG. Development of Therapeutics That Induce Mitochondrial Biogenesis for the Treatment of Acute and Chronic Degenerative Diseases. *J Med Chem.* 2016;59(23):10411-34.
66. Moulin C, Caumont-Sarcos A, and Ieva R. Mitochondrial presequence import: Multiple regulatory knobs fine-tune mitochondrial biogenesis and homeostasis. *Biochim Biophys Acta Mol Cell Res.* 2019;1866(5):930-44.

67. Demishtein-Zohary K, and Azem A. The TIM23 mitochondrial protein import complex: function and dysfunction. *Cell Tissue Res.* 2017;367(1):33-41.
68. Zamora M, and Villena JA. Targeting mitochondrial biogenesis to treat insulin resistance. *Curr Pharm Des.* 2014;20(35):5527-57.
69. Fridovich I. Oxygen toxicity: a radical explanation. *J Exp Biol.* 1998;201(Pt 8):1203-9.
70. Grivennikova VG, and Vinogradov AD. Mitochondrial production of reactive oxygen species. *Biochemistry (Mosc).* 2013;78(13):1490-511.
71. Bienert GP, and Chaumont F. Aquaporin-facilitated transmembrane diffusion of hydrogen peroxide. *Biochim Biophys Acta.* 2014;1840(5):1596-604.
72. Andreyev AY, Kushnareva YE, and Starkov AA. Mitochondrial metabolism of reactive oxygen species. *Biochemistry (Mosc).* 2005;70(2):200-14.
73. Murphy MP. Mitochondrial thiols in antioxidant protection and redox signaling: distinct roles for glutathionylation and other thiol modifications. *Antioxid Redox Signal.* 2012;16(6):476-95.
74. Bonekamp NA, Völkl A, Fahimi HD, and Schrader M. Reactive oxygen species and peroxisomes: struggling for balance. *Biofactors.* 2009;35(4):346-55.
75. Halliwell B, and Gutteridge JM. *Free radicals in biology and medicine.* Oxford university press, USA; 2015.
76. Mailloux RJ, McBride SL, and Harper ME. Unearthing the secrets of mitochondrial ROS and glutathione in bioenergetics. *Trends Biochem Sci.* 2013;38(12):592-602.
77. Tew KD, and Townsend DM. Glutathione-s-transferases as determinants of cell survival and death. *Antioxid Redox Signal.* 2012;17(12):1728-37.
78. Cox AG, Winterbourn CC, and Hampton MB. Mitochondrial peroxiredoxin involvement in antioxidant defence and redox signalling. *Biochem J.* 2009;425(2):313-25.
79. Schrader M, and Fahimi HD. Peroxisomes and oxidative stress. *Biochim Biophys Acta.* 2006;1763(12):1755-66.
80. Cox MM, and Nelson DL. *Lehninger principles of biochemistry.* Wh Freeman New York; 2008.
81. Nordgren M, and Fransen M. Peroxisomal metabolism and oxidative stress. *Biochimie.* 2014;98:56-62.
82. Harris IS, and DeNicola GM. The Complex Interplay between Antioxidants and ROS in Cancer. *Trends Cell Biol.* 2020;30(6):440-51.
83. Lee RC, Feinbaum RL, and Ambros V. The C. elegans heterochronic gene lin-4 encodes small RNAs with antisense complementarity to lin-14. *Cell.* 1993;75(5):843-54.
84. O'Brien J, Hayder H, Zayed Y, and Peng C. Overview of MicroRNA Biogenesis, Mechanisms of Actions, and Circulation. *Frontiers in Endocrinology.* 2018;9(402).
85. Ha M, and Kim VN. Regulation of microRNA biogenesis. *Nat Rev Mol Cell Biol.* 2014;15(8):509-24.
86. Okada C, Yamashita E, Lee SJ, Shibata S, Katahira J, Nakagawa A, et al. A high-resolution structure of the pre-microRNA nuclear export machinery. *Science.* 2009;326(5957):1275-9.

87. Climent M, Viggiani G, Chen YW, Coulis G, and Castaldi A. MicroRNA and ROS Crosstalk in Cardiac and Pulmonary Diseases. *Int J Mol Sci.* 2020;21(12).
88. Stalder L, Heusermann W, Sokol L, Trojer D, Wirz J, Hean J, et al. The rough endoplasmatic reticulum is a central nucleation site of siRNA-mediated RNA silencing. *Embo j.* 2013;32(8):1115-27.
89. Ladomery MR, Maddocks DG, and Wilson ID. MicroRNAs: their discovery, biogenesis, function and potential use as biomarkers in non-invasive prenatal diagnostics. *Int J Mol Epidemiol Genet.* 2011;2(3):253-60.
90. Bartel DP. MicroRNAs: target recognition and regulatory functions. *Cell.* 2009;136(2):215-33.
91. Maurel M, and Chevet E. Endoplasmic reticulum stress signaling: the microRNA connection. *Am J Physiol Cell Physiol.* 2013;304(12):C1117-26.
92. Heyam A, Lagos D, and Plevin M. Dissecting the roles of TRBP and PACT in double-stranded RNA recognition and processing of noncoding RNAs. *Wiley Interdiscip Rev RNA.* 2015;6(3):271-89.
93. Kawamata T, Seitz H, and Tomari Y. Structural determinants of miRNAs for RISC loading and slicer-independent unwinding. *Nat Struct Mol Biol.* 2009;16(9):953-60.
94. Lee Y, Hur I, Park SY, Kim YK, Suh MR, and Kim VN. The role of PACT in the RNA silencing pathway. *Embo j.* 2006;25(3):522-32.
95. Chakravarthy S, Sternberg SH, Kellenberger CA, and Doudna JA. Substrate-specific kinetics of Dicer-catalyzed RNA processing. *J Mol Biol.* 2010;404(3):392-402.
96. Lee HY, Zhou K, Smith AM, Noland CL, and Doudna JA. Differential roles of human Dicer-binding proteins TRBP and PACT in small RNA processing. *Nucleic Acids Res.* 2013;41(13):6568-76.
97. Kok KH, Ng MH, Ching YP, and Jin DY. Human TRBP and PACT directly interact with each other and associate with dicer to facilitate the production of small interfering RNA. *J Biol Chem.* 2007;282(24):17649-57.
98. Noland CL, Ma E, and Doudna JA. siRNA repositioning for guide strand selection by human Dicer complexes. *Mol Cell.* 2011;43(1):110-21.
99. Noland CL, and Doudna JA. Multiple sensors ensure guide strand selection in human RNAi pathways. *Rna.* 2013;19(5):639-48.
100. Wilson RC, Tambe A, Kidwell MA, Noland CL, Schneider CP, and Doudna JA. Dicer-TRBP complex formation ensures accurate mammalian microRNA biogenesis. *Mol Cell.* 2015;57(3):397-407.
101. Emde A, and Hornstein E. miRNAs at the interface of cellular stress and disease. *Embo j.* 2014;33(13):1428-37.
102. Kim VN, Han J, and Siomi MC. Biogenesis of small RNAs in animals. *Nat Rev Mol Cell Biol.* 2009;10(2):126-39.
103. Gantier MP, and Williams BR. The response of mammalian cells to double-stranded RNA. *Cytokine Growth Factor Rev.* 2007;18(5-6):363-71.
104. Kok KH, Lui PY, Ng MH, Siu KL, Au SW, and Jin DY. The double-stranded RNA-binding protein PACT functions as a cellular activator of RIG-I to facilitate innate antiviral response. *Cell Host Microbe.* 2011;9(4):299-309.

105. Lui PY, Wong LR, Ho TH, Au SWN, Chan CP, Kok KH, et al. PACT Facilitates RNA-Induced Activation of MDA5 by Promoting MDA5 Oligomerization. *J Immunol.* 2017;199(5):1846-55.
106. Peters GA, Li S, and Sen GC. Phosphorylation of specific serine residues in the PKR activation domain of PACT is essential for its ability to mediate apoptosis. *J Biol Chem.* 2006;281(46):35129-36.
107. Singh M, Fowlkes V, Handy I, Patel CV, and Patel RC. Essential role of PACT-mediated PKR activation in tunicamycin-induced apoptosis. *J Mol Biol.* 2009;385(2):457-68.
108. Bennett RL, Blalock WL, and May WS. Serine 18 phosphorylation of RAX, the PKR activator, is required for PKR activation and consequent translation inhibition. *J Biol Chem.* 2004;279(41):42687-93.
109. Singh M, and Patel RC. Increased interaction between PACT molecules in response to stress signals is required for PKR activation. *J Cell Biochem.* 2012;113(8):2754-64.
110. Li S, Peters GA, Ding K, Zhang X, Qin J, and Sen GC. Molecular basis for PKR activation by PACT or dsRNA. *Proc Natl Acad Sci U S A.* 2006;103(26):10005-10.
111. St Johnston D, Brown NH, Gall JG, and Jantsch M. A conserved double-stranded RNA-binding domain. *Proc Natl Acad Sci U S A.* 1992;89(22):10979-83.
112. Peters GA, Hartmann R, Qin J, and Sen GC. Modular structure of PACT: distinct domains for binding and activating PKR. *Mol Cell Biol.* 2001;21(6):1908-20.
113. Chang KY, and Ramos A. The double-stranded RNA-binding motif, a versatile macromolecular docking platform. *Febs j.* 2005;272(9):2109-17.
114. Takahashi T, Miyakawa T, Zenno S, Nishi K, Tanokura M, and Ui-Tei K. Distinguishable in vitro binding mode of monomeric TRBP and dimeric PACT with siRNA. *PLoS One.* 2013;8(5):e63434.
115. Chendrimada TP, Gregory RI, Kumaraswamy E, Norman J, Cooch N, Nishikura K, et al. TRBP recruits the Dicer complex to Ago2 for microRNA processing and gene silencing. *Nature.* 2005;436(7051):740-4.
116. Haase AD, Jaskiewicz L, Zhang H, Lainé S, Sack R, Gatignol A, et al. TRBP, a regulator of cellular PKR and HIV-1 virus expression, interacts with Dicer and functions in RNA silencing. *EMBO Rep.* 2005;6(10):961-7.
117. MacRae IJ, Ma E, Zhou M, Robinson CV, and Doudna JA. In vitro reconstitution of the human RISC-loading complex. *Proc Natl Acad Sci U S A.* 2008;105(2):512-7.
118. Laraki G, Clerzius G, Daher A, Melendez-Peña C, Daniels S, and Gatignol A. Interactions between the double-stranded RNA-binding proteins TRBP and PACT define the Medipal domain that mediates protein-protein interactions. *RNA Biol.* 2008;5(2):92-103.
119. Yoda M, Kawamata T, Paroo Z, Ye X, Iwasaki S, Liu Q, et al. ATP-dependent human RISC assembly pathways. *Nat Struct Mol Biol.* 2010;17(1):17-23.
120. Luthra P, Ramanan P, Mire CE, Weisend C, Tsuda Y, Yen B, et al. Mutual antagonism between the Ebola virus VP35 protein and the RIG-I activator PACT determines infection outcome. *Cell Host Microbe.* 2013;14(1):74-84.

121. Siu KL, Yeung ML, Kok KH, Yuen KS, Kew C, Lui PY, et al. Middle east respiratory syndrome coronavirus 4a protein is a double-stranded RNA-binding protein that suppresses PACT-induced activation of RIG-I and MDA5 in the innate antiviral response. *J Virol.* 2014;88(9):4866-76.
122. Fairman-Williams ME, Guenther UP, and Jankowsky E. SF1 and SF2 helicases: family matters. *Curr Opin Struct Biol.* 2010;20(3):313-24.
123. Das S, Ferlito M, Kent OA, Fox-Talbot K, Wang R, Liu D, et al. Nuclear miRNA regulates the mitochondrial genome in the heart. *Circ Res.* 2012;110(12):1596-603.
124. Das S, Bedja D, Campbell N, Dunkerly B, Chenna V, Maitra A, et al. miR-181c regulates the mitochondrial genome, bioenergetics, and propensity for heart failure in vivo. *PLoS One.* 2014;9(5):e96820.
125. Guo R, Gu J, Zong S, Wu M, and Yang M. Structure and mechanism of mitochondrial electron transport chain. *Biomed J.* 2018;41(1):9-20.
126. Bertero E, and Maack C. Metabolic remodelling in heart failure. *Nat Rev Cardiol.* 2018;15(8):457-70.
127. Indrieri A, Carrella S, Romano A, Spaziano A, Marrocco E, Fernandez-Vizarra E, et al. miR-181a/b downregulation exerts a protective action on mitochondrial disease models. *EMBO Mol Med.* 2019;11(5).
128. Zhao MW, Yang P, and Zhao LL. Chlorpyrifos activates cell pyroptosis and increases susceptibility on oxidative stress-induced toxicity by miR-181/SIRT1/PGC-1α/Nrf2 signaling pathway in human neuroblastoma SH-SY5Y cells: Implication for association between chlorpyrifos and Parkinson's disease. *Environ Toxicol.* 2019;34(6):699-707.
129. Latronico MV, and Condorelli G. The might of microRNA in mitochondria. *Circ Res.* 2012;110(12):1540-2.
130. Cannon B, and Nedergaard J. Brown adipose tissue: function and physiological significance. *Physiol Rev.* 2004;84(1):277-359.
131. Scheja L, and Heeren J. Metabolic interplay between white, beige, brown adipocytes and the liver. *J Hepatol.* 2016;64(5):1176-86.
132. Garretson JT, Szymanski LA, Schwartz GJ, Xue B, Ryu V, and Bartness TJ. Lipolysis sensation by white fat afferent nerves triggers brown fat thermogenesis. *Mol Metab.* 2016;5(8):626-34.
133. Puigserver P, Wu Z, Park CW, Graves R, Wright M, and Spiegelman BM. A cold-inducible coactivator of nuclear receptors linked to adaptive thermogenesis. *Cell.* 1998;92(6):829-39.
134. Kajimura S, Spiegelman BM, and Seale P. Brown and Beige Fat: Physiological Roles beyond Heat Generation. *Cell Metab.* 2015;22(4):546-59.
135. Wu J, Cohen P, and Spiegelman BM. Adaptive thermogenesis in adipocytes: is beige the new brown? *Genes Dev.* 2013;27(3):234-50.
136. Harms M, and Seale P. Brown and beige fat: development, function and therapeutic potential. *Nat Med.* 2013;19(10):1252-63.
137. Sustarsic EG, Ma T, Lynes MD, Larsen M, Karavaeva I, Havelund JF, et al. Cardiolipin Synthesis in Brown and Beige Fat Mitochondria Is Essential for Systemic Energy Homeostasis. *Cell Metab.* 2018;28(1):159-74.e11.

138. Xu D, Xu S, Kyaw AMM, Lim YC, Chia SY, Chee Siang DT, et al. RNA Binding Protein Ybx2 Regulates RNA Stability During Cold-Induced Brown Fat Activation. *Diabetes.* 2017;66(12):2987-3000.
139. Pihlajamäki J, Lerin C, Itkonen P, Boes T, Floss T, Schroeder J, et al. Expression of the splicing factor gene SFRS10 is reduced in human obesity and contributes to enhanced lipogenesis. *Cell Metab.* 2011;14(2):208-18.
140. Huot M, Vogel G, Zabarauskas A, Ngo CT, Coulombe-Huntington J, Majewski J, et al. The Sam68 STAR RNA-binding protein regulates mTOR alternative splicing during adipogenesis. *Mol Cell.* 2012;46(2):187-99.
141. Chou CF, Lin YY, Wang HK, Zhu X, Giovarelli M, Briata P, et al. KSRP ablation enhances brown fat gene program in white adipose tissue through reduced miR-150 expression. *Diabetes.* 2014;63(9):2949-61.
142. Thomou T, Mori MA, Dreyfuss JM, Konishi M, Sakaguchi M, Wolfrum C, et al. Corrigendum: Adipose-derived circulating miRNAs regulate gene expression in other tissues. *Nature.* 2017;545(7653):252.
143. Oliverio M, Schmidt E, Mauer J, Baitzel C, Hansmeier N, Khani S, et al. Dicer1-miR-328-Bace1 signalling controls brown adipose tissue differentiation and function. *Nat Cell Biol.* 2016;18(3):328-36.
144. Liu W, Bi P, Shan T, Yang X, Yin H, Wang YX, et al. miR-133a regulates adipocyte browning in vivo. *PLoS Genet.* 2013;9(7):e1003626.
145. Zhang H, Guan M, Townsend KL, Huang TL, An D, Yan X, et al. MicroRNA-455 regulates brown adipogenesis via a novel HIF1an-AMPK-PGC1α signaling network. *EMBO Rep.* 2015;16(10):1378-93.
146. Sun L, and Trajkovski M. MiR-27 orchestrates the transcriptional regulation of brown adipogenesis. *Metabolism.* 2014;63(2):272-82.
147. Hu F, Wang M, Xiao T, Yin B, He L, Meng W, et al. miR-30 promotes thermogenesis and the development of beige fat by targeting RIP140. *Diabetes.* 2015;64(6):2056-68.
148. Trajkovski M, and Lodish H. MicroRNA networks regulate development of brown adipocytes. *Trends Endocrinol Metab.* 2013;24(9):442-50.
149. Shamsi F, Zhang H, and Tseng YH. MicroRNA Regulation of Brown Adipogenesis and Thermogenic Energy Expenditure. *Front Endocrinol (Lausanne).* 2017;8:205.
150. Acosta-Alvear D, Karagöz GE, Fröhlich F, Li H, Walther TC, and Walter P. The unfolded protein response and endoplasmic reticulum protein targeting machineries converge on the stress sensor IRE1. *Elife.* 2018;7.
151. Karise I, Bargut TC, Del Sol M, Aguila MB, and Mandarim-de-Lacerda CA. Metformin enhances mitochondrial biogenesis and thermogenesis in brown adipocytes of mice. *Biomed Pharmacother.* 2019;111:1156-65.
152. Heusch G. 25 years of remote ischemic conditioning: from laboratory curiosity to clinical outcome. *Basic Res Cardiol.* 2018;113(3):15.
153. Heusch G. Coronary microvascular obstruction: the new frontier in cardioprotection. *Basic Res Cardiol.* 2019;114(6):45.
154. Tai Y, Li L, Peng X, Zhu J, Mao X, Qin N, et al. Mitochondrial uncoupler BAM15 inhibits artery constriction and potently activates AMPK in vascular smooth muscle cells. *Acta Pharm Sin B.* 2018;8(6):909-18.

155. Zhao J, Gao JL, Zhu JX, Zhu HB, Peng X, Jiang M, et al. The different response of cardiomyocytes and cardiac fibroblasts to mitochondria inhibition and the underlying role of STAT3. *Basic Res Cardiol.* 2019;114(2):12.
156. Zhou H, Ma Q, Zhu P, Ren J, Reiter RJ, and Chen Y. Protective role of melatonin in cardiac ischemia-reperfusion injury: From pathogenesis to targeted therapy. *J Pineal Res.* 2018;64(3).
157. Andres AM, Tucker KC, Thomas A, Taylor DJ, Sengstock D, Jahania SM, et al. Mitophagy and mitochondrial biogenesis in atrial tissue of patients undergoing heart surgery with cardiopulmonary bypass. *JCI Insight.* 2017;2(4):e89303.
158. Zhou H, Wang S, Hu S, Chen Y, and Ren J. ER-Mitochondria Microdomains in Cardiac Ischemia-Reperfusion Injury: A Fresh Perspective. *Front Physiol.* 2018;9:755.
159. Lochner A, Marais E, and Huisamen B. Melatonin and cardioprotection against ischaemia/reperfusion injury: What's new? A review. *J Pineal Res.* 2018;65(1):e12490.
160. Vela D. Keeping heart homeostasis in check through the balance of iron metabolism. *Acta Physiol (Oxf).* 2020;228(1):e13324.
161. Sprenger HG, and Langer T. The Good and the Bad of Mitochondrial Breakups. *Trends Cell Biol.* 2019;29(11):888-900.
162. Forini F, Nicolini G, Kusmic C, and Iervasi G. Protective Effects of Euthyroidism Restoration on Mitochondria Function and Quality Control in Cardiac Pathophysiology. *Int J Mol Sci.* 2019;20(14).
163. Yellon DM, He Z, Khambata R, Ahluwalia A, and Davidson SM. The GTN patch: a simple and effective new approach to cardioprotection? *Basic Res Cardiol.* 2018;113(3):20.
164. Sharp WW, Fang YH, Han M, Zhang HJ, Hong Z, Banathy A, et al. Dynamin-related protein 1 (Drp1)-mediated diastolic dysfunction in myocardial ischemia-reperfusion injury: therapeutic benefits of Drp1 inhibition to reduce mitochondrial fission. *Faseb j.* 2014;28(1):316-26.
165. Zhou H, Hu S, Jin Q, Shi C, Zhang Y, Zhu P, et al. Mff-Dependent Mitochondrial Fission Contributes to the Pathogenesis of Cardiac Microvasculature Ischemia/Reperfusion Injury via Induction of mROS-Mediated Cardiolipin Oxidation and HK2/VDAC1 Disassociation-Involved mPTP Opening. *J Am Heart Assoc.* 2017;6(3).
166. Zhou H, Wang J, Zhu P, Zhu H, Toan S, Hu S, et al. NR4A1 aggravates the cardiac microvascular ischemia reperfusion injury through suppressing FUNDC1-mediated mitophagy and promoting Mff-required mitochondrial fission by CK2α. *Basic Res Cardiol.* 2018;113(4):23.
167. Guan L, Che Z, Meng X, Yu Y, Li M, Yu Z, et al. MCU Up-regulation contributes to myocardial ischemia-reperfusion Injury through calpain/OPA-1-mediated mitochondrial fusion/mitophagy Inhibition. *J Cell Mol Med.* 2019;23(11):7830-43.
168. Pirzeh L, Babapour V, Badalzadeh R, and Panahi N. Pretreatment with vildagliptin boosts ischemic-postconditioning effects on cardioprotection and expression profile of genes regulating autophagy and mitochondrial fission/fusion

in diabetic heart with reperfusion injury. *Naunyn Schmiedebergs Arch Pharmacol.* 2019;392(11):1371-82.
169. Shen T, Zheng M, Cao C, Chen C, Tang J, Zhang W, et al. Mitofusin-2 is a major determinant of oxidative stress-mediated heart muscle cell apoptosis. *J Biol Chem.* 2007;282(32):23354-61.
170. Song M, Mihara K, Chen Y, Scorrano L, and Dorn GW, 2nd. Mitochondrial fission and fusion factors reciprocally orchestrate mitophagic culling in mouse hearts and cultured fibroblasts. *Cell Metab.* 2015;21(2):273-86.
171. Mouton AJ, DeLeon-Pennell KY, Rivera Gonzalez OJ, Flynn ER, Freeman TC, Saucerman JJ, et al. Mapping macrophage polarization over the myocardial infarction time continuum. *Basic Res Cardiol.* 2018;113(4):26.
172. Morales PE, Arias-Durán C, Ávalos-Guajardo Y, Aedo G, Verdejo HE, Parra V, et al. Emerging role of mitophagy in cardiovascular physiology and pathology. *Mol Aspects Med.* 2020;71:100822.
173. Cadete VJJ, Vasam G, Menzies KJ, and Burelle Y. Mitochondrial quality control in the cardiac system: An integrative view. *Biochim Biophys Acta Mol Basis Dis.* 2019;1865(4):782-96.
174. Li J, Cai SX, He Q, Zhang H, Friedberg D, Wang F, et al. Intravenous miR-144 reduces left ventricular remodeling after myocardial infarction. *Basic Res Cardiol.* 2018;113(5):36.
175. Sun T, Ding W, Xu T, Ao X, Yu T, Li M, et al. Parkin Regulates Programmed Necrosis and Myocardial Ischemia/Reperfusion Injury by Targeting Cyclophilin-D. *Antioxid Redox Signal.* 2019;31(16):1177-93.
176. Zhou H, Zhang Y, Hu S, Shi C, Zhu P, Ma Q, et al. Melatonin protects cardiac microvasculature against ischemia/reperfusion injury via suppression of mitochondrial fission-VDAC1-HK2-mPTP-mitophagy axis. *J Pineal Res.* 2017;63(1).
177. Baker JE, Holman P, Kalyanaraman B, Griffith OW, and Pritchard KA, Jr. Adaptation to chronic hypoxia confers tolerance to subsequent myocardial ischemia by increased nitric oxide production. *Ann N Y Acad Sci.* 1999;874:236-53.
178. Eells JT, Henry MM, Gross GJ, and Baker JE. Increased mitochondrial K(ATP) channel activity during chronic myocardial hypoxia: is cardioprotection mediated by improved bioenergetics? *Circ Res.* 2000;87(10):915-21.
179. Opie LH, and Sack MN. Metabolic plasticity and the promotion of cardiac protection in ischemia and ischemic preconditioning. *J Mol Cell Cardiol.* 2002;34(9):1077-89.
180. Eliseev RA, Vanwinkle B, Rosier RN, and Gunter TE. Diazoxide-mediated preconditioning against apoptosis involves activation of cAMP-response element-binding protein (CREB) and NFkappaB. *J Biol Chem.* 2004;279(45):46748-54.
181. Lucas DT, and Szweda LI. Cardiac reperfusion injury: aging, lipid peroxidation, and mitochondrial dysfunction. *Proc Natl Acad Sci U S A.* 1998;95(2):510-4.
182. Zweier JL. Measurement of superoxide-derived free radicals in the reperfused heart. Evidence for a free radical mechanism of reperfusion injury. *J Biol Chem.* 1988;263(3):1353-7.

183. Chen Z, Siu B, Ho YS, Vincent R, Chua CC, Hamdy RC, et al. Overexpression of MnSOD protects against myocardial ischemia/reperfusion injury in transgenic mice. *J Mol Cell Cardiol.* 1998;30(11):2281-9.
184. St-Pierre J, Lin J, Krauss S, Tarr PT, Yang R, Newgard CB, et al. Bioenergetic analysis of peroxisome proliferator-activated receptor gamma coactivators 1alpha and 1beta (PGC-1alpha and PGC-1beta) in muscle cells. *J Biol Chem.* 2003;278(29):26597-603.
185. Wang J, and Zhou H. Mitochondrial quality control mechanisms as molecular targets in cardiac ischemia-reperfusion injury. *Acta Pharm Sin B.* 2020;10(10):1866-79.
186. Tufanli O, Telkoparan Akillilar P, Acosta-Alvear D, Kocaturk B, Onat UI, Hamid SM, et al. Targeting IRE1 with small molecules counteracts progression of atherosclerosis. *Proc Natl Acad Sci U S A.* 2017;114(8):E1395-e404.
187. Hamid SM, Citir M, Terzi EM, Cimen I, Yildirim Z, Dogan AE, et al. Inositol-requiring enzyme-1 regulates phosphoinositide signaling lipids and macrophage growth. *EMBO Rep.* 2020;21(12):e51462.
188. Karagöz GE, Acosta-Alvear D, Nguyen HT, Lee CP, Chu F, and Walter P. An unfolded protein-induced conformational switch activates mammalian IRE1. *Elife.* 2017;6.
189. Zhang K, Liu H, Song Z, Jiang Y, Kim H, Samavati L, et al. The UPR Transducer IRE1 Promotes Breast Cancer Malignancy by Degrading Tumor Suppressor microRNAs. *iScience.* 2020;23(9):101503.
190. Rowe TM, Rizzi M, Hirose K, Peters GA, and Sen GC. A role of the double-stranded RNA-binding protein PACT in mouse ear development and hearing. *Proc Natl Acad Sci U S A.* 2006;103(15):5823-8.
191. Zhang X, Goncalves R, and Mosser DM. The isolation and characterization of murine macrophages. *Curr Protoc Immunol.* 2008;Chapter 14:Unit 14.1.
192. Aune UL, Ruiz L, and Kajimura S. Isolation and differentiation of stromal vascular cells to beige/brite cells. *J Vis Exp.* 2013(73).
193. Erbay E, Babaev VR, Mayers JR, Makowski L, Charles KN, Snitow ME, et al. Reducing endoplasmic reticulum stress through a macrophage lipid chaperone alleviates atherosclerosis. *Nat Med.* 2009;15(12):1383-91.
194. Livak KJ, and Schmittgen TD. Analysis of relative gene expression data using real-time quantitative PCR and the 2(-Delta Delta C(T)) Method. *Methods.* 2001;25(4):402-8.
195. Allen JJ, Li M, Brinkworth CS, Paulson JL, Wang D, Hübner A, et al. A semisynthetic epitope for kinase substrates. *Nat Methods.* 2007;4(6):511-6.
196. Wessel D, and Flügge UI. A method for the quantitative recovery of protein in dilute solution in the presence of detergents and lipids. *Anal Biochem.* 1984;138(1):141-3.
197. He L, Diedrich J, Chu YY, and Yates JR, 3rd. Extracting Accurate Precursor Information for Tandem Mass Spectra by RawConverter. *Anal Chem.* 2015;87(22):11361-7.
198. Xu T, Park SK, Venable JD, Wohlschlegel JA, Diedrich JK, Cociorva D, et al. ProLuCID: An improved SEQUEST-like algorithm with enhanced sensitivity and specificity. *J Proteomics.* 2015;129:16-24.

199. Tabb DL, McDonald WH, and Yates JR, 3rd. DTASelect and Contrast: tools for assembling and comparing protein identifications from shotgun proteomics. *J Proteome Res.* 2002;1(1):21-6.
200. Peng J, Elias JE, Thoreen CC, Licklider LJ, and Gygi SP. Evaluation of multidimensional chromatography coupled with tandem mass spectrometry (LC/LC-MS/MS) for large-scale protein analysis: the yeast proteome. *J Proteome Res.* 2003;2(1):43-50.
201. Beausoleil SA, Villén J, Gerber SA, Rush J, and Gygi SP. A probability-based approach for high-throughput protein phosphorylation analysis and site localization. *Nat Biotechnol.* 2006;24(10):1285-92.
202. Wei Y, Wang D, Topczewski F, and Pagliassotti MJ. Saturated fatty acids induce endoplasmic reticulum stress and apoptosis independently of ceramide in liver cells. *Am J Physiol Endocrinol Metab.* 2006;291(2):E275-81.
203. Diakogiannaki E, Welters HJ, and Morgan NG. Differential regulation of the endoplasmic reticulum stress response in pancreatic beta-cells exposed to long-chain saturated and monounsaturated fatty acids. *J Endocrinol.* 2008;197(3):553-63.
204. Bertolotti A, Zhang Y, Hendershot LM, Harding HP, and Ron D. Dynamic interaction of BiP and ER stress transducers in the unfolded-protein response. *Nature Cell Biology.* 2000;2(6):326-32.
205. Ghosh R, Wang L, Wang Eric S, Perera BGayani K, Igbaria A, Morita S, et al. Allosteric Inhibition of the IRE1α RNase Preserves Cell Viability and Function during Endoplasmic Reticulum Stress. *Cell.* 2014;158(3):534-48.
206. Harnoss JM, Le Thomas A, Shemorry A, Marsters SA, Lawrence DA, Lu M, et al. Disruption of IRE1α through its kinase domain attenuates multiple myeloma. *Proc Natl Acad Sci U S A.* 2019;116(33):16420-9.
207. Harrington PE, Biswas K, Malwitz D, Tasker AS, Mohr C, Andrews KL, et al. Unfolded Protein Response in Cancer: IRE1α Inhibition by Selective Kinase Ligands Does Not Impair Tumor Cell Viability. *ACS Med Chem Lett.* 2015;6(1):68-72.
208. Papandreou I, Denko NC, Olson M, Van Melckebeke H, Lust S, Tam A, et al. Identification of an Ire1alpha endonuclease specific inhibitor with cytotoxic activity against human multiple myeloma. *Blood.* 2011;117(4):1311-4.
209. Mimura N, Fulciniti M, Gorgun G, Tai YT, Cirstea D, Santo L, et al. Blockade of XBP1 splicing by inhibition of IRE1α is a promising therapeutic option in multiple myeloma. *Blood.* 2012;119(24):5772-81.
210. Gomez JA, and Rutkowski DT. Experimental reconstitution of chronic ER stress in the liver reveals feedback suppression of BiP mRNA expression. *Elife.* 2016;5.
211. Shimazawa M, Inokuchi Y, Ito Y, Murata H, Aihara M, Miura M, et al. Involvement of ER stress in retinal cell death. *Mol Vis.* 2007;13:578-87.
212. Nakamura S, Takizawa H, Shimazawa M, Hashimoto Y, Sugitani S, Tsuruma K, et al. Mild endoplasmic reticulum stress promotes retinal neovascularization via induction of BiP/GRP78. *PLoS One.* 2013;8(3):e60517.
213. Dabo S, Maillard P, Collados Rodriguez M, Hansen MD, Mazouz S, Bigot DJ, et al. Inhibition of the inflammatory response to stress by targeting interaction between PKR and its cellular activator PACT. *Sci Rep.* 2017;7(1):16129.

214. Koscianska E, Starega-Roslan J, and Krzyzosiak WJ. The role of Dicer protein partners in the processing of microRNA precursors. *PLoS One.* 2011;6(12):e28548.
215. Barnett SA, and Dickson RG. Wild mice in the cold: some findings on adaptation. *Biol Rev Camb Philos Soc.* 1989;64(4):317-40.
216. Oelkrug R, Polymeropoulos ET, and Jastroch M. Brown adipose tissue: physiological function and evolutionary significance. *J Comp Physiol B.* 2015;185(6):587-606.
217. Mottillo EP, Balasubramanian P, Lee YH, Weng C, Kershaw EE, and Granneman JG. Coupling of lipolysis and de novo lipogenesis in brown, beige, and white adipose tissues during chronic β3-adrenergic receptor activation. *J Lipid Res.* 2014;55(11):2276-86.
218. Tilokani L, Nagashima S, Paupe V, and Prudent J. Mitochondrial dynamics: overview of molecular mechanisms. *Essays Biochem.* 2018;62(3):341-60.
219. Rodriguez-Ortiz CJ, Baglietto-Vargas D, Martinez-Coria H, LaFerla FM, and Kitazawa M. Upregulation of miR-181 decreases c-Fos and SIRT-1 in the hippocampus of 3xTg-AD mice. *J Alzheimers Dis.* 2014;42(4):1229-38.
220. Lee YH, Kim SN, Kwon HJ, and Granneman JG. Metabolic heterogeneity of activated beige/brite adipocytes in inguinal adipose tissue. *Sci Rep.* 2017;7:39794.
221. Murley A, and Nunnari J. The Emerging Network of Mitochondria-Organelle Contacts. *Mol Cell.* 2016;61(5):648-53.
222. Abrisch RG, Gumbin SC, Wisniewski BT, Lackner LL, and Voeltz GK. Fission and fusion machineries converge at ER contact sites to regulate mitochondrial morphology. *J Cell Biol.* 2020;219(4).
223. Kleele T, Rey T, Winter J, Zaganelli S, Mahecic D, Perreten Lambert H, et al. Distinct fission signatures predict mitochondrial degradation or biogenesis. *Nature.* 2021;593(7859):435-9.
224. Wu Z, Puigserver P, Andersson U, Zhang C, Adelmant G, Mootha V, et al. Mechanisms controlling mitochondrial biogenesis and respiration through the thermogenic coactivator PGC-1. *Cell.* 1999;98(1):115-24.
225. Scarpulla RC. Transcriptional paradigms in mammalian mitochondrial biogenesis and function. *Physiol Rev.* 2008;88(2):611-38.
226. Altshuler-Keylin S, and Kajimura S. Mitochondrial homeostasis in adipose tissue remodeling. *Sci Signal.* 2017;10(468).
227. Zheng M, Kim SK, Joe Y, Back SH, Cho HR, Kim HP, et al. Sensing endoplasmic reticulum stress by protein kinase RNA-like endoplasmic reticulum kinase promotes adaptive mitochondrial DNA biogenesis and cell survival via heme oxygenase-1/carbon monoxide activity. *Faseb j.* 2012;26(6):2558-68.
228. Kato H, Okabe K, Miyake M, Hattori K, Fukaya T, Tanimoto K, et al. ER-resident sensor PERK is essential for mitochondrial thermogenesis in brown adipose tissue. *Life Science Alliance.* 2020;3(3):e201900576.
229. Camargos S, Scholz S, Simón-Sánchez J, Paisán-Ruiz C, Lewis P, Hernandez D, et al. DYT16, a novel young-onset dystonia-parkinsonism disorder: identification of a segregating mutation in the stress-response protein PRKRA. *Lancet Neurol.* 2008;7(3):207-15.

230. Dos Santos CO, da Silva-Júnior FP, Puga RD, Barbosa ER, Azevedo Silva SMC, Borges V, et al. The prevalence of PRKRA mutations in idiopathic dystonia. *Parkinsonism Relat Disord.* 2018;48:93-6.
231. Bernstein E, Caudy AA, Hammond SM, and Hannon GJ. Role for a bidentate ribonuclease in the initiation step of RNA interference. *Nature.* 2001;409(6818):363-6.
232. Letts JA, and Sazanov LA. Clarifying the supercomplex: the higher-order organization of the mitochondrial electron transport chain. *Nat Struct Mol Biol.* 2017;24(10):800-8.
233. Shan B, Wang X, Wu Y, Xu C, Xia Z, Dai J, et al. The metabolic ER stress sensor IRE1α suppresses alternative activation of macrophages and impairs energy expenditure in obesity. *Nat Immunol.* 2017;18(5):519-29.
234. Yu EPK, Reinhold J, Yu H, Starks L, Uryga AK, Foote K, et al. Mitochondrial Respiration Is Reduced in Atherosclerosis, Promoting Necrotic Core Formation and Reducing Relative Fibrous Cap Thickness. *Arterioscler Thromb Vasc Biol.* 2017;37(12):2322-32.
235. Vilne B, Skogsberg J, Foroughi Asl H, Talukdar HA, Kessler T, Björkegren JLM, et al. Network analysis reveals a causal role of mitochondrial gene activity in atherosclerotic lesion formation. *Atherosclerosis.* 2017;267:39-48.
236. Wang Y, Wang GZ, Rabinovitch PS, and Tabas I. Macrophage mitochondrial oxidative stress promotes atherosclerosis and nuclear factor-κB-mediated inflammation in macrophages. *Circ Res.* 2014;114(3):421-33.
237. Wang Y, Subramanian M, Yurdagul A, Jr., Barbosa-Lorenzi VC, Cai B, de Juan-Sanz J, et al. Mitochondrial Fission Promotes the Continued Clearance of Apoptotic Cells by Macrophages. *Cell.* 2017;171(2):331-45.e22.
238. Hotamisligil GS. Inflammation, metaflammation and immunometabolic disorders. *Nature.* 2017;542(7640):177-85.
239. Myoishi M, Hao H, Minamino T, Watanabe K, Nishihira K, Hatakeyama K, et al. Increased endoplasmic reticulum stress in atherosclerotic plaques associated with acute coronary syndrome. *Circulation.* 2007;116(11):1226-33.

COPYRIGHT PERMISSIONS

Keywords: mitochondria-associated ER membrane, cardiovascular diseases, SR-mitochondrial contact, mitochondrial bioenergetics, metabolic transition

Citation: Gao P, Yan Z and Zhu Z (2020) Mitochondria-Associated Endoplasmic Reticulum Membranes in Cardiovascular Diseases. *Front. Cell Dev. Biol.* 8:604240. doi: 10.3389/fcell.2020.604240

Received: 09 September 2020; **Accepted:** 21 October 2020;
Published: 09 November 2020.

Edited by:
Giampaolo Morciano, University of Ferrara, Italy

Reviewed by:
Cláudia Pereira, University of Coimbra, Portugal
Riccardo Filadi, Institute of Neuroscience, Italian National Research Council, Italy
Ester Zito, Mario Negri Institute for Pharmacological Research, Italy

License Number	5331290157196
License date	Jun 17, 2022

Printable Details

Licensed Content

Licensed Content Publisher	Elsevier
Licensed Content Publication	Trends in Cell Biology
Licensed Content Title	The Complex Interplay between Antioxidants and ROS in Cancer
Licensed Content Author	Isaac S. Harris,Gina M. DeNicola
Licensed Content Date	Jun 1, 2020
Licensed Content Volume	30
Licensed Content Issue	6
Licensed Content Pages	12

Order Details

Type of Use	reuse in a thesis/dissertation
Portion	figures/tables/illustrations
Number of figures/tables/illustrations	1
Format	both print and electronic
Are you the author of this Elsevier article?	No
Will you be translating?	No

About Your Work

Title	CHARACTERIZATION OF A NOVEL IRE1 SUBSTRATE PACT AND INTERACTING miRNAS
Institution name	Bilkent University
Expected presentation date	Jun 2022

Additional Data

Portions	Figure 1

Requestor Location

Requestor Location	Bilkent University 1200 N Olive Dr. Unit 314 WEST HOLLYWOOD, CA 90069 United States Attn: Bilkent University

Tax Details

Publisher Tax ID	98-0397604

Price

Total	0.00 USD

License Number	5331290369977
License date	Jun 17, 2022

Printable Details

Licensed Content

Licensed Content Publisher	John Wiley and Sons
Licensed Content Publication	The EMBO Journal
Licensed Content Title	miRNAs at the interface of cellular stress and disease
Licensed Content Author	Eran Hornstein, Anna Emde
Licensed Content Date	May 27, 2014
Licensed Content Volume	33
Licensed Content Issue	13
Licensed Content Pages	10

Order Details

Type of use	Dissertation/Thesis
Requestor type	University/Academic
Format	Print and electronic
Portion	Figure/table
Number of figures/tables	1
Will you be translating?	No

About Your Work

Title	CHARACTERIZATION OF A NOVEL IRE1 SUBSTRATE PACT AND INTERACTING miRNAS
Institution name	Bilkent University
Expected presentation date	Jun 2022

Additional Data

Portions	Figure 1

Requestor Location

Requestor Location	Bilkent University 1200 N Olive Dr. Unit 314 WEST HOLLYWOOD, CA 90069 United States Attn: Bilkent University

Tax Details

Publisher Tax ID	EU826007151

Price

Total	0.00 USD

License Number	5331290566500
License date	Jun 17, 2022

Printable Details

Licensed Content

Licensed Content Publisher	John Wiley and Sons
Licensed Content Publication	WILEY INTERDISCIPLINARY REVIEWS: RNA
Licensed Content Title	Dissecting the roles of TRBP and PACT in double-stranded RNA recognition and processing of noncoding RNAs
Licensed Content Author	Michael Plevin, Dimitris Lagos, Alex Heyam
Licensed Content Date	Jan 28, 2015
Licensed Content Volume	6
Licensed Content Issue	3
Licensed Content Pages	19

Order Details

Type of use	Dissertation/Thesis
Requestor type	University/Academic
Format	Print and electronic
Portion	Figure/table
Number of figures/tables	1
Will you be translating?	No

About Your Work

Title	CHARACTERIZATION OF A NOVEL IRE1 SUBSTRATE PACT AND INTERACTING miRNAS
Institution name	Bilkent University
Expected presentation date	Jun 2022

Additional Data

Portions	Figure 1

Requestor Location

Requestor Location	Bilkent University 1200 N Olive Dr. Unit 314 WEST HOLLYWOOD, CA 90069 United States Attn: Bilkent University

Tax Details

Publisher Tax ID	EU826007151

Price

Total	0.00 USD

License Number	5331290830544
License date	Jun 17, 2022

Printable Details

Licensed Content

Licensed Content Publisher	Wolters Kluwer Health, Inc.
Licensed Content Publication	Circulation Research
Licensed Content Title	The Might of MicroRNA in Mitochondria
Licensed Content Author	Michael V.G. Latronico, Gianluigi Condorelli
Licensed Content Date	Jun 8, 2012
Licensed Content Volume	110
Licensed Content Issue	12

Order Details

Type of Use	Dissertation/Thesis
Requestor type	University/College
Sponsorship	No Sponsorship
Format	Print and electronic
Will this be posted online?	Yes, on a secure website
Portion	Figures/tables/illustrations
Number of figures/tables/illustrations	1
Author of this Wolters Kluwer article	No
Will you be translating?	No
Intend to modify/change the content	No

About Your Work

Title	CHARACTERIZATION OF A NOVEL IRE1 SUBSTRATE PACT AND INTERACTING miRNAS
Institution name	Bilkent University
Expected presentation date	Jun 2022

Additional Data

Portions	Figure

Requestor Location

Requestor Location	Bilkent University 1200 N Olive Dr. Unit 314 WEST HOLLYWOOD, CA 90069 United States Attn: Bilkent University

Tax Details

Publisher Tax ID	13-2932696

Price

Total	0.00 USD

PUBLICATIONS

Dogan AE, Hamid SM, Yildirim AD, Yildirim Z, Sen G, Riera CE, Gottlieb RA, Erbay E. PACT Establishes a Post-transcriptional Brake on Mitochondrial Biogenesis by Promoting the Maturation of miR-181c. J Biol Chem. 2022 May 19:102050. doi: 10.1016/j.jbc.2022.102050. Epub ahead of print. PMID: 35598827.

Hamid SM, Citir M, Terzi EM, Cimen I, Yildirim Z, Dogan AE, Kocaturk B, Onat UI, Arditi M, Weber C, Traynor-Kaplan A, Schultz C, Erbay E. Inositol-requiring enzyme-1 regulates phosphoinositide signaling lipids and macrophage growth. EMBO Rep. 2020 Dec 3;21(12):e51462. doi: 10.15252/embr.202051462. Epub 2020 Nov 2. PMID: 33140520; PMCID: PMC7726810.